IDENTIFYING KEY MARKERS AND MECHANISMS UNDERLYING ADULT NEURAL STEM AND PROGENITOR CELLS AND NEUROGENESIS

by

Yi Zhou

A dissertation submitted to Johns Hopkins University

In conformity with the requirements for the degree of Doctor of Philosophy

Baltimore, Maryland

August, 2018

Abstract

The adult mammalian brain is a dynamic structure, capable of undergoing cellular and molecular remodeling in response to an animal's interactions with the outside world. One dramatic example of brain plasticity is the birth and addition of functional newborn cells to an existing circuit. This process, arising from adult neural stem cells, recapitulates many hallmarks of neural development events into adulthood in two specialized environments: the subventricular zone along the lateral ventricle and the subgranular zone in the dentate gyrus of the hippocampus. The hippocampus draws much interest as a model system because adult-born neurons adapt the brain to temporal events in external space including spatial learning and retention, pattern discrimination, and clearance of memory traces, regulating cognitive and affective behaviors as well as neural plasticity. Deficits in adult hippocampal neurogenesis have been implicated in various brain disorders and psychiatric diseases. Importantly, adult neurogenesis is also present in the human hippocampus and may serve as a cellular mechanism that mediates or augments recovery from mental disorders and neural damage.

In the adult hippocampus, quiescent radial glia-like neural stem cells (RGLs) continuously give rise to newborn dentate granule neurons and astrocytes. It is well established that both extrinsic environmental signals and intrinsic signaling pathways regulate the sequential process of neurogenesis ranging from quiescent RGL activation, persistence, division, fate specification, to newborn neuron development, migration, and integration. Therefore, understanding how adult neural stem cells and their progeny are regulated during development and in adulthood has implications for brain plasticity and regenerative medicine. My thesis research presented here examines how adult

neurogenesis occurs at a cellular level throughout neural development from stem cell to nerve cell.

The first part of my thesis examines how neural stem cells are maintained to sustain adult neurogenesis. Stem cell quiescence is highly regulated by their local microenvironment to sustain continuous neurogenesis in the adult brain, whereas dysregulation leads to stem cell depletion. Quiescence has also been suggested to be essential for establishing the adult neural stem cell pool during development. However, how the stem cell population is maintained throughout early development to ensure a sufficient number of adult neural stem cells to support life-long neurogenesis is not well understood. I identified for the first time, a novel stem cell-derived niche factor that maintains quiescence and prevents developmental exhaustion of neural stem cells to sustain continuous neurogenesis in the adult mammalian brain. My finding highlights the complexity of prospective regulatory mechanisms to maintain a viable stem cell pool over the lifespan.

The second part of my thesis focuses on imaging technology development that enables real-time observation on the dentate gyrus at a single-cell resolution. Stem cells exhibit two defining characteristics, the capacity to simultaneously give rise to the differentiated progeny through asymmetric cell differentiation, and to make more copies of themselves through symmetric cell division. How neural stem cells divide are carefully balanced to ensure correct number of cells located in the neurogenic niche. Moreover, brain injuries were known to largely alter the neural stem cell division pattern, potentially to replace cells lost through injury. Accurate proliferation control of adult neural stem cells raises hope for their potential in regenerative therapies for brain repair. However,

the dynamics of hippocampal neural stem cell division in adult mammals remain unclear; the hippocampus in the mammalian brain is located hundreds of millimeters from the brain surface, rendering it technically difficult for direct observations. I developed a live imaging system, with easy access to the hippocampus, which allows for the integrative view on the changes in behavior of adult neural stem cells and their progeny at a single-cell resolution.

The third part of my thesis characterizes how newborn neurons migrate within the adult hippocampus. Mammalian brain development is a complex, ordered process whereby newborn neurons follow stereotyped migration modes to organize into specific patterns required for complicated neural circuit formation. Classically, principal excitatory neurons are thought to organize into radial columns that underlie the basic brain circuits, whereas inhibitory neurons disperse tangentially across these columns to modulate the principal circuits. These principles are thought to be fundamental to the genesis of the complex mammalian brain. Surprisingly, I, in collaboration with Gerry Sun, found that precursors for excitatory principal neurons exhibit tangential migration in the adult mammalian brain, which utilizes direct contacts with niche vasculature as a migration substrate. This finding represents a novel form of glutamatergic cell migration in the adult mammalian nervous system.

In summary, the work I accomplished during graduate school, including the thesis work presented here, has contributed significant novel discoveries in neural development in the adult brain (see summarized in **Figure 19**). I have found novel molecular and cellular mechanisms regulating adult neural stem cell quiescence and persistence (Zhou et al., 2018), division, fate decision (Sun et al., 2015a), and newborn neuron migration

(Sun et al., 2015b). I developed live imaging technology allowing real-time observation on single-cell behaviors, as well as the ongoing work (not included in this thesis) where I utilize single-cell RNA sequencing technology with bioinformatics pipeline to identify novel key molecular signature during human hippocampal neurogenesis. Overall, my findings have great relevance to better understanding brain development and regenerative medicine.

Ph.D. Dissertation Referees

Hongjun Song, Ph.D. (Faculty Sponsor): Perelman Professor, Department of Neuroscience, University of Pennsylvania; Adjunct Professor, Department of Neuroscience, the Johns Hopkins University, School of Medicine

Erika Matunis, Ph.D.: Professor, Department of Cell Biology, the Johns Hopkins University, School of Medicine

This thesis is dedicated to

the courage that has been taking me through the darkest moments in life,

and the sources where it comes from,

my parents, Zhou Junmin and Zhuang Dayu,

my grandparents, Zhou Hai’ao and Xu Jinghua,

and Yuan Qian.

Preface

First of all, I am grateful to my mentor, Hongjun Song, for providing a rich, resourceful environment that allows me to exchange scientific ideas, establish collaborations, and have access to cutting-edge technologies, great networks and possibilities. He, my role model, has inspired me with qualities and skillsets that I need to become a driven, resourceful professional and a positive, confident person. I thank Gerry Sun, a 'big brother' who took me under his wing at the beginning of my graduate career, teaching me not only scientific knowledge and techniques, but also scientific rigid, integrity, responsibility, time management, and all the things that I benefited tremendously throughout my graduate school. I also thank Yijing Su, Chun Zhong, and Tong Ma for their great support during the past few years both in lab and in life, with whom I became close friends with. None of the work would have been possible if not for the tremendous amount of help from all the Song and Ming lab members, especially Michael Bonaguidi, Allison Bond, Xinyuan Wang, Yi-lan Weng, Daniel Berg, Ryan Stadel, Eunchai Kang, Wei Huang, Kim Christian, Lihong Liu, Yuan Cai, Darin Johnson, and Jordan Schnoll. And I am thankful for a few young and brilliant minds that worked with me, Shiori Ito, Zhengyun Ji, Nick Kawasaki, Nik Modak, Justin Oh, Alex Phan, Jamie Shade, and Adeline Yong. I am fortunate to have collaborators that made generous contributions to my research projects, Guo-li Ming, David Nauen, Nicolas Toni, Jonathan Moss, Kamran Atabai, Chung-ha Davis, Shiying Li, Hao Wu, Armen Saghatelyan, and researchers from the NIH brain and tissue bank at University of Maryland, and University of Miami. And I thank the funding support from American Heart Association.

I also thank my thesis committee, Erika Matunis, Jeremy Nathans, and Seth Blackshaw for providing helpful feedback on my projects and supporting me in the back throughout my graduate career. I am very grateful to Nicholas Marsh-Armstrong for believing in me and giving me the opportunity to come to Hopkins, as well as for serving as a patient, responsive rotation mentor, and for being a reliable collaborator. I also would like to thank BCMB, the best graduate program in the world, in particular Carolyn Machamer and Arhonda Gogos, who really hold the big family together and nurturing every student in the program.

I would like to take the opportunity to appreciate my previous research mentors, Alex Kolodkin, James Bamburg, John Rash, John O'Brien, Yue Sun, and Xiaotao Li, who guided me into the scientific world, a journey I enjoyed very much. I thank Hao Jia, Zixuan Pang, Felix Yu, Chris DeMarco, who have been close friends and 'comrades' in preparing together a career in consulting, venture capital, and private equity. I appreciate the connections and support from old friends at different stages of my life, in particular Zhenghui Deng, Junjie Bian, Shi Zheng, and Phil Head, who provided guidance and backed me up as the going got tough.

Finally, I thank my family, my parents, Junmin Zhou and Dayu Zhuang, my grandparents, Hai'ao Zhou and Jinghua Xu, and Qian Yuan, for their unconditional and endless trust, patience, and love. They have been and will forever be the sources and motivation for me to work hard and live prosper.

Contents

List of Figures

List of Tables

List of Movies

Abbreviations

A: astrocyte or astroglial cell

aCSF: artificial cerebrospinal fluid

BV: blood vessel

GCL: granule cell layer

IN: immature neuron

IPC: intermediate progenitor cell

Mfge8: milk-fat globule-EGF factor 8

ML: molecular layer

N: mature neuron or neuronal lineage

NB: neuroblast

NPC: neural progenitor cell

NSC: neural stem cell

PFA: paraformaldehyde

RGL / RG / R: radial glia-like neural stem cell

SGZ: subgranular zone

SVZ: subventricular zone

1 – General Introduction

The mature central nervous system was often thought of as inhospitable to cell growth or genesis (Ramon y Cajal, 1930). Pioneer work from five decades ago demonstrated that neurogenesis, a process of generating functional neurons from neural precursor cells, occurs beyond development and continues into adulthood (Altman and Das, 1965). This concept became widely accepted and thereby exerted a strong scientist and public attention since the beginning of the 21st century, when adult-born neurons were identified by the incorporation of Bromodeoxyuridine (BrdU), a nucleotide analogue, in humans (Eriksson et al., 1998; Gage, 2000), as well as in almost all mammalian species (Ming and Song, 2011). Findings of neurogenesis in humans was confirmed by a recent study that estimated neuronal birth and turnover rate by measuring the ^{14}C content of genomic DNA in neurons from human post-mortem tissue (Spalding et al., 2013). It is now established that adult neurogenesis persists in mammals throughout their lives mainly in two discrete regions, the subgranular zone (SGZ) in the dentate gyrus of the hippocampus and the subventricular zone (SVZ) of the lateral ventricles. This process adapts existing hippocampus circuits to an animal's interactions with the outside world and contributes to functional recovery in response to neural injury, which represents a striking form of structural plasticity in the adult mammalian brain (Bond et al., 2015).

In the adult hippocampus, radial glia-like cells (RGLs) are the bona fide stem cells that continuously give rise to newborn dentate granule neurons and astrocytes (Ming and Song, 2011). It is well established that both extrinsic environmental signals and intrinsic signaling pathways regulate the sequential process of neurogenesis ranging from quiescent RGL activation, persistence, division, fate specification, to newborn neuron

migration, development, and integration (Bond et al., 2015; Goncalves et al., 2016; Ninkovic and Gotz, 2007). Accumulative evidence has demonstrated critical roles of new neurons in the adult hippocampus in regulating neural plasticity as well as cognitive and affective behaviors, whereas deficits in adult hippocampal neurogenesis have been implicated in various brain disorders (Anacker and Hen, 2017; Christian et al., 2014; Kempermann and Gage, 1999). Therefore, understanding how adult neural stem cells and their progenitors are regulated during development and in adulthood has implications for brain plasticity and regenerative medicine.

2 – General Methods

2.1 Animals

All animal procedures used in this study were performed in accordance with the protocol approved by the Institutional Animal Care and Use Committee of Johns Hopkins University School of Medicine and University of Pennsylvania. All mice in the study were backcrossed to the C57BL/6 background for at least six generations. Animals were housed in a 14-hour light/10-hour dark cycle and had free access to food and water. Housing and husbandry conditions followed standard settings.

2.2 Tamoxifen administration

Tamoxifen (66.67 mg/ml, Sigma, T5648) was prepared in a 5:1 corn oil (Sigma) to ethanol mixture. A dose of 375 mg/kg body weight was intraperitoneally injected into 15-day-old or 2-month-old male and female mice every 12 hours for 3 times. To achieve sparse labeling for clonal analysis (~ 8-16 clones per hemisphere), a single dose of tamoxifen (77.5 mg/kg for the *Rosa-YFP*$^{f/+}$ reporter, 250 mg/kg for the *Confetti*$^{f/+}$ reporter) was intraperitoneally injected into adult 8-10 week-old male and female mice. Mice were analyzed at 1, 3, 7, 30, or 60 days post-tamoxifen injection.

2.3 Tissue processing, immunostaining and confocal imaging

Animals were transcardiac perfused with cold 4% paraformaldehyde [wt/vol, in 0.1 M phosphate buffer, PB, pH 7.4], and cryoprotected with 30% sucrose [wt/vol]. Serial 40 μm-thick coronal brain sections were cut on a frozen sliding microtome (Leica,

SM2010R) for immunohistology. Antibodies diluted in TBS with 0.05% Triton X-100 and 3% donkey serum, were used. See the complete list of antibodies in **Table 1**.

The mT-labeled cells and non-specific blood vessel labeling were removed, and MCM2, Nestin, and NeuN antigens were retrieved by incubating brain sections in 1X target retrieval solution (DAKO) at 92.5 °C for 10 min, followed by a 20-min cooling to room temperature. BrdU antigen was retrieved by incubating brain sections in 2N HCl for 1 hour in room temperature, followed by 0.1M boric acid neutralization for 30 min. Cy2-, Cy3- or Cy5-conjugated secondary antibodies (Jackson ImmunoResearch; 1:500) to appropriate species were incubated at room temperature for 2 hours. Stained sections were imaged at 40x on a Zeiss LSM 710 or 800 confocal microscope (Carl Zeiss).

2.4 Image processing and data analyses

All confocal images were analyzed with Imaris 7.2, 7.6, or 9.0 software (Bitplane) or Fiji Image J (NIH) and analyzed. For illustrative purposes, some cells and features were volume-rendered using the Surface module in Imaris. The Spots module in Imaris was used to digitize cell nucleus locations in the 3D space and to code cell type classifications, according to distinct morphological and molecular markers. The Clipping Plane module in Imaris was used to estimate the local SGZ plane for 2D clone projections. Spots and clipping planes were exported to Matlab (The MathWorks) for further distance measurements, calculations, and analyses. During data acquisition, clones that spanned multiple serial sections were reconstructed using Reconstruct software (John C. Fiala, NIH) and exported at full resolution for 3D visualization into Imaris.

2.5 Quantification and statistical analyses

The studies were blinded during data collection and quantification. Data in figure panels reflect several independent experiments performed on different days. No data were excluded. An estimate of variation within each group of data is indicated using standard error of the mean (SEM). Statistical analysis was performed with on one-way ANOVA (with Tukey post hoc test), one-tailed unpaired Student's t test, two-sample Kolmogorov-Smirnov test, or Wilcoxon rank sum test (with Bonferroni correction for multiple comparisons, where applicable), as indicated in the text and figures. All statistical analyses were performed in the Origin software (OriginLab).

ANTIBODY	SOURCE	IDENTIFIER
Cy2-, Cy3-, or Cy5-conjugated donkey secondary	JacksonImmunoResearch	
Cy3-conjugated goat anti-Armenian Hamster secondary	JacksonImmunoResearch	127-165-160
Chicken anti-GFP	Aves Labs	GFP-1020
Goat anti-GFP	Rockland	
Armenian Hamster anti-Mfge8	MBL	D199-3
Mouse anti-Mfge8	R&D Systems	MAB2767
Mouse anti-Mfge8	Santa Cruz	sc-8029
Mouse anti-GM130	BD Biosciences	610822
Rabbit anti-Ki67	Leica	NCL-Ki67p
Mouse anti-Ki67	BD Biosciences	550609
Mouse anti-BM28 (aka Mcm2)	BD Biosciences	610701
Rat anti-BrdU	Novus	NB500-169
Goat anti-Nestin	Santa Cruz	sc-21248
Chicken anti-Nestin	Aves Labs	NES
Mouse anti-GFAP	Millipore	MAB360
Rabbit anti-GFAP	DAKO	Z0334
Rabbit anti-Tbr2	Abcam	ab23345
Goat anti-DCX	Santa Cruz	sc-8067
Mouse anti-NeuN	Millipore	MAB377

Mouse anti-NeuN, Alexa Fluor 488 conjugated	Millipore	MAB377X
Guinea pig anti-NeuN	Millipore	
Rabbit anti-Prox1	Abcam	
Mouse anti-Prox1	Millipore	
Rabbit anti-S100β	Sigma	2644
Guinea pig anti-Olig2	A generous gift from B. Novitch (UCLA)	
Goat anti-Itga8	R&D Systems	AF4076
Sheep anti-Itgb5	R&D Systems	AF3824
Rat anti-Itgb1	Millipore	MAB1997; (Brooker et al., 2016)
Mouse anti-S6 (54D2)	Cell Signaling	#2317; (Kim et al., 2009)
Rabbit anti-pS6 (Ser235/236)	Cell Signaling	#2211; (Kim et al., 2009)
Rabbit anti-4EBP1 (53H11)	Cell Signaling	#9644
Rabbit anti-p4EBP1 (T37/46)	Cell Signaling	#2855
Mouse anti-Akt (5G3)	Cell Signaling	#2966
Rabbit anti-pAkt (Thr308)	Cell Signaling	#9275S
Rat anti-CD68	Bio-Rad	MCA1957GA
Rabbit anti-Iba1	WAKO	019-19741
Anti-fluorescein peroxidase	Roche	11426346910

Hamster anti-rat CD29	BD Biosciences	555002
Mouse IgG1 isotype control	BD Biosciences	554121
Rat anti-mouse CD51, integrin αv	BioLegend	104107
Mouse anti-β-actin	Sigma	A1978
Goat anti-rabbit IgG-HRP	Cell Signaling	7074S
Goat anti-mouse IgG-HRP	Santa Cruz	sc-2031
Rat anti-CD31	BD Biosciences	
Rabbit anti-γ-tubulin	BioLegend	

Table 1. Primary antibodies used.

3 – Neural stem cell-enriched Mfge8 promotes quiescence and prevents developmental exhaustion of adult neural stem cell pool

(This chapter was published (Zhou et al., 2018). I am the first author and was involved in all aspects of the study.)

3.1 Introduction

Neurogenesis persists throughout life in the subgranular zone (SGZ) in the dentate gyrus of the hippocampus and the subventricular zone (SVZ) of the lateral ventricles and represents a striking form of structural plasticity in the adult mammalian brain (Gage, 2000). In the adult hippocampus, quiescent radial glia-like neural stem cells (RGLs) continuously give rise to newborn dentate granule neurons and astrocytes (Goncalves et al., 2016; Ming and Song, 2011; Seri et al., 2004). Accumulative evidence has demonstrated critical roles of new neurons in the adult hippocampus in regulating neural plasticity as well as cognitive and affective behaviors, whereas deficits in adult hippocampal neurogenesis have been implicated in various brain disorders (Anacker and Hen, 2017; Christian et al., 2014; Kempermann and Gage, 1999). Therefore, understanding how the pool of adult neural stem cells is regulated during development and maintained in adulthood has implications for brain plasticity and regenerative medicine.

It is well established that both extrinsic environmental signals and intrinsic signaling pathways regulate the sequential process of neurogenesis in both adult SGZ and SVZ, ranging from quiescent neural stem cell activation and fate specification, to new neuron development and integration (Bond et al., 2015; Goncalves et al., 2016; Ninkovic and Gotz, 2007). Multiple lines of evidence suggest that RGL quiescence is a highly

regulated state and is critical to maintain continuous neurogenesis in the adult brain. First, single-cell transcriptome analyses have revealed high expression levels of many signaling pathway receptors and intracellular mediators during quiescence, which become down-regulated upon RGL activation (Llorens-Bobadilla et al., 2015; Shin et al., 2015). Second, dysregulation of cytoplasmic signaling pathways, such as FoxO (Paik et al., 2009; Renault et al., 2009) and PTEN (Bonaguidi et al., 2011), activates quiescent RGLs. Third, activation of quiescent RGLs can lead to their depletion in both adult SGZ and SVZ (Calzolari et al., 2015; Encinas et al., 2011; Groszer et al., 2006; Mira et al., 2010; Seib et al., 2013). Understanding how adult neural stem cell quiescence is regulated remains an important cornerstone in the field and may have implications for understanding other somatic stem cells in various tissues (Cheung and Rando, 2013). Among niche factors identified so far that regulate adult RGL quiescence, almost all of them are paracrine factors, including neurotransmitters and peptides released from axon terminals (Berg et al., 2013; Karadottir and Kuo, 2018; Paez-Gonzalez et al., 2014; Paul et al., 2017; Song et al., 2012; Tong et al., 2014), the Wnt inhibitor sFRP3 released from mature granule cells (Jang et al., 2013), Notch ligand DLL1 from newborn neurons (Kawaguchi et al., 2013), and growth factors NT-3 and VEGF released from endothelial cells (Delgado et al., 2014). Much less is known about whether RGL quiescence is also regulated by neural stem cell-derived factors.

Quiescence has also been suggested to be essential for establishing the adult neural stem cell pool during development. Adult SVZ neural stem cells are set aside and remain quiescent during development (Fuentealba et al., 2015; Furutachi et al., 2015). Importantly, activation of these quiescent or slowly dividing populations during

development, by deletion of either the cyclin-dependent kinase inhibitor p57 (Furutachi et al., 2015) or VCAM1 (Hu et al., 2017), reduces the pool of adult SVZ neural stem cells. The niche mechanism that regulates the adult neural stem cell pool during development is completely unknown.

Our recent single-cell transcriptomic analysis has provided insight into the molecular signature of quiescent RGLs in the adult mouse dentate gyrus (Shin et al., 2015). We noted that the transcript of milk-fat globule-EGF factor 8 (Mfge8, also known as SED1 or lactadherin) is highly enriched during the quiescent state compared to the activated state of RGLs (**Figure 1A**) (Shin et al., 2015). Mfge8 is traditionally known to play a critical role in phagocytosis (Nagata et al., 2010; Raymond et al., 2009). Phagocytes secrete Mfge8, which binds to 'eat-me' signals secreted by dying cells, such as exposed phosphatidylserine. Mfge8 then binds to integrin receptors $\alpha_v\beta_3$ or $\alpha_v\beta_5$ expressed on phagocytes to promote engulfment of apoptotic cells (Hanayama et al., 2002). In the nervous system, activated microglia or astrocytes during neuroinflammation or ischemic injury secrete Mfge8 and phagocytose dying cells and fragments (Fricker et al., 2012; Mills et al., 2015; Neher et al., 2013). Here we investigated the potential role and mechanism of Mfge8 in regulating neurogenesis in the early postnatal and adult mouse dentate gyrus under physiological conditions.

3.2 Methods

3.2.1 Animals

All animal procedures used in this study were performed in accordance with the protocol approved by the Institutional Animal Care and Use Committee of Johns Hopkins University School of Medicine and University of Pennsylvania. All mice in the study were backcrossed to the C57BL/6 background for at least six generations. Animals were housed in a 14-hour light/10-hour dark cycle and had free access to food and water. Housing and husbandry conditions followed standard settings. Both 15-day-old mice (postnatal) and 2-month-old mice (adult) were used in this study. For immunohistology, C57Bl6/J wild-type mice and *Nestin-GFP* transgenic mice (Encinas et al., 2006) were used. For knockout and rapamycin rescue analysis, mice used in different groups were housed as littermates: C57Bl6/J WT mice, and *Mfge8*$^{-/-}$(KO). For conditional knockout analyses, *Gli-CreER*^{T2}*; Mfge8*$^{f/f}$; *mT/mG*$^{f/-}$, and *Gli1-CreER*^{T2}*; mT/mG*$^{f/-}$ were generated by crossing *Gli1-CreER*^{T2} driver (Ahn and Joyner, 2005) with *mT/mG*$^{f/-}$ reporter (Muzumdar et al., 2007) and *Mfge8*$^{f/f}$ mice (Atabai lab), where applicable.

The following primers were used for mouse genotyping: eGFP (F: 5'-GCT GTT CAC CGG GGT GGT GC-3'; R: 5'-GGC AGC AGC ACG GGG CCG TC-3'), CreER (F: 5'-TGCCACGACCAAGTGACAGCAATG-3'; R: 5'-ACCAGAGACGGAAATCCATGGCTC-3'), *Mfge8* germline knockout mice (WT: 5'-GTGAACCTTCTGCGGAAGAT-3'; Mutant: 5'-CGTGGGATCATTGTTTTTCT-3'; Common antisense primer: 5'-GGGCATAAACTCCAGCTCAC-3'), *Mfge8* conditional knockout mice (F: 5'-CCTTAAGGCCCCTCTCATTC-3'; 5'-TGTCAAGCATTGCAGAGTCC-3'), and mT/mG (WT: 5'-

CGAGGCGGATCACAAGCAATA-3'; Mutant: 5'-TCAATGGGCGGGGGTCGTT-3'; Common: 5'-CTCTGCTGCCTCCTGGCTTCT-3').

3.2.2 BrdU administration

For analysis of cell proliferation in the dentate gyrus, P15 or P60 mice were injected with BrdU (200 mg/kg body weight, i.p.) and analyzed 2 hours or 30 days later. Tissue processing and quantification of $BrdU^+$ cells within the SGZ and granule cell layer were carried out as previously described (Jang et al., 2013).

3.2.3 Tamoxifen administration

Tamoxifen (66.67 mg/ml, Sigma, T5648) was prepared in a 5:1 corn oil (Sigma) to ethanol mixture (Sun et al., 2015a; Sun et al., 2015b). A dose of 375 mg/kg body weight was intraperitoneally injected into P15 or P60 male and female mice every 12 hours for 3 times. Mice were analyzed 3 or 30 days post-tamoxifen injection.

3.2.4 Rapamycin administration

Rapamycin (LC Laboratories) was first dissolved in ethanol at a stock concentration of 25 mg/ml and was further diluted with a final concentration of 1 mg/ml in 4% ethanol, 5% Tween 80, and 5% PEG 400 as previously described (Kim et al., 2009). Rapamycin was intraperitoneally delivered twice to mice at 20 mg/kg body weight at P11 and P13, analyzed at P15, or injected at P60 and P62 and analyzed at P64.

3.2.5 Tissue processing, immunostaining, and confocal imaging

Animals were perfused with cold 4% paraformaldehyde [wt/vol; in 0.1 M phosphate buffer (PB), pH 7.4], and cryoprotected with 30% sucrose (wt/vol). Serial 40-μm-thick coronal brain sections were cut on a frozen sliding microtome (Leica; SM2010R) for immunohistology as previously described (Sun et al., 2015a; Sun et al., 2015b). Every 6th section was taken for immunohistology throughout the anterior to posterior axis of the dentate gyrus. Antibodies were diluted in TBS (Tris buffered saline) with 0.1% Triton X-100 and 3% (vol/vol) donkey serum. Sections were incubated with primary antibodies at 4 °C overnight. The following primary antibodies were used: BrdU (Novus; rat; 1:300), CD68 (Bio-Rad; rat; 1:300), DCX (Santa Cruz, goat, 1:100), GFAP (Millipore, mouse, rabbit, 1:1,000), GFP (Aves Labs, chicken, 1:500), GM130 (BD Biosciences, mouse, 1:300), Iba1 (WAKO; rabbit; 1:500), integrin α_8 (R&D Systems; goat; 1:100), integrin β_1 (Millipore; rat; 1:300), integrin α_5 (R&D Systems; sheep; 1:500), Ki67 (Leica; rabbit; 1:500; BD Bioscience; mouse; 1:500), Mcm2 (aka BM28; BD Biosciences; mouse; 1:300), Mfge8 (MBL; Armenian Hamster; 1:500; R&D Systems; Mouse; 1:100; Santa Cruz; mouse; 1:300), Nestin (Santa Cruz; Goat; 1:250; Aves Labs; chicken; 1:500), NeuN (Millipore; mouse; 1:500; and Alexa Fluor 488 conjugated), Olig2 (guinea pig; 1:500); p4EBP1 (Cell Signaling; rabbit; 1:500), pS6 (Ser-235/236; Cell Signaling; rabbit; 1:500), S-100β (Sigma; rabbit; 1:300); and Tbr2 (Abcam; rabbit; 1:250).

The mT-labeled cells and non-specific blood vessel labeling were removed, and Mcm2 and NeuN antigens were retrieved by incubating brain sections in 1x target retrieval solution (DAKO) at 92.5 °C for 10 min, followed by a 20-min cooling to room

temperature. BrdU antigen was retrieved by incubating brain sections in 2N HCl for 1 hour in room temperature, followed by 0.1M boric acid neutralization for 30 min. Cy2-, Cy3- or Cy5-conjugated secondary antibodies (Jackson ImmunoResearch; 1:500) to appropriate species were incubated at room temperature for 2 hours. Stained sections were imaged at 40x on a Zeiss LSM 710 or 800 confocal microscope (Carl Zeiss).

3.2.6 *In-situ* hybridization

In-situ hybridization was performed on PFA-fixed brain sections (40 μm thickness) as described previously (Mills et al., 2015). Fluorescein-conjugated antisense riboprobe for *Mfge8* mRNA was generated by in vitro transcription. Hybridization of the riboprobes on sections was performed at 65 °C overnight and followed by washing once with 5x SSC and 1% SDS, then twice with 0.2x SSC for 1 hour each at 72 °C. The sections were incubated with anti-fluorescein peroxidase (Roche) at 4 °C for overnight, and were visualized using Cy3-conjugated Tyramide Signal Amplification system (Perkin-Elmer) at room temperature. The *in-situ* hybridization was followed by immunostaining for Nestin (goat anti-Nestin, Santa Cruz, 1:500), and GFAP (Millipore, mouse, rabbit, 1:1,000) incubated at 4 °C overnight and followed by incubation of Cy2- and Cy5-conjugated secondary antibodies (Jackson ImmunoResearch; 1:500) for 2 hours at room temperature.

3.2.7 Adult neural progenitor culture and analyses

Adult mouse hippocampal neural progenitor cells were derived from adult mouse dentate gyrus as previously described (Ma et al., 2008; Song et al., 2002). To determine whether

Mfge8 was secreted by adult neural progenitors in culture, cells were cultured to reach 75% confluency and media were collected and concentrated 5-10 times by centrifugation at 4˚C with Amicon Ultra-4 Centrifugal Filter Units (Millipore, 10,000 NMWL) at 4,000 x g. Samples were processed for Western blot analysis to detect Mfge8 protein at ~50 KD.

To examine neural progenitor proliferation, adult neural progenitors were incubated with exogenous recombinant Mfge8 (R&D Systems) for 2 days. Blocking antibodies against integrin α_v (BioLegend; 0.625 μg/ml) or β_1 (BD Biosciences; 0.625 μg/ml), or IgG control (BD Biosciences; 0.625 μg/ml) were added for 24 hours before an EdU (Thermo Fisher Scientific, 10 μM) pulse for 40 min followed by PFA fixation for immunostaining, imaging and quantification. EdU was detected by Click-iT Imaging Kit (Invitrogen), in combination with immunostaining for Nestin (goat anti-Nestin, Santa Cruz, 1:500).

Biochemical analyses were performed as previously described (Kim et al., 2009). Adult neural progenitor culture was lysed in cold RIPA buffer containing 50 mM Tris HCl (pH 7.5), 150 mM NaCl, 1% NP-40, 0.5% sodium deoxycholate, 0.1% SDS supplemented with protease and phosphatase inhibitor cocktail (Cell Signaling; Sigma) at 4˚C for 10 min, followed by sonication on ice for 30 sec for 3 times. Protein concentration was determined by Bradford assay (Bio-Rad). Equal amounts of protein were loaded to be separated by SDS-PAGE on 4-20% resolving gels (Bio-Rad) and transblotted onto PVDF membranes (Bio-Rad). Membranes were incubated in primary antibodies at a 1:1,000 dilution at 4 °C overnight against 4EBP1 (Cell Signaling; rabbit), p4EBP1 (Cell Signaling; rabbit), S6 (Cell Signaling; mouse), pS6 (Cell Signaling;

rabbit), β-actin (Sigma; mouse), Mfge8 (R&D Systems; mouse; Santa Cruz; mouse), Akt (Cell Signaling; mouse), and pAkt (Cell Signaling; rabbit), followed by a secondary HRP-conjugated antibody (Cell Signaling; rabbit; Santa Cruz; mouse). For evaluation of total 4EBP1, S6, and Akt, we stripped and reprobed membranes that had been blotted for phospho-versions of these proteins.

3.2.8 Image processing and data analyses

All confocal images were blindly acquired between experimental and control groups under the same laser power and gain, and were analyzed with Imaris 7.2, 7.6, 9.0 software (BitPlane), or ImageJ (NIH) without adjusting image brightness or contrast, as previously described (Sun et al., 2015a; Sun et al., 2015b). The Spots module in Imaris was used to digitize cell-nucleus locations in the 3D space and to code cell type classifications according to distinct morphological and molecular markers. The Clipping Plane module in Imaris was used to estimate the local SGZ plane for 2D clone projections. For illustrative purposes, some cells and features were volume-rendered using the Surface module in Imaris (**Figure 1C-F**; bottom panels). A qualified RGL needed to satisfy the following criteria, (1) located in the SGZ of the dentate gyrus; (2) have a distinct $Nestin^{+}GFAP^{+}$ radial process; (3) have a $DAPI^{+}$ nuclei that is largely wrapped around by GFAP immunostaining signal in the same focal plane. A cell nucleus located within the granule cell layer and having overlapped immunostaining signals of DAPI, BrdU/Mcm2, and Tbr2 or NeuN in the same focal plane, is qualified as a $BrdU^{+}/Mcm2^{+}$ intermediate progenitor cell or dentate granule neuron, respectively. A $BrdU^{+}/Mcm2^{+}$ DCX^{+} neuroblast should be located in the granule cell layer, and have a

$DAPI^+$ and $BrdU^+/Mcm2^+$ nuclei that is largely wrapped around by DCX immunostaining signal in the same focal plane.

3.2.9 Quantification and statistical analysis

The studies were blinded during data collection and quantification. Data in figure panels reflect several independent experiments performed on different days. No data were excluded. An estimate of variation within each group of data is indicated using standard error of the mean (SEM). Statistical analysis was performed with one-way ANOVA (with Tukey post hoc test), or one-tailed unpaired Student's t-test, as indicated in the text and figures. All statistical analyses were performed in Origin software (OriginLab).

3.3 Results

3.3.1 Mfge8 is enriched in quiescent RGLs in adult mouse dentate gyrus

Our recent single-cell RNA-sequencing analysis of Nestin-CFP labeled neural progenitors in the adult mouse dentate gyrus suggested an enrichment of *Mfge8* mRNA in quiescent, but not active neural progenitors (**Figure 1A**) (Shin et al., 2015). To validate this result, we performed *in situ* hybridization in combination with immunohistology for markers of RGLs. Indeed, *Mfge8* mRNA was present in $Nestin^{+}GFAP^{+}$ RGLs, as well as $Nestin^{-}GFAP^{+}$ astrocytes in the adult dentate gyrus (**Figure 1B**). We further performed immunohistological analysis using anti-Mfge8 antibodies, which we validated with *Mfge8* knockout mice (**Figure 2A**). Using Nestin-GFP transgenic mice (Encinas et al., 2006) to label RGLs in the adult dentate gyrus, we detected the presence of Mfge8 protein at the base of radial fibers in most $Nestin\text{-}GFP^{+}GFAP^{+}$ RGLs (94.7 ± 3.3%; n = 3 mice), and in particular at the $GM130^{+}$ Golgi apparatus (**Figure 1C-D**). Consistent with single-cell RNA-sequencing results (**Figure 1A**), few proliferating $Mcm2^{+}$ RGLs (16.2 ± 3.5%; n = 3 mice; **Figure 1E** and **Movie 1**) or $Tbr2^{+}$ intermediate progenitor cells (IPCs; 6.1 ± 1.1%; n = 3 mice; **Figure 1F**) expressed Mfge8 protein. Among other cell types in the adult dentate gyrus, Mfge8 protein was present in $s100\beta^{+}$ astrocytes (95.3 ± 4.5%; n = 3 mice; **Figure 2B**), but was not detectable in $NeuN^{+}$ mature granule cells, $Iba1^{+}$ microglia, or $Olig2^{+}$ oligodendrocyte precursors (n = 3; **Figure 2C-E**). Together, these results revealed highly enriched expression of Mfge8 in quiescent RGLs and astrocytes in the adult dentate gyrus.

Figure 1. Mfge8 is enriched in quiescent adult mouse hippocampal neural stem cells.

(**A**) Enrichment of *Mfge8* mRNA in quiescent radial glia-like neural stem cells (RGLs). Shown is an expression profile of *Mfge8* from single-cell RNA-seq analysis of Nestin-CFP marked neural progenitors in adult mouse dentate gyrus (Shin et al., 2015). Each data point represents the expression level of *Mfge8* of a single cell along a pseudotime trajectory from quiescent RGLs to activated RGLs to proliferating IPCs. Data points are fitted with local polynomial regression fitting (red line) with 95% confidence intervals (gray area). The superimposed Violin plots represent a summary of expression from different stages along the neurogenesis trajectory.

(**B**) Sample confocal images of *Mfge8* fluorescent *in-situ* hybridization, and Nestin and GFAP immunostaining in the adult mouse dentate gyrus. Note the presence of *Mfge8* mRNA in $Nestin^{+}GFAP^{+}$ RGLs (an example is shown in box 1 with solid line) and in $Nestin^{-}GFAP^{+}$ astrocytes (an example is shown in box 2 with dashed line). The region in box 1 is shown at a higher magnification (right panels). Scale bar: 10 μm.

(**C-F**) Sample confocal images of immunostaining for Mfge8 and GFAP (**C**), Golgi marker GM130 (**D;** arrow points to Mfge8 and GM130 colocalization at the base of RGL radial fiber), proliferating cell marker Mcm2 (**E;** yellow arrowheads point to $Mcm2^{-}$ RGLs and orange arrows point to a $Mcm2^{+}$ RGL), and an intermediate progenitor cell (IPC) marker Tbr2 (**F;** arrow points to a $Tbr2^{+}$ cell)**,** in Nestin-GFP^{+} cells in adult mouse dentate gyrus. Bottom panel shows 3D volume-rendered Mfge8 immunostaining. Scale bars: 10 μm. Note the presence of Mfge8 in $GM130^{+}$ Golgi compartment in $Mcm2^{-}$ Nestin-$GFP^{+}GFAP^{+}$ quiescent RGLs, but not in $Tbr2^{+}$ IPCs. Also see **Movie 1** for (**E**).

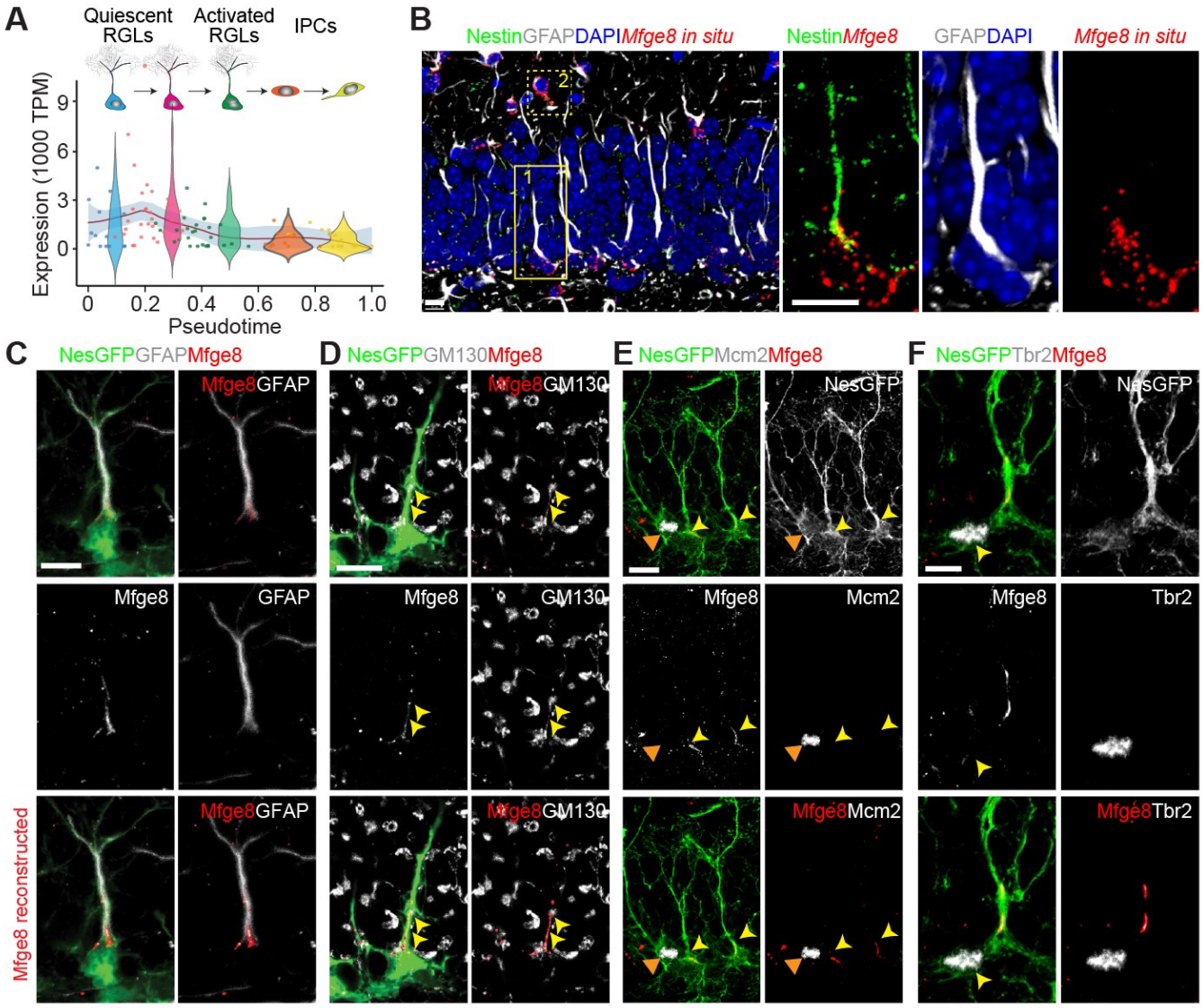
A
Quiescent RGLs
Activated RGLs
IPCs
Expression (1000 TPM)
9
6
3
0
0
0.2
0.4
0.6
0.8
1.0
Pseudotime
B
NestinGFAPDAPIMfge8 in situ
NestinMfge8
GFAPDAPI
Mfge8 in situ
1
2
C
NesGFPGFAPMfge8
Mfge8GFAP
Mfge8
GFAP
Mfge8 reconstructed
Mfge8GFAP
D
NesGFPGM130Mfge8
Mfge8GM130
Mfge8
GM130
Mfge8GM130
E
NesGFPMcm2Mfge8
NesGFP
Mfge8
Mcm2
Mfge8Mcm2
F
NesGFPTbr2Mfge8
NesGFP
Mfge8
Tbr2
Mfge8Tbr2

Figure 2. Immunohistological characterization of Mfge8 expression in the adult dentate gyrus.

(**A**) Specificity of antibodies against Mfge8 was validated by immunostaining on dentate gyrus sections from adult *Mfge8* germline knockout mice. Shown are sample confocal images immunostained for Mfge8 and GM130. Scale bar: 10 μm.

(**B-E**) Expression of Mfge8 in astrocytes, but not in mature granule cells, microglia or oligodendrocyte precursors in the adult dentate gyrus. Shown are sample confocal images of immunostaining for Mfge8, astrocyte marker S100β (**B**), mature granule neuron marker NeuN (**C**), microglia marker Iba1 (**D**), and oligodendrocyte precursor marker Olig2 (**E**). Scale bars: 10 μm.

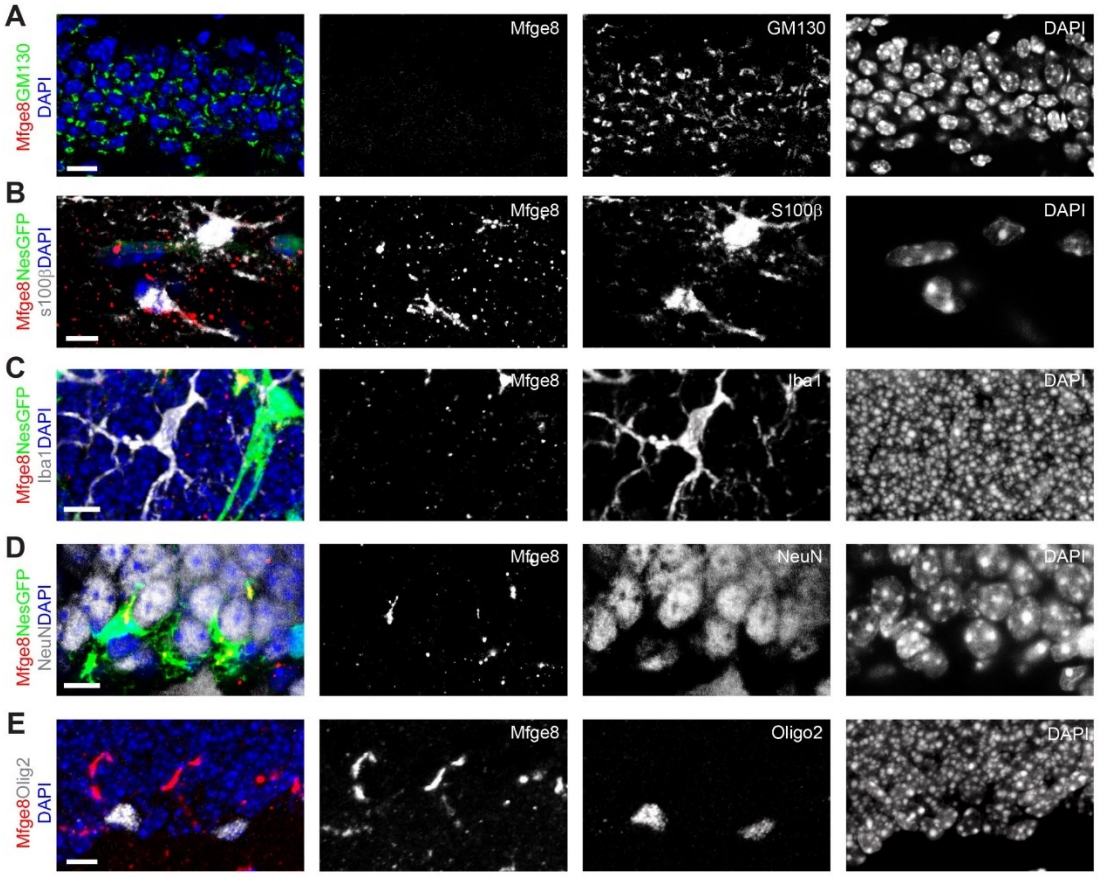
A
Mfge8GM130
DAPI
Mfge8
GM130
DAPI
B
Mfge8NesGFP
s100βDAPI
Mfge8
S100β
DAPI
C
Mfge8NesGFP
Iba1DAPI
Mfge8
Iba1
DAPI
D
Mfge8NesGFP
NeuNDAPI
Mfge8
NeuN
DAPI
E
Mfge8Olig2
DAPI
Mfge8
Oligo2
DAPI

Movie 1. Mfge8 is enriched in quiescent RGLs in the adult mouse dentate gyrus. Shown is a confocal image of immunostaining for DAPI (blue), GFP (green), Mfge8 (red), and Mcm2 (white) in a *Nestin-GFP* reporter mouse. Note there is one $Mcm2^{+}GFP^{+}$ activated RGL (the furthest left) that was $Mfge8^{-}$. There are three $Mcm2^{-}GFP^{+}Mfge8^{+}$ quiescent RGLs (right). Also shown is a surface rendering of Mfge8 immunostaining (red).

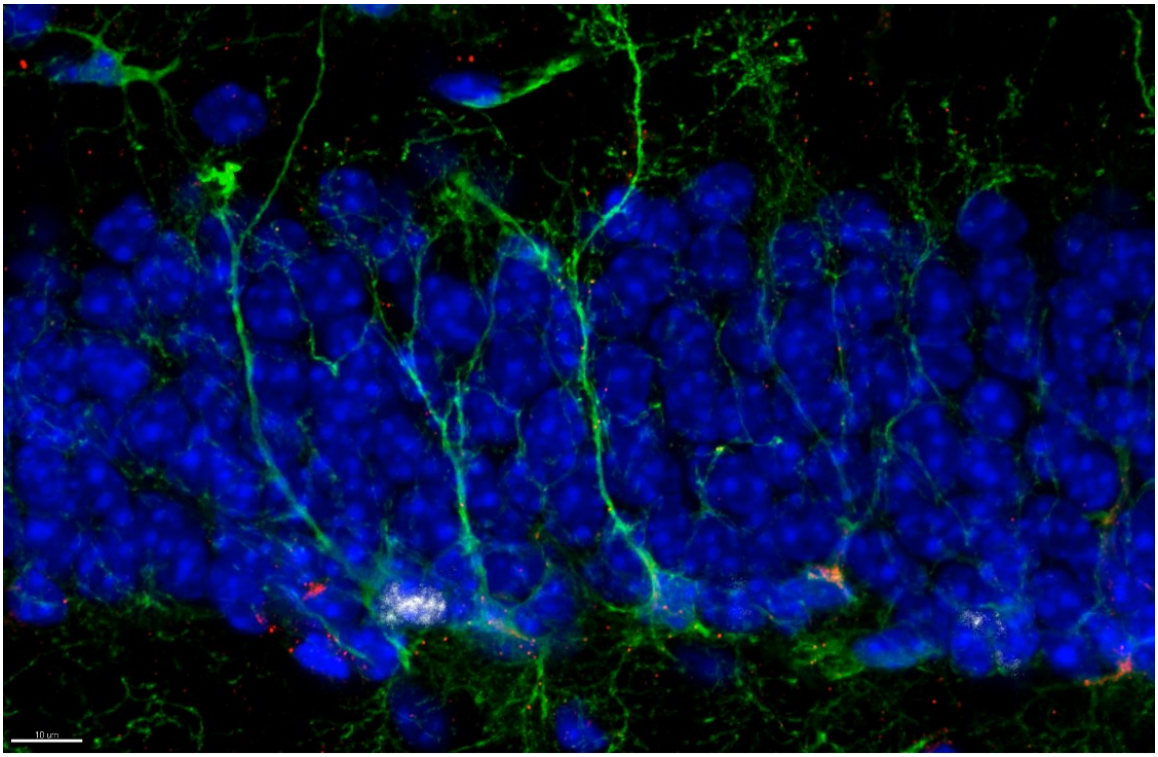
10 um

3.3.2 *Mfge8* deletion leads to reduced adult hippocampal neurogenesis

To explore the potential function of Mfge8 in the adult hippocampal neurogenesis, we first examined *Mfge8* homozygous germline knockout mice (KO) and their wild-type (WT) littermates (Hanayama et al., 2004). We injected bromodeoxyuridine (BrdU) into P60 mice and collected tissue 2 hours later (**Figure 3A**). Quantification showed reduced densities of $BrdU^+Nestin^+GFAP^+$ RGLs, $BrdU^+Tbr2^+$ IPCs, and $BrdU^+DCX^+$ neuroblasts (NBs) in KO mice compared to WT littermates (**Figure 3B-C**). We also examined proliferating cells independent of BrdU labeling with Mcm2 immunostaining and found similar results (**Figure 3D-E**). To examine the production of adult-born neurons, we injected P60 animals with BrdU five times at 12-hour intervals, and collected tissue 30 days later (**Figure 3F**). We found a significant decrease in the density of $BrdU^+NeuN^+$ adult-born neurons in KO (**Figure 3G-H**). Together, these results showed that Mfge8 is required to maintain a proper level of adult hippocampal neurogenesis.

Given that Mfge8 is expressed by both RGLs and astrocytes in the adult dentate gyrus, we next examined the specific contribution of Mfge8 from RGLs on adult neurogenesis. We generated the *Gli-CreER^{T2}::mT/mG$^{f/+}$::Mfge8$^{f/f}$* (cKO) model by crossing *Mfge8$^{f/f}$* conditional allele with the *Gli1-CreER^{T2}* driver, which specifically targets RGLs within the adult mouse dentate gyrus (Ahn and Joyner, 2005; Sun et al., 2015a), and with an *mT/mG$^{f/+}$* reporter (Muzumdar et al., 2007). We injected P60 mice with multiple doses of tamoxifen for analysis 30 days later (**Figure 3I**). Quantification showed a significant decrease in the density of GFP^+ RGLs in the adult SGZ (**Figure 3J-K**). In parallel, we observed a decrease in the number of GFP^+ neuronal progeny, but an increase in GFP^+ astrocytes (**Figure 3K**). These results suggest that adult RGL-derived

Mfge8 is required to maintain proper RGL numbers and adult neurogenesis levels, and to prevent RGL depletion via differentiation into astrocytes.

Figure 3. *Mfge8* deletion leads to decreased adult hippocampal neurogenesis.

(**A-E**) Reduced densities of proliferating RGLs, IPCs, and neuroblasts (NBs) in the dentate gyrus of P60 *Mfge8* KO mice. Shown in (**A**) is a schematic diagram of experimental design of a 2-hour BrdU pulse-chase in P60 mice. Also shown are sample confocal images (**B, D**) and quantification (**C, E**) of $Nestin^+GFAP^+$ RGLs, $Tbr2^+$ IPCs, and DCX^+ NBs that are $BrdU^+$ or $Mcm2^+$. Arrows point to $BrdU^+$ or $Mcm2^+$ $marker^+$ cells. Scale bars: 10 μm. Values represent mean ± SEM (n = 5 for **C** and **E**; ** $P < 0.001$; * $P < 0.01$; unpaired Student's t-test).

(F-H) Reduced generation of adult-born neurons in the dentate gyrus of *Mfge8* KO mice. Shown in (**F**) is a schematic diagram of the experimental design of 30 day BrdU pulse-chase in P60 mice. Also shown are sample confocal images (**G**) and quantification (**H**) of adult-born $BrdU^+NeuN^+$ dentate granule neurons. Scale bar: 10 μm. Values represent mean ± SEM (n = 5; ** $P < 0.001$; unpaired Student's t-test).

(**I-K**) Reduced RGL maintenance and neurogenesis, but increased astrocyte production upon conditional *Mfge8* deletion specifically in adult RGLs. Shown in (**I**) is a schematic diagram of experimental design of 30-day chase post tamoxifen induction of P60 mice. Also shown are sample confocal images (**J**) and quantification of composition of GFP^+ cells in the dentate gyrus 1 month after induction (**K**). Scale bar: 10 μm. Values represent mean ± SEM (n = 5; ** $P < 0.001$; unpaired Student's t-test). IN: immature neuron; N: mature neuron; A: astrocyte.

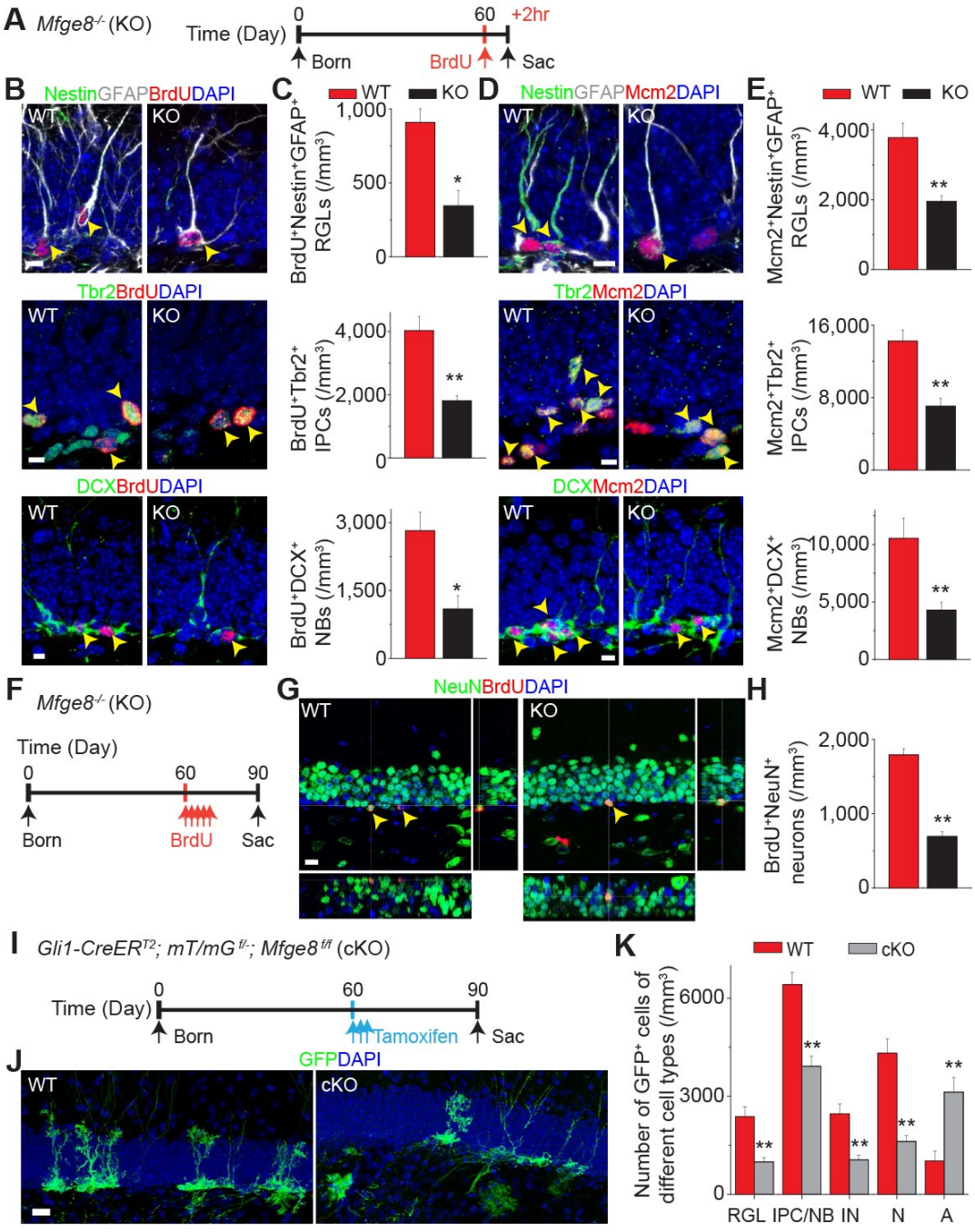
A Mfge8-/- (KO)
Time (Day)
0
60
+2hr
Born
BrdU
Sac
B NestinGFAPBrdUDAPI
C
WT
KO
BrdU+Nestin+GFAP+ RGLs (/mm3)
1,000
500
0
*
D NestinGFAPMcm2DAPI
E
Mcm2+Nestin+GFAP+ RGLs (/mm3)
4,000
2,000
0
**
Tbr2BrdUDAPI
BrdU+Tbr2+ IPCs (/mm3)
4,000
2,000
Tbr2Mcm2DAPI
Mcm2+Tbr2+ IPCs (/mm3)
16,000
8,000
DCXBrdUDAPI
BrdU+DCX+ NBs (/mm3)
3,000
1,500
DCXMcm2DAPI
Mcm2+DCX+ NBs (/mm3)
10,000
5,000
F Mfge8-/- (KO)
Time (Day)
90
Born
BrdU
Sac
G NeuNBrdUDAPI
H
BrdU+NeuN+ neurons (/mm3)
2,000
1,000
I Gli1-CreERT2; mT/mGf/-; Mfge8f/f (cKO)
Tamoxifen
J GFPDAPI
cKO
K
Number of GFP+ cells of different cell types (/mm3)
6000
3000
RGL
IPC/NB
IN
N
A

3.3.3 Mfge8 suppresses RGL proliferation in the adult and early postnatal dentate gyrus

Previous studies have shown that activation of quiescent RGLs can lead to their depletion via differentiation into astrocytes in the adult SGZ (Bonaguidi et al., 2011; Encinas et al., 2011). To determine whether RGLs were overactivated, we performed short-term fate-mapping upon adult RGL-specific *Mfge8* deletion. We injected tamoxifen into P60 cKO mice and analyzed 3 days later (**Figure 4A**). Quantification of $Mcm2^+$ GFP^+ RGLs among all GFP^+ RGLs showed a significant increase in cKO compared to control mice (**Figure 4B-C**). Thus, Mfge8 functions to promote RGL quiescence in the adult dentate gyrus.

This result of increased RGL activation from adult RGL-specific cKO is in contrast to the finding of decreased density of dividing RGLs in the adult SGZ of germline KO mice (**Figure 3B-E**). One possibility is that the loss of Mfge8 leads to premature activation and depletion of RGLs during early postnatal development, resulting in a decreased total number of RGLs, which in turn leads to a reduced number of proliferating RGLs and decreased level of adult dentate neurogenesis (**Figure 5A**).

We directly tested this model by analyzing early postnatal dentate neurogenesis. Immunohistological analyses showed that Mfge8 was expressed in most $Mcm2^-$ quiescent RGLs from P3 to adult (**Figure 5B**). To examine the impact of *Mfge8* deletion on postnatal dentate neurogenesis, we pulsed WT and KO mice at P15 with BrdU and analyzed 2 hours later (**Figure 4D**). Quantification showed significantly increased densities of $BrdU^+Nestin^+GFAP^+$ RGLs, $BrdU^+Tbr2^+$ IPCs, and $BrdU^+DCX^+$ NBs in KO mice compared to WT littermates (**Figure 4E-F**). Analysis of proliferating cells based on

Mcm2 expression showed similar results (**Figure 4G-H**). To examine the long-term consequences, we pulsed animals with multiple BrdU injections at P15 and examined 30 days later (**Figure 4I**). Consistent with increased RGL activation and increased numbers of IPCs and NBs at P15, we found an increased density of $BrdU^+NeuN^+$ mature neurons in KO (**Figure 4J-K**). Importantly, the density of $BrdU^+Nestin^+GFAP^+$ labeling-retaining RGLs was significantly reduced in KO mice (**Figure 4L-M**), indicating a reduced pool of adult RGLs in the absence of Mfge8. Similarly, conditional deletion of *Mfge8* with *Gli-CreER*^{T2} at P15 led to a reduced number of GFP^+ RGLs examined 30 days later (**Figure 4N-O**). At the population level, we observed a slight increase of $Nestin^+GFAP^+$ RGLs and significant increase of $Tbr2^+$ IPCs, and $BrdU^+$ or $Mcm2^+$ proliferating progenitors at P15 in KO, in contrast to significant decreases in these cell populations at P60 (**Figure 5D-F**).

Together, these results support the model that RGL-derived Mfge8 promotes RGL quiescence and maintenance in early postnatal stages to sustain a proper level of dentate neurogenesis into adulthood.

Figure 4. Mfge8 suppresses RGL activation and prevents developmental exhaustion of RGLs in the dentate gyrus.

(**A-C**) Conditional deletion of *Mfge8* in adult RGLs leads to their activation. Shown in (**A**) is a schematic diagram of experimental design. Shown in (**B**) are sample confocal images. Arrowhead points to a $Mcm2^+GFP^+$ RGL. Scale bar: 10 μm. Shown in (**C**) are quantifications. Values represent mean ± SEM (n = 4; ** $P < 0.001$; unpaired Student's t-test).

(**D-H**) Lack of *Mfge8* leads to an increased number of proliferating RGLs, IPCs and NBs in P15 dentate gyrus. Shown in (**D**) is a schematic diagram of experimental design of a 2-hour BrdU pulse-chase in P15 mice. Also shown are sample confocal images (**E, G**) and quantifications (**F, H**) of $Nestin^+GFAP^+$ RGLs, $Tbr2^+$ IPCs, and DCX^+ NBs that are $BrdU^+$or $Mcm2^+$. Scale bars: 10 μm. Arrowheads point to $BrdU^+$ or $Mcm2^+$ and $marker^+$ cells. Values represent mean ± SEM (n = 4 for **E** and **H**; * $P < 0.01$; unpaired Student's t-test).

(**I-M**) Loss of Mfge8 leads to increased neurogenesis in early postnatal dentate gyrus, but reduced number of RGLs in the adult dentate gyrus. Shown in (**I**) is a schematic diagram of the experimental design of 30 day BrdU pulse-chase in P15 mice. Also shown are sample confocal images (**J, L**) and quantification of $BrdU^+NeuN^+$ early postnatally born granule neurons (**K**) and $BrdU^+Nestin^+GFAP^+$ label-retaining RGLs (**M**) 30 days after BrdU injection. Yellow arrows point to $BrdU^+NeuN^+$ neurons (**J**) or $BrdU^+Nestin^+GFAP^+$ label-retaining RGL (**L**). An orange arrowhead points to a $BrdU^+Nestin^-GFAP^-$ cell (**L**). Scale bars: 10 μm. Values represent mean ± SEM (n = 5 for **K** and **M**; * $P < 0.01$; ** $P < 0.001$; unpaired student's t-test).

(**N-O**) Conditional deletion of *Mfge8* in RGLs at P15 leads to a decreased number of RGLs at P45. Shown are a schematic diagram of experimental design (**N**) and quantification (**O**). Values represent mean ± SEM (n = 4; * $P < 0.01$; unpaired Student's t-test).

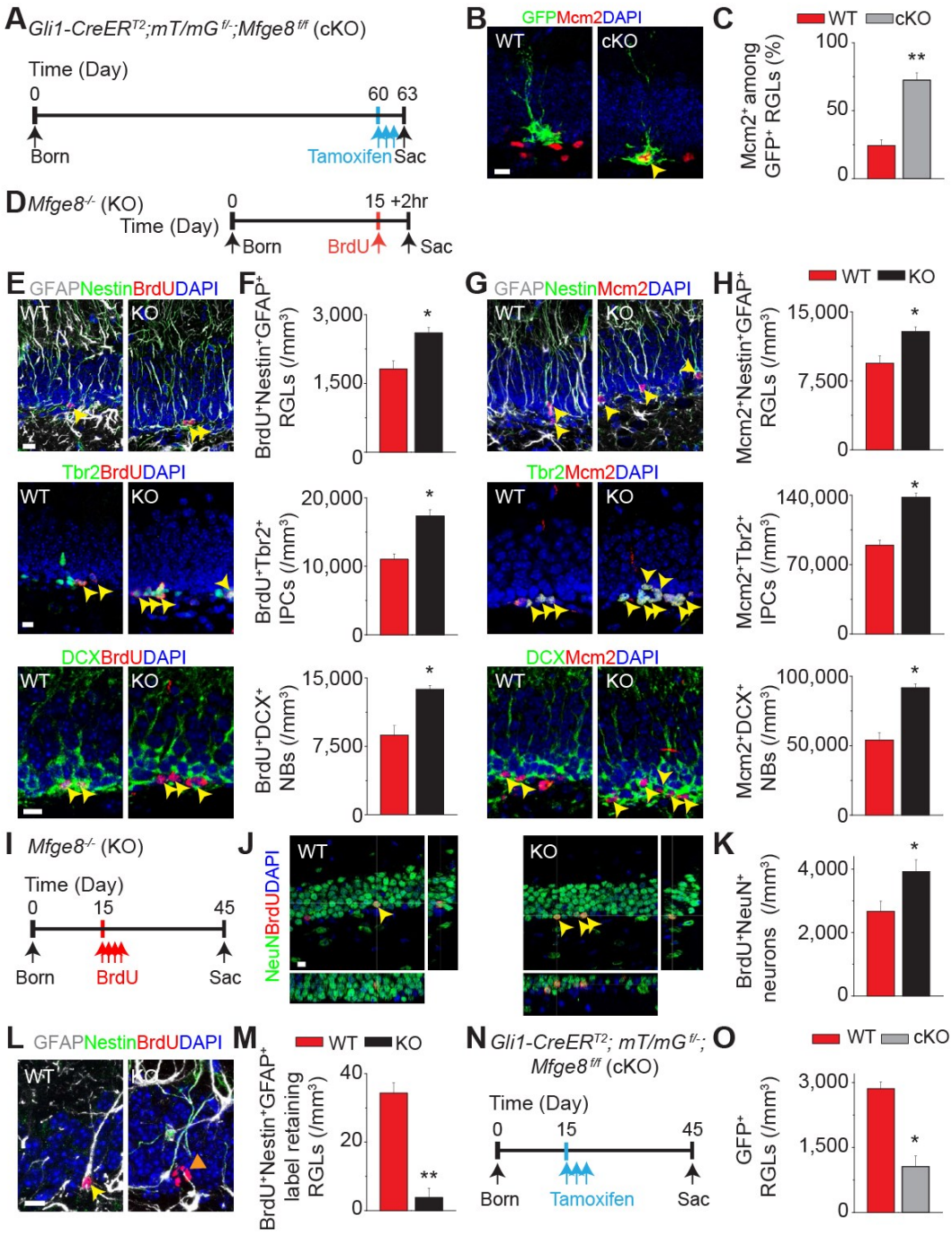
A Gli1-CreER^T2;mT/mG^f/-;Mfge8^f/f (cKO)
Time (Day)
0
60 63
Born
Tamoxifen
Sac
B
GFPMcm2DAPI
WT
cKO
C
WT
cKO
Mcm2+ among GFP+ RGLs (%)
100
50
0
**
D Mfge8-/- (KO)
Time (Day)
0
15 +2hr
Born
BrdU
Sac
E GFAPNestinBrdUDAPI
WT
KO
F
BrdU+Nestin+GFAP+ RGLs (/mm3)
3,000
1,500
0
*
Tbr2BrdUDAPI
BrdU+Tbr2+ IPCs (/mm3)
20,000
10,000
DCXBrdUDAPI
BrdU+DCX+ NBs (/mm3)
15,000
7,500
G GFAPNestinMcm2DAPI
H
Mcm2+Nestin+GFAP+ RGLs (/mm3)
15,000
7,500
Tbr2Mcm2DAPI
Mcm2+Tbr2+ IPCs (/mm3)
140,000
70,000
DCXMcm2DAPI
Mcm2+DCX+ NBs (/mm3)
100,000
50,000
I Mfge8-/- (KO)
Time (Day)
0
15
45
Born
BrdU
Sac
J
NeuNBrdUDAPI
K
BrdU+NeuN+ neurons (/mm3)
4,000
2,000
L GFAPNestinBrdUDAPI
M
BrdU+Nestin+GFAP+ label retaining RGLs (/mm3)
40
20
**
N Gli1-CreER^T2; mT/mG^f/-; Mfge8^f/f (cKO)
Time (Day)
0
15
45
Born
Tamoxifen
Sac
O
GFP+ RGLs (/mm3)
3,000
1,500

Figure 5. Expression of Mfge8 in the early postnatal dentate gyrus.

(**A**) A working model on the role of Mfge8 in suppressing RGL over-activation and depletion during development to maintain the adult neural stem cell pool in the dentate gyrus.

(**B**) Mfge8 is enriched in quiescent RGLs during postnatal development. Shown are sample confocal images (left panel; Scale bar: 10 μm) and quantification (right panel) of the percentage of $Mfge8^+$ cells among $Mcm2^-$Nestin-GFP^+ quiescent RGLs at P3, P7, P15, and P60. Yellow arrowheads point to $Mfge8^+Mcm2^-$ RGLs and orange arrows point to an $Mfge8^-Mcm2^+$ RGL. Values represent mean ± SEM (n = 3 mice).

(**C**) Sample confocal images of $S100\beta^+$ astrocytes in the developing dentate gyrus. Scale bar: 10 μm. Note the sparse presence of astrocytes in early postnatal dentate gyrus.

(**D-F**) Neurogenesis is transiently increased in the early postnatal dentate gyrus, but reduced in adult in *Mfge8* KO mice. Shown are quantifications of total numbers of $Nestin^+GFAP^+$ RGLs (**D**), $Tbr2^+$ IPCs (**E**), and $BrdU^+$ or $Mcm2^+$ proliferating cells (**F**) in KO and WT littermates at P15 and P60. BrdU injection paradigm at P15 and P60 follows **Figure 4D** and **3A**, respectively. Values represent mean ± SEM (n = 4; * $P < 0.05$; ** $P < 0.01$; unpaired student's t-test).

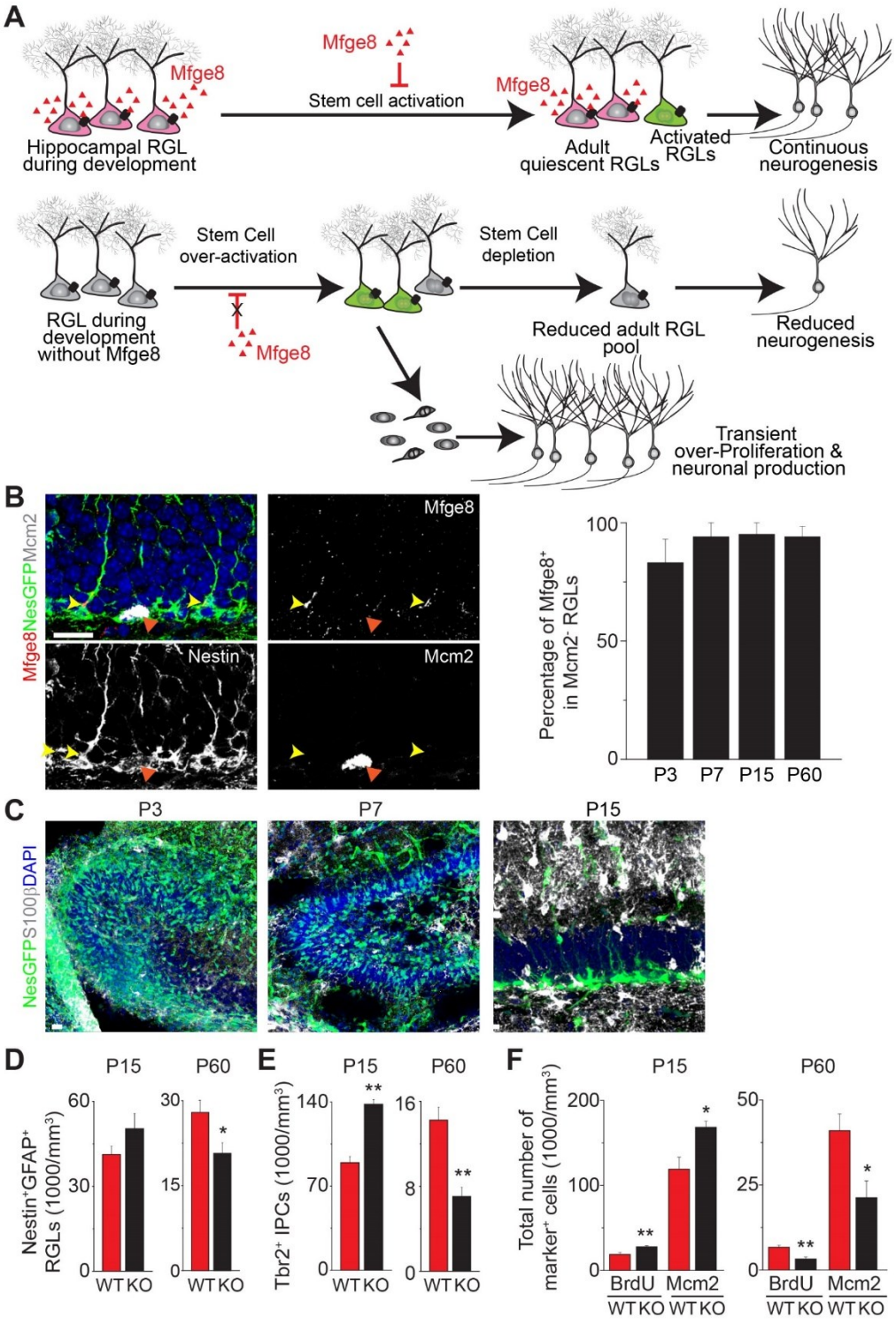
A
Mfge8
Hippocampal RGL during development
Mfge8
Stem cell activation
Mfge8
Adult quiescent RGLs
Activated RGLs
Continuous neurogenesis
Stem Cell over-activation
RGL during development without Mfge8
Mfge8
Stem Cell depletion
Reduced adult RGL pool
Reduced neurogenesis
Transient over-Proliferation & neuronal production
B
Mfge8NesGFPMcm2
Mfge8
Nestin
Mcm2
Percentage of Mfge8+ in Mcm2- RGLs
100
50
0
P3
P7
P15
P60
C
P3
P7
P15
NesGFPS100βDAPI
D
P15
P60
Nestin+GFAP+ RGLs (1000/mm3)
60
30
0
30
15
0
WT KO
WT KO
*
E
P15
P60
Tbr2+ IPCs (1000/mm3)
140
70
0
16
8
0
WT KO
WT KO
**
**
F
P15
P60
Total number of marker+ cells (1000/mm3)
200
100
0
50
25
0
BrdU
Mcm2
BrdU
Mcm2
WT KO
WT KO
WT KO
WT KO
**
*
**
*

3.3.4 Mfge8 promotes RGL quiescence via suppression of mTOR1 pathway

We next examined the mechanism by which Mfge8 maintains RGL quiescence. Integrin $\alpha_v\beta_{3/5}$ is the best known Mfge8 receptor for phagocytosis (Nagata et al., 2010) (**Figure 6A**). However, immunohistological analysis showed that integrin β_5 does not appear to be expressed by RGLs, but instead is co-localized almost exclusively with Iba1$^+$ microglia in the adult dentate gyrus (**Figure 6B, D**). This result raised the question of whether Mfge8-dependent regulation of RGLs involves microglia. Quantitative analyses showed no detectable differences in the densities of Iba1$^+$Itgb5$^+$ microglia or Iba1$^+$CD68$^+$ activated microglia (Mosher et al., 2012) between the WT and KO adult dentate gyrus (**Figure 6D-E**). Thus, microglia activity does not appear to be affected by the loss of Mfge8 in the dentate gyrus.

Integrin receptor $\alpha_8\beta_1$ was recently identified as a non-canonical Mfge8 receptor in regulating gastrointestinal motility (**Figure 6A**) (Khalifeh-Soltani et al., 2016). Integrin β_1 is known to be expressed in neural progenitor cells in the adult SVZ and SGZ (Brooker et al., 2016; Shen et al., 2008). Indeed, immunohistological analysis showed expression of both integrin α_8 and β_1 by Nestin-GFP$^+$ RGLs in the P15 and adult dentate gyrus (**Figure 7A** and **6C**). We next used an in vitro adult neural progenitor cell culture model (Ma et al., 2008) to examine the role of integrin β_1 in regulating neural stem cell proliferation. We first confirmed that Mfge8 protein is released into the culture medium by adult neural progenitors (**Figure 7B**). Addition of recombinant Mfge8 protein reduced proliferation of adult neural progenitors (**Figure 7C-E and 6F**). Importantly, addition of functional blocking antibodies for integrin β_1 (Goh et al., 2008), but not integrinα_v,

abolished the effect of Mfge8 on suppression of adult neural progenitor proliferation (**Figure 7C-E**).

Previous studies in the gastrointestinal system have shown that Mfge8 can either upregulate (Khalifeh-Soltani et al., 2014) or downregulate (Khalifeh-Soltani et al., 2016) the intracellular PTEN-PI3K-Akt pathway by binding to integrin receptors $\alpha_v\beta_{3/5}$ or $\alpha_8\beta_1$, respectively (**Figure 6A**). One major target of the PTEN-Akt pathway is mTOR1, which is known to be required for neural stem cell proliferation (Ka et al., 2014; Sato et al., 2010). We found that in cultured adult neural progenitors exogenous Mfge8 reduced levels of phosphorylated AKT (pAKT), phosphorylated 4EBP1 protein (p4EBP1), and phosphorylated S6 protein (pS6) (**Figure 7F-G**), which have commonly been used to monitor Akt-mTOR1 activation (Shaw et al., 2004; Xu et al., 2011). Such effects were blocked by anti-integrin β_1 antibodies, but not by anti-α_v antibodies (**Figure 7F-G**). Immunohistological analyses also showed a significant increase in densities of p4EBP1$^+$ and pS6$^+$ GFAP$^+$ RGLs in KO mice compared to WT littermates at P15 (**Figure 7G-H**) and in the cKO model in the adult dentate gyrus (**Figure 6G-H**), indicating in vivo elevated levels of mTOR1 activity in RGLs upon loss of *Mfge8*. Together, these results suggest that Mfge8 serves as a suppressor of mTOR1 activation in neural stem cells (**Figure 8A**).

To assess the functional role of the mTOR1 pathway in Mfge8-dependent regulation of RGL quiescence, we pharmacologically inhibited mTOR1 activation with rapamycin injections at P11 and P13 and performed analysis at P15 (**Figure 7I**). Immunohistological analysis confirmed the effectiveness of rapamycin treatment on reducing p4EBP1 and pS6 expression (**Figure 8B-C**). Quantification of Mcm2$^+$

Nestin^{+}GFAP^{+} RGLs in the dentate gyrus showed that, while rapamycin had no effect on WT animals, it completely abolished elevated RGL activation in *Mfge8* KO mice (**Figure 7J**). Similarly, rapamycin treatment abolished *Mfge8*-deletion induced adult RGL activation in the cKO model (**Figure 8D-F**).

Figure 6. Potential signaling mechanism by Mfge8.

(**A**) A schematic diagram showing that Mfge8 can either upregulate (Khalifeh-Soltani et al., 2014) or downregulate (Khalifeh-Soltani et al., 2016) the intracellular PTEN-PI3K-Akt pathway by binding to integrin receptors $\alpha_v\beta_{3/5}$ or $\alpha_8\beta_1$, respectively.

(**B-C**) Expression of Mfge8 receptor integrin β_5, β_1 and α_5 in the adult dentate gyrus. Shown are sample confocal images of immunostaining for integrin β_5 (**B**) and β_1 and α_8 (**C**). Scale bars: 10 μm. Note the expression of $\alpha_8\beta_1$, but not β_5, in Nestin-GFP$^+$ RGLs.

(**D-E**) Loss of Mfge8 does not appear to affect microglia in the adult dentate gyrus. Shown are sample confocal images and quantification of Iba1$^+$Itgb5$^+$ microglia (**D**) and Iba1$^+$CD68$^+$ activated microglia (**E**) in *Mfge8* KO and WT littermates. Scale bars: 100 μm (left panels) and 10 μm (inserts; right three panels).Values represent mean ± SEM (n = 3 mice).

(**F**) Adult mouse neural progenitor proliferation was suppressed by exogenous recombinant Mfge8 in a dose-dependent manner. Neural progenitor cells were cultured in the presence of different doses of exogenous Mfge8 or IgG control for 2 days before a 40-min EdU chase. Shown is quantification of EdU$^+$Nestin$^+$ proliferating cells among all Nestin$^+$ cells. Values represent mean ± SEM (n = 4; * $P < 0.05$; ** $P < 0.01$; one-way ANOVA).

(**G-H**) Increased mTOR1 signaling in RGLs in conditional *Mfge8* knockout mice. Shown are a schematic diagram of the experimental design (**G**) and quantifications (**H**) of the number of p4EBP1$^+$ or pS6$^+$ and GFAP$^+$GFP$^+$ RGLs 3 days after tamoxifen induction. Values represent mean ± SEM (n = 4; * $P < 0.05$; unpaired student's t-test).

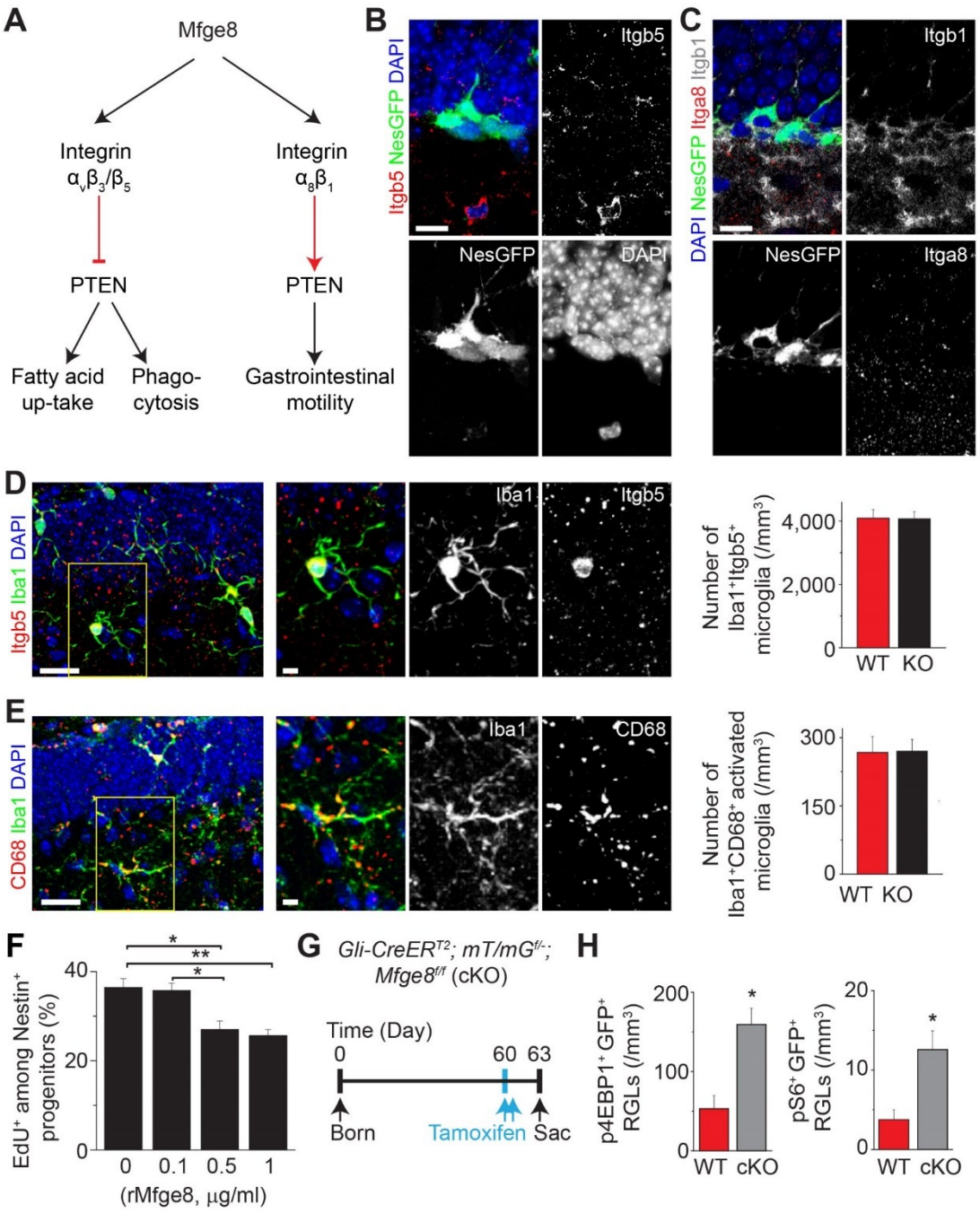
A
Mfge8
Integrin $\alpha_v\beta_3/\beta_5$
Integrin $\alpha_8\beta_1$
PTEN
PTEN
Fatty acid up-take
Phago-cytosis
Gastrointestinal motility
B
Itgb5 NesGFP DAPI
Itgb5
NesGFP
DAPI
C
DAPI NesGFP Itga8 Itgb1
Itgb1
NesGFP
Itga8
D
Itgb5 Iba1 DAPI
Iba1
Itgb5
Number of Iba1+Itgb5+ microglia (/mm3)
4,000
2,000
0
WT KO
E
CD68 Iba1 DAPI
Iba1
CD68
Number of Iba1+CD68+ activated microglia (/mm3)
300
150
0
WT KO
F
EdU+ among Nestin+ progenitors (%)
40
20
0
0 0.1 0.5 1
(rMfge8, μg/ml)
G
Gli-CreER^{T2}; mT/mG$^{f/-}$; Mfge8$^{f/f}$ (cKO)
Time (Day)
0
60 63
Born
Tamoxifen
Sac
H
p4EBP1+ GFP+ RGLs (/mm3)
200
100
0
WT cKO
pS6+ GFP+ RGLs (/mm3)
20
10
0
WT cKO

Figure 7. Mfge8 promotes RGL quiescence by suppressing mTOR1 signaling.

(**A**) Sample confocal images of immunostaining for Mfge8, integrin receptor $\alpha_8\beta_1$ in Nestin-GFP$^+$ RGLs in the P15 dentate gyrus. Scale bar: 10 μm.

(**B**) Release of Mfge8 protein into the culture medium of adult neural progenitors. Shown is a sample Western blot of concentrated culture medium (10x, 5x) and whole cell lysate.

(**C-E**) Mfge8 suppresses proliferation of adult neural progenitors. Shown are a schematic diagram of the experimental design (**C**), sample confocal images (**D**; scale bar: 20 μm) and quantifications (**E**) of adult mouse dentate gyrus-derived neural progenitors cultured in the presence or absence of rMfge8 (0.5 μg/ml), anti-α_v integrin antibodies (av; 0.625 μg/ml), or anti-β_1 integrin antibodies (b1; 0.625 μg/ml). Values represent mean ± SEM (n = 4; ** $P < 0.001$; * $P < 0.01$; n.s.: not significant; one-way ANOVA).

(**F**) Mfge8 suppresses mTOR1 signaling in adult neural progenitors. Adult neural progenitors were similarly treated as in (**C**) and then subject to Western blot analysis. Shown are sample Western blot images (top panels) and quantifications (bottom panel). Values represent mean ± SEM (n = 4; ** $P < 0.001$; * $P < 0.01$; one-way ANOVA).

(**G-H**) Increased mTOR1 signaling in RGLs in *Mfge8* KO mice. Shown are sample confocal images and quantifications of numbers of p4EBP1$^+$ (**G**) and pS6$^+$ (**H**) Nestin$^+$GFAP$^+$ RGLs in P15 mice. Arrowheads point to p4EBP1$^+$ or pS6$^+$ Nestin$^+$GFAP$^+$ RGLs. Scale bar: 10 μm. Values represent mean ± SEM (n = 4; * $P < 0.01$; unpaired Student's t-test).

(**I-J**) Rapamycin treatment rescues RGL overactivation in the P15 dentate gyrus of *Mfge8* KO mice. Shown in (**I**) is a schematic diagram of the experimental design. Rapamycin (20 mg/kg body weight) or vehicle was i.p. injected. Shown in (**J**) is the quantification of

$BrdU^+Nestin^+GFAP^+$ RGLs. Values represent mean ± SEM (n = 4; * $P < 0.01$; one-way ANOVA).

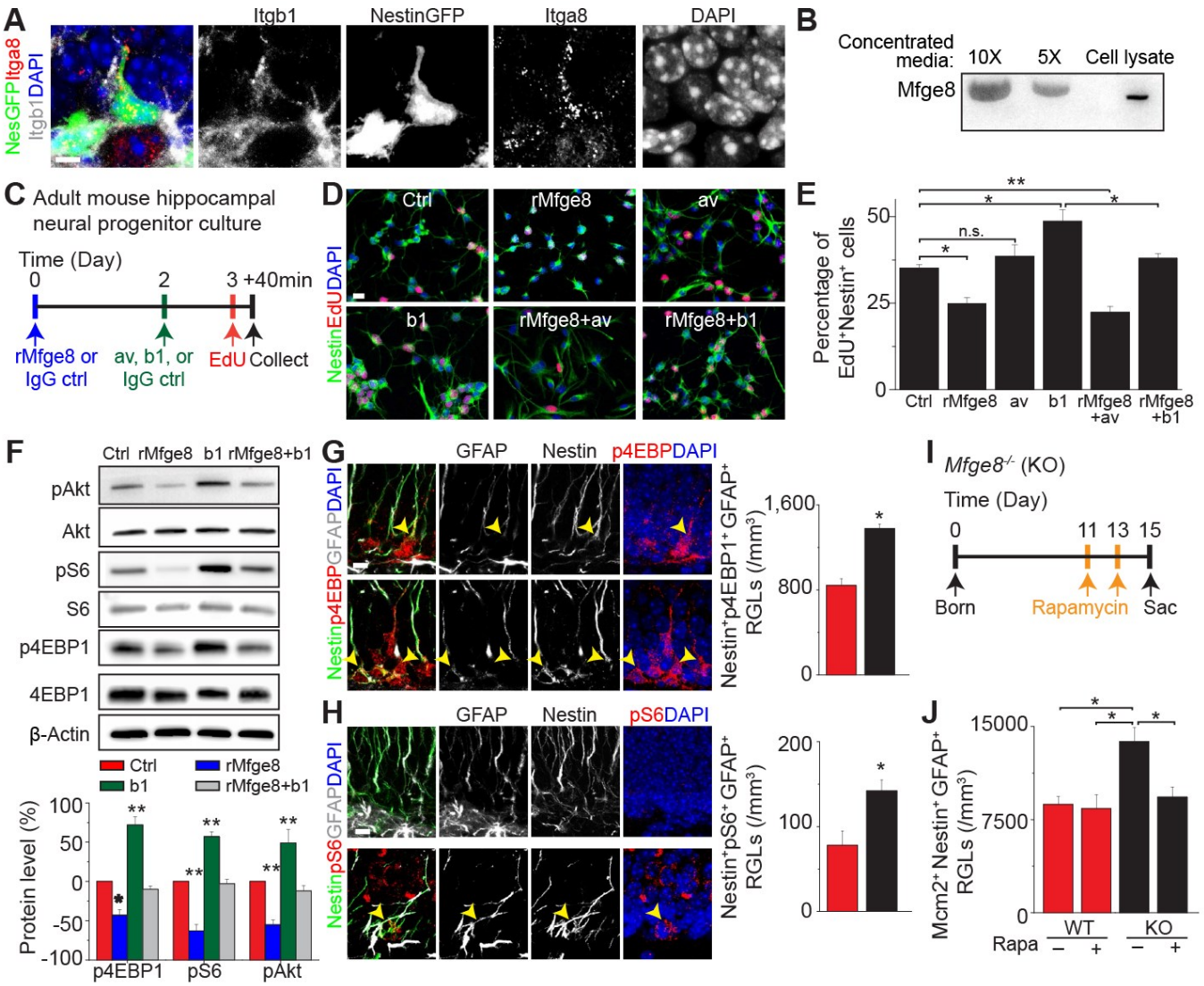
A
Itgb1
NestinGFP
Itga8
DAPI
NesGFPItga8
Itgb1DAPI
B
Concentrated media:
10X
5X
Cell lysate
Mfge8
C
Adult mouse hippocampal neural progenitor culture
Time (Day)
0
2
3 +40min
rMfge8 or IgG ctrl
av, b1, or IgG ctrl
EdU
Collect
D
Ctrl
rMfge8
av
b1
rMfge8+av
rMfge8+b1
NestinEdUDAPI
E
Percentage of EdU+Nestin+ cells
n.s.
Ctrl
rMfge8
av
b1
rMfge8 +av
rMfge8 +b1
F
Ctrl
rMfge8
b1
rMfge8+b1
pAkt
Akt
pS6
S6
p4EBP1
4EBP1
β-Actin
Protein level (%)
p4EBP1
pS6
pAkt
G
GFAP
Nestin
p4EBPDAPI
Nestinp4EBPGFAPDAPI
Nestin+p4EBP1+ GFAP+ RGLs (/mm3)
H
pS6DAPI
NestinpS6GFAPDAPI
Nestin+pS6+ GFAP+ RGLs (/mm3)
I
Mfge8-/- (KO)
Time (Day)
0
11
13
15
Born
Rapamycin
Sac
J
Mcm2+Nestin+GFAP+ RGLs (/mm3)
WT
KO
Rapa

Figure 8. Mfge8 promotes neural stem cell quiescence via suppression of mTOR1 pathway.

(**A**) A model of Mfge8 regulation of RGL quiescence by suppressing mTOR1 pathway. (**B-C**) Rapamycin, an mTOR1 inhibitor, effectively abolished mTOR1 activity in RGLs. Shown are sample confocal images (**B**) and quantification (**C**) of immunostaining for mTOR1 activation markers, p4EBP1 and pS6 in RGLs upon rapamycin treatment. Scale bar: 10 μm. Values represent mean ± SEM (n = 4; ** $P < 0.001$; one-way ANOVA). (**D-F**) Rapamycin treatment rescues RGL overactivation in the P15 dentate gyrus of *Mfge8* conditional knockout mice. Shown in (**D**) is a schematic diagram of the experimental design. Rapamycin (20 mg/kg body weight) or vehicle was i.p. injected after tamoxifen induction. Also shown are sample images (**E**) and quantification (**F**) of GFP^+Mcm2^+ $GFAP^+$ RGLs in cKO and controls. Values represent mean ± SEM (n = 4; ** $P < 0.01$; * $P < 0.05$; one-way ANOVA).

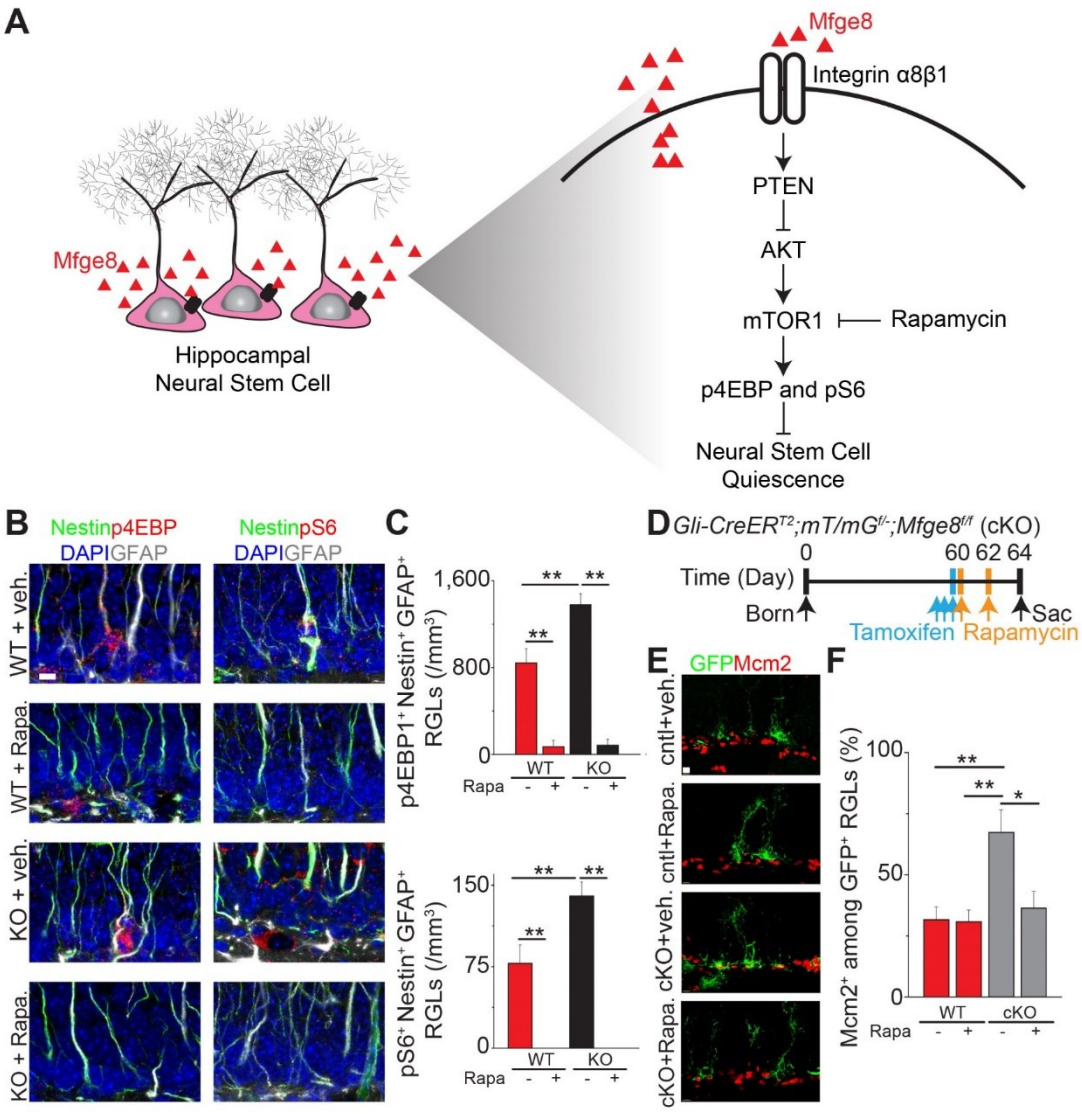
A
Mfge8
Integrin α8β1
PTEN
AKT
mTOR1
Rapamycin
p4EBP and pS6
Neural Stem Cell
Quiescence
Mfge8
Hippocampal
Neural Stem Cell
B
Nestinp4EBP
DAPIGFAP
NestinpS6
DAPIGFAP
WT + veh.
WT + Rapa.
KO + veh.
KO + Rapa.
C
p4EBP1+ Nestin+ GFAP+ RGLs (/mm3)
1,600
800
0
WT
KO
Rapa
pS6+ Nestin+ GFAP+ RGLs (/mm3)
150
75
0
D
Gli-CreER^T2;mT/mG^f/-;Mfge8^f/f (cKO)
Time (Day)
0
60 62 64
Born
Sac
Tamoxifen
Rapamycin
E
GFPMcm2
cntl+veh.
cntl+Rapa.
cKO+veh.
cKO+Rapa.
F
Mcm2+ among GFP+ RGLs (%)
100
50
0
WT
cKO
Rapa

3.4 Discussion

How the neural stem cell pool is maintained throughout early development to ensure a sufficient number of adult neural stem cells to support life-long neurogenesis is not well understood (Berg et al., 2018). Here we identified Mfge8 as a stem cell-enriched niche factor that maintains the adult neural stem cell pool during early postnatal development and in adulthood by promoting RGL quiescence (**Figure 5A**). In addition to a large number of previously identified paracrine factors released by other niche cell types, our finding illustrates the complexity of neurogenesis regulation that is also modulated by a stem cell-derived factor *in vivo*. While Mfge8 is best known to mediate phagocytosis, here we identified a non-canonical role of Mfge8 signaling in maintaining neural stem cell quiescence by suppressing mTOR1 activation (**Figure 8A**). Interestingly, recent transcriptome analyses have also found enrichment of Mfge8 in different stem cell populations, such as neural stem cells in the embryonic cortex (Pollen et al., 2015; Yuzwa et al., 2017; Zeisel et al., 2015), developing and adult dentate gyrus (Hochgerner et al., 2018), adult SVZ (Dulken et al., 2017), hair follicle stem cells (Lay et al., 2016), embryonic stem cells (Yan et al., 2013), and induced pluripotent stem cells (Asai et al., 2017), raising the possibility that Mfge8 may play a general role as an autocrine signal for various types of stem cells.

Mfge8 is traditionally known to be involved in phagocytosis by phagocytes and microglia (Raymond et al., 2009). In the adult dentate gyrus, however, Mfge8 is selectively expressed by quiescent RGLs and astrocytes, but not by RGL progeny or microglia. Through adult RGL-specific deletion, we provide evidence that the RGL population regulates its own quiescence and maintenance via Mfge8. One advantage of

autocrine regulation is the spatial proximity of signals for fine tuning of stem cell behavior. Given diffusion limits of secreted molecules in the adult mammalian brain, especially when their receptors are in proximity for efficient binding/trapping, the effect could be rather local. Astrocytes are known to modulate adult dentate neurogenesis via secreted factors (Lie et al., 2005; Song et al., 2002), it will be interesting to specifically examine whether astrocyte-derived Mfge8 also regulates RGL quiescence when genetic tools become available in the future. Since astrocytes are born during later postnatal stages (**Figure 5C**), it is likely that RGL-derived Mfge8 plays a more dominant role in regulating RGL quiescence during early postnatal development. Our study also identifies the signaling mechanism whereby Mfge8 promotes RGL quiescence (**Figure 8A**). Our results are consistent with previous findings that loss of integrin β_1 depletes RGLs, promotes astrocyte differentiation, and reduces neurogenesis in the adult dentate gyrus (Brooker et al., 2016). Notably, genetic deletion of *Ilk* (integrin-linked kinase) or *Pten* also leads to quiescent RGL activation in the adult dentate gyrus (Bonaguidi et al., 2011; Porcheri et al., 2014). Together, these findings identify the PTEN-Akt-mTOR1 pathway as a hub that integrates stem cell-activation signals to regulate RGL quiescence and maintenance.

How the adult neural stem cell pool is regulated during development is not well understood. Recent studies have suggested a critical role of quiescence in establishing the somatic stem cell pool during development. For example, the adult muscle stem cell pool is established during puberty by sex hormone-dependent regulation of Notch signaling that converts cycling juvenile stem cells to a quiescent stem cell population (Kim et al., 2016). For epidermal stem cells, NFATc1 (Horsley et al., 2008) and Lrig1 (Jensen et al.,

2009) play a critical role in governing the quiescence of a reservoir of stem cells throughout hair follicle morphogenesis, which is retained during adulthood. In the central nervous system, activation of the reserve neural stem cells during development by deletion of p57 or VCAM1 reduces their numbers in the adult SVZ (Furutachi et al., 2015; Hu et al., 2017). Similarly, deletion of FoxOs leads to increased early postnatal hippocampal neurogenesis, but reduced number of RGLs and decreased neurogenesis in the adult hippocampus (Paik et al., 2009; Renault et al., 2009), a phenotype very similar to Mfge8 KO mice. Our study identifies, for the first time, a niche mechanism that maintains neural stem cell quiescence to sustain neurogenesis in the adult hippocampus. Our finding also highlights the complexity of prospective regulatory mechanisms to maintain a viable stem cell pool over the lifespan, involving both paracrine and autocrine signaling from a stem cell-derived factor.

4 – Developing *ex vivo* live imaging technology to observe adult neural stem and progenitor cells at a single-cell resolution

4.1 Introduction

While the majority of neural stem cells (NSCs) stay quiescent most of the time, they are capable of both populating the developing and adult brain and repopulating injured or diseased brain through cell division. Once they enter cell cycle and become activated, they can choose between different modes of division (Gotz and Huttner, 2005). Asymmetric division is self-renewing and yields one more progenitor, while symmetric division yields either two NSCs (self-renewing) or two progenitors (not self-renewing). Progenitor cells, in contrast to NSCs, can only differentiate into one particular cell type (Morrison and Kimble, 2006). This ability, to simultaneously give rise to the differentiated progeny and to make more copies of themselves, is known to be the hallmark of stem cells. The balance between asymmetric or symmetric division are carefully regulated by both intrinsic signaling and environmental signals, which ensures the correct number of cells located in the neural stem cell pool (Knoblich, 2008). The existence and accurate proliferation control of adult NSCs raises hope for their potential in regenerative therapies for brain repair.

In the developing neocortex, NSCs primarily undergo symmetric divisions to expand stem-cell pools during embryonic development. In contrast, NSCs primarily use asymmetric divisions to expand differentiated cell numbers. Modes of division are regulated by niche signaling and is altered during diseases or injury conditions (Homem et al., 2015). It was shown that physiological injuries increase both the rate of cell division and the number of rounds of symmetric division, potentially to replace cells lost

through injury (Morrison and Kimble, 2006). However, how NSCs behave in the adult dentate gyrus of the hippocampus, where stem cells and neurogenesis persist in adulthood, remains not clear and has recently exerted attention from multiple groups (Barbosa et al., 2015; Pilz et al., 2018).

The dentate gyrus of the hippocampus in the mammalian brain is located tens or hundreds of millimeters from the brain surface, rendering it technically difficult for direct observations (Barbosa et al., 2015). *Ex vivo* acute slice live imaging, with easy access to the dentate gyrus, allows for the integrative view on the changes in the behavior of individual adult NSCs and their progeny (Khlghatyan and Saghatelyan, 2012). Here we developed real-time imaging methods to observe the dynamics of adult hippocampal NSCs and progeny.

4.2 Detailed Procedure

4.2.1 Pre-requisites for materials and recipes for aCSF

All glassware / spatulas used should have never ever come in contact with paraformaldehyde (PFA) or detergents. If ethanol is used to sterilize beakers or section holding chamber, be sure to evaporate all ethanol before using.

Artificial cerebrospinal fluid (aCSF) is made to mimic brain cerebrospinal fluid conditions *in vivo*. The composition is listed in **Table 2**, modified from Saghatelyan's group (Khlghatyan and Saghatelyan, 2012). Stock solutions for 10x aCSF/cutting solution, 1 M $MgCl_2$ solution, and 1 M $CaCl_2$ solution should be prepared according to **Table 3** and **Table 4**.

Chemical	**MW**	**Catalog**	**Company**	**Cutting solution (mM)**	**aCSF (mM)**
Sucrose	342.3	S1888	Sigma	210.3	--
D(+) glucose (dextrose)	180	G7528	Sigma	20	20
KCl	74.56	3040-01	J.T. Baker	3	3
NaCl	58.5	BP358-1	Fisher Science	--	125
$MgCl_2$	95.21	M8266	Sigma	3	1.3
$NaHCO_3$	84.01	S5761	Sigma	26	26
NaH_2PO_4	119.98	S8282	Sigma	1.25	1.25
$CaCl_2 \cdot 2H_2O$	147.01	C7902	Sigma	0.5	2

Table 2. The aCSF solution.

Modified from (Khlghatyan and Saghatelyan, 2012). MW: molecular weight

Chemical	MW	Catalog	Company	Molarity (mM)	10x, 1L (g)
KCl	74.56	3040-01	J.T. Baker	30	2.238
NaH_2PO_4	119.98	S8282	Sigma	12.5	1.4998
$NaHCO_3$	84.01	S5761	Sigma	260	21.840

Table 3. The 10x aCSF/cutting solution stock.

Modified from (Khlghatyan and Saghatelyan, 2012). Add reagents in the order listed above. Sterile filter the stock (Nalgene, 597-3320) and store at room temperature. In order to prevent precipitates or mold, sucrose, D(+) glucose (dextrose), NaCl, $MgCl_2 \cdot 6H_2O$, and $CaCl_2 \cdot 2H_2O$ should be freshly added when making the 1x aCSF/cutting solution.

Chemical	MW	Catalog	Company	Molarity (mM)	For 50ml stock (g)
$MgCl_2 \cdot 6H_2O$	203.31	M8266	Sigma	3	10.165
$CaCl_2 \cdot 2H_2O$	147.01	C7902	Sigma	0.5	7.350

Table 4. The 1 M $MgCl_2$ and $CaCl_2$ solution stock.

Modified from (Khlghatyan and Saghatelyan, 2012). Sterile filter the stock (Nalgene, 597-3320) and store at room temperature.

4.2.2 Make 1x aCSF solution

- Add ~700 ml ddH_2O into the 1 L glass beaker
- Place 3.602 g dextrose and 7.305 g NaCl
- Add 1.3 ml of 1 M $MgCl_2 \cdot 6H_2O$ stock and 2 ml of 1 M $CaCl_2 \cdot 2H_2O$ stock
- Add 100 ml of 10x aCSF/cutting solution stock
- Add ddH_2O up to 1L using a volumetric flask
- Measure and expect osmolality ~310 mOsm, using a osmometer (Precision Systems, μ OSMETTE 5002)
- Measure and expect pH ~7.6, using a pH meter (Thermo Scientific, Orion Star A211 pH Benchtop Meter)
- Oxygenate the solution with 95% O_2 / 5% CO_2 (carbogenated O_2) overnight
- Measure and adjust pH to ~7.4 after bubbling with carbogenated O_2, using a pH meter

We prepare 1 L 1x aCSF solution in a glass beaker designated solely for this purpose the day before the experiment. It is critical to follow the order of reagents added to avoid any precipitates. Tiring the solution with a stir bar can help completely dissolve solution.

4.2.3 Make 1x cutting solution

- Add ~150 ml ddH_2O into a 250 mL glass beaker
- Place 18 g sucrose and 0.901 g dextrose
- Add 750 µl of 1 M $MgCl_2 \cdot 6H_2O$ stock and 125 µl of 1 M $CaCl_2 \cdot 2H_2O$ stock
- Add 25 ml of 10x aCSF/cutting solution stock

- Add ddH_2O up to 250 ml using a volumetric flask
- Measure and expect osmolality ~310 mOsm, using a osmometer (Precision Systems, μ OSMETTE 5002)
- Measure and expect pH ~7.6, using a pH meter (Thermo Scientific, Orion Star A211 pH Benchtop Meter)
- Oxygenate the solution with 95% O_2 / 5% CO_2 till pH reaching ~7.4

We prepare 250 ml of 1x cutting solution on the day of the experiment.

4.2.4 Set up vibratome

- Turn on hot water bath to allow it to equilibrate to 32 °C
- Cap the cutting solution beaker with petri dish and place in –80 °C freezer for 30 min in order to partially freeze the solution
- Pour ~3 ml/well 1x aCSF solution into a 6-well plate (Corning 353046), which is submerged in 32 °C water bath
- Bubble with carbogenated O_2
- Add a cell strainer (BD falcon, ref 3352350) to hold brain slices
- Turn on vibratome (Leica, VT 1000S)
- Put the cutting chamber inside a stage mount
- Cover the cutting chamber with plastic chamber cap to prevent ice from getting in
- Surround and fill stage mount with ice
- Break the feather blade (TedPella imported; product #121-9) in half and attach it to the vibratome

- Mix the slushy cutting solution with a spatula

4.2.5 Capture dentate gyrus in a pseudo whole-mount view

The *Nestin-GFP* mice (Encinas et al., 2006) and the tamoxifen-inducible *Ascl1*^{CreERT2};*mTmG*$^{f/-}$ mice (Sun et al., 2015b) were used in this study. For the *Ascl1* mice, a dose of 375 mg/kg body weight tamoxifen was intraperitoneally injected into 15-day-old or 2-month-old male and female mice every 12 hours for 3 times, as previously described (Sun et al., 2015b). Mice were analyzed 3 or 5 days post-tamoxifen injection.

- Perfuse animal with cold cutting solution to clear out blood, as previously described (Khlghatyan and Saghatelyan, 2012; Sun et al., 2015b). Be aware that tools should never have contact with PFA
- Remove brain from skull and place into a petri dish containing 5 ml ice-cold cutting solution to half immerse the brain
- Cut off the cerebellum coronally; section the brain in half sagittally (**Figure 9**)

Ideally, the entire procedure, from getting the animal to starting imaging, should be completed within 30 min; the steps from vibratome sectioning the brain and on, should be completed within 10 min.

4.2.5.1 Capture posterior dentate gyrus

- Mount the brain midline-down and vibratome cut the brain sagittally (**Figure 9**)
- The ideal section with a big piece of dentate gyrus should appear in more lateral portions of the hippocampus

4.2.5.2 Capture anterior dentate gyrus

- In order to maximize the chance of getting as much anterior dentate gyrus in one section, for each hemisphere, trim the ventral side at an angle as depicted in **Figure 10**
- Cut off the anterior portion of brain coronally
- Mount ventral side of the brain down, with rostral side facing the blade

4.2.6 Section brain

- From this step on, brain sections should be protected from lights.
- Apply a drop of Vetbond (3M, sc-361931) to the vibratome stage in the area where the brain will be mounted
- Place the grossly-trimmed brain from **Section 4.2.5** into the drop of Vetbond, keeping medial side facing up
- Gently pipet the remaining cutting solution into the stage chamber, being very careful not to have ice fall on the tissue
- Vibratome cut sections at 250 μm. For every slice, use the blunt spatula end to help press against the blade and separate the tissue, as the blade nears the end of cutting the tissue
- Once the vibratome gets to the level where hippocampus can be visualized, start collecting sections with a blunt end transfer pipette into the cell strainer in the glass bubbling chamber
- Optional: tissue sections go directly from ice-cold to 32 °C, therefore, you may let sections rest for 30-60 min in the imaging chamber before imaging

Figure 9. Schematic representation of the preparation of acute live slices.

(**A**) Schematic representation of one caudal, one intra-hemispheric and two sagittal cuts. (**B**) Schematic representation of placing the mouse brain on the platform of the vibratome. (**C**) Schematic representation of acute slice incubation chamber. (**D**) Schematic representation of the imaging chamber.

Figure adapted from (Khlghatyan and Saghatelyan, 2012).

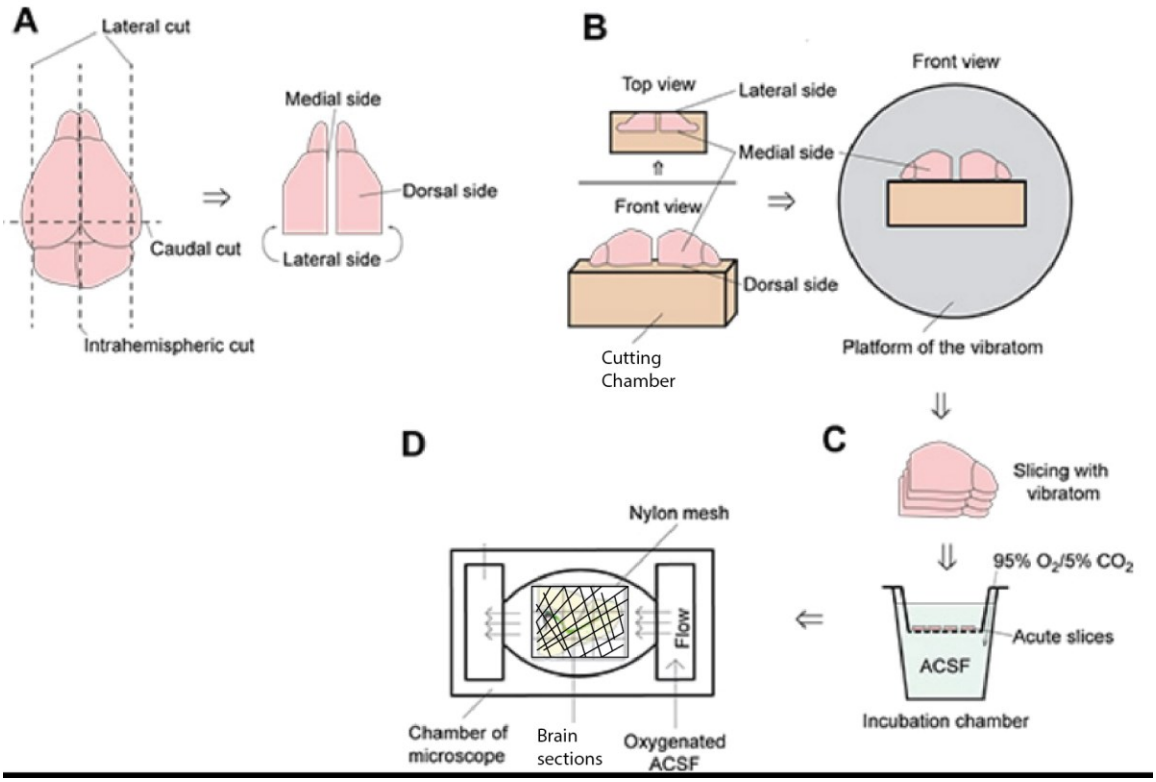
A
Lateral cut
Medial side
Dorsal side
Caudal cut
Lateral side
Intrahemispheric cut
B
Top view
Lateral side
Medial side
Front view
Front view
Dorsal side
Cutting
Chamber
Platform of the vibratom
C
Slicing with
vibratom
95% O2/5% CO2
Acute slices
ACSF
Incubation chamber
D
Nylon mesh
Flow
Chamber of
microscope
Brain
sections
Oxygenated
ACSF

Figure 10. Capture the anterior dentate gyrus of the hippocampus.

An illustration showing the angle and location (magenta line) to trim the brain before further vibratome-sectioning in order to capture as much dentate gyrus as possible in one section. See **Section 4.2.5.2** for details.

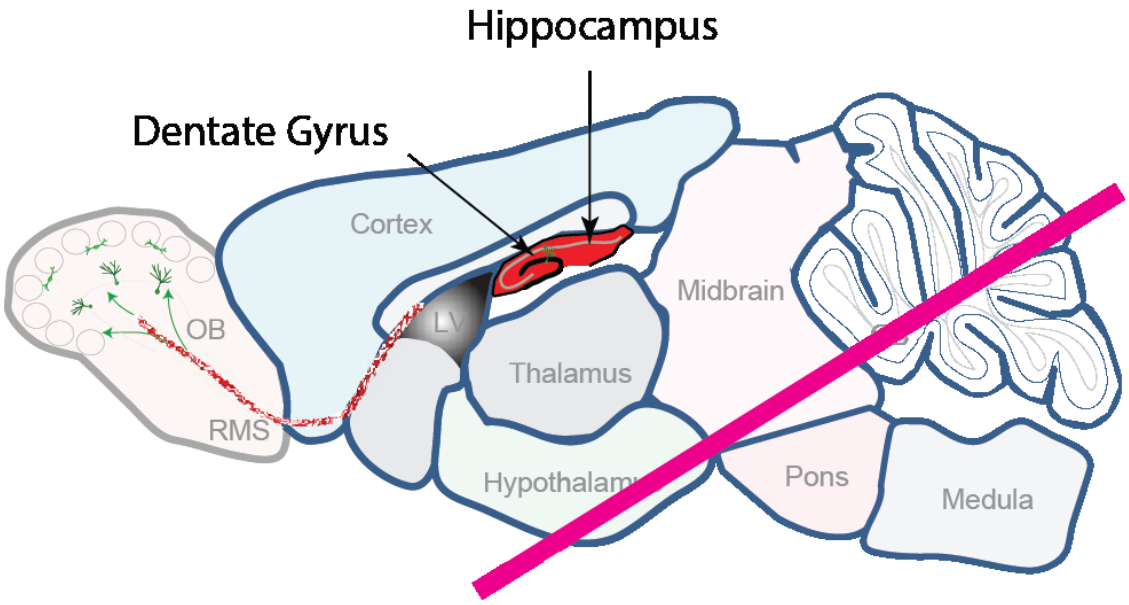
Hippocampus
Dentate Gyrus
Cortex
OB
RMS
LV
Thalamus
Midbrain
Pons
Medula

4.2.7 Imaging setup

- Turn on two-photon imaging system (Chameleon) 1-2 hours before the experiment to stabilize the system
- Turn on heated stage and adjust temperature to 32 °C (tempcontrol, 37-2 digital). 1-2 hours before the experiment to equilibrate the system
- Put on a 20x water immersion objective (Objective W Plan-Apochromat 20x/1.0 DIC M27 75mm; Zeiss 421452-9601-000). Lower the objective into POC-R chamber (Pecon) filled with aCSF solution
- Set up MasterFlex CL peristaltic pump (#EW-77122-22 or -26, ColeParmer) with two sets of Tygon R-3603 tubing (0.89 mm ID/2.82 mm OD; #EW-95609-26, ColeParmer), one entering, one leaving the POC-R chamber, to perfuse the imaging chamber with aCSF from the beaker in the water bath
- Transfer the brain sections from the 6-well plate to imaging chamber using a blunt-cut transfer pipette
- To avoid drifting of slice during imaging, stabilize it by carefully placing a nylon mesh (Warner Instruments) on top of the slice. The mesh is 0.12 mm thick and the openings range from 0.3 to 1.13 mm. Position the mesh so that it does not obstruct the imaging field
- Adjust flow rate to ~2 ml/min
- Specify the time lapse microscope with imaging interval (every 15 min) and number of cycles (80-120 cycles)
- Identify dentate gyrus using eyepieces, adjust to 100% camera, and start imaging

- Warping of the tissue occurs very often. Leave extra 30% blank Z-sections when setting up Z-stack. Severe warping happens when the conditions this tissue was resting in do not exactly match the conditions on the imaging stage

Instrument	**Vendor**	**Catalog**
pH meter	Thermo Scientific	Orion Star A211 pH Benchtop Meter
Osmometer	Precision Systems	μ OSMETTE 5002
Vibratome	Leica	VT 1000S
6-well plate	Corning	353046
Cell strainer	BD falcon	3352350
Feather blade	TedPella imported	#121-9
Vetbond	3M	sc-361931
Two-photon imaging system	Chameleon	N/A
Heat stage	tempcontrol	37-2 digital
Objective W Plan-Apochromat 20x/1.0 DIC M27 75mm	Zeiss	421452-9601-000
POC-R chamber	Pecon	N/A

MasterFlex CL peristaltic pump	ColeParmer	#EW-77122-22 or -26
Tube	Tygon	R-3603
Nylon mesh	Warner Instruments	64-0198
Nalgene Rapid-Flow Sterile Disposable Bottle	Nalgene	597-3320

Table 5. Instruments required for this study.

4.3 Results and Discussion

I imaged 219 cells in total in the SGZ during 27 imaging sessions, among which 131 cells were GFP^+ adult NSCs with a distinct radial process. One imaging session usually lasts ~12-24 hours. Throughout the imaging time, 81.7% of the labeled adult NSCs (107 of 131 NSCs) in the dentate gyrus stayed quiescent without changing their identity. 14.1% (19 of 131 cells) of adult NSCs divided asymmetrically to get rise to a progenitor cell, while 3.8% (5 of 131 cells) divided to give rise to a cell that extends a radial process. No stem cell depletion or astrocyte differentiation were observed. Notably, NSC divisions displayed a similar pattern, as was summarized in a schematic drawing (**Figure 11**) and shown in representative movies (**Movie 2, 3 and 4**). Briefly, before cell division occurs, the NSC retracts its radial process to ~20 μm within 30 min. The cell soma then transforms into a round shape within 30 min before it divides into two cells. After that, the mother stem cell re-extends and branches its radial process while the newly divided daughter cell will slowly detach from its mother stem cell. The entire mitosis process takes less than one hour.

Interestingly, 16 of the 24 dividing NSCs (66.7%) have at least one neighboring NSC that is dividing either simultaneously or one after the other within a few hours apart. (**Movie 2 and 3**). This result suggests that environmental niche signals may be influencing NSC activation and division (Bond et al., 2015). Taken together, we concluded that adult NSCs in the dentate gyrus are locally influenced by extrinsic environmental signals and undergo symmetric or asymmetric divisions to sustain the hippocampal neurogenic niche under physiological conditions.

There are a few limitations to the *ex vivo* acute slice imaging technology. First, the niche signaling is altered *ex vivo* and is different from its physiological condition. Second, sectioning the brain for *ex vivo* imaging causes a much more severe injury response in the dentate gyrus niche than *in vivo* imaging (Pilz et al., 2018). Third, tissue health decreases severely over time in aCSF, which limits one imaging session to less than 24 hours. Due to (1) the quiescent nature of the adult NSC niche and (2) transient NSC division time window, only two or three dividing cells can be captured during one imaging session. Because of these limitations, we were not able to perform clone lineage tracing under live imaging or to detect any long-term cell behaviors, for example, cell cycle re-entry or clone expansion that takes days or weeks to occur.

Despite these limitations, it still serves as a valuable methodology to observe the short-term behavior of adult NSCs and progeny at a single-cell resolution. It can be applied to future experiments, such as exploring the orientation of the cleavage plane during stem cell divisions, and the acute response of stem cells to exogenously-added drugs, etc.

Figure 11. A schematic model of neural stem cell division pattern.

Before cell division occurs, the NSC retracts its radial process to ~20 μm within 30 min. The cell soma then transforms into a round shape within 30 min before it divides into two cells. After that, the mother stem cell re-extends and branches its radial process while the newly divided daughter cell will slowly detach from its mother stem cell.

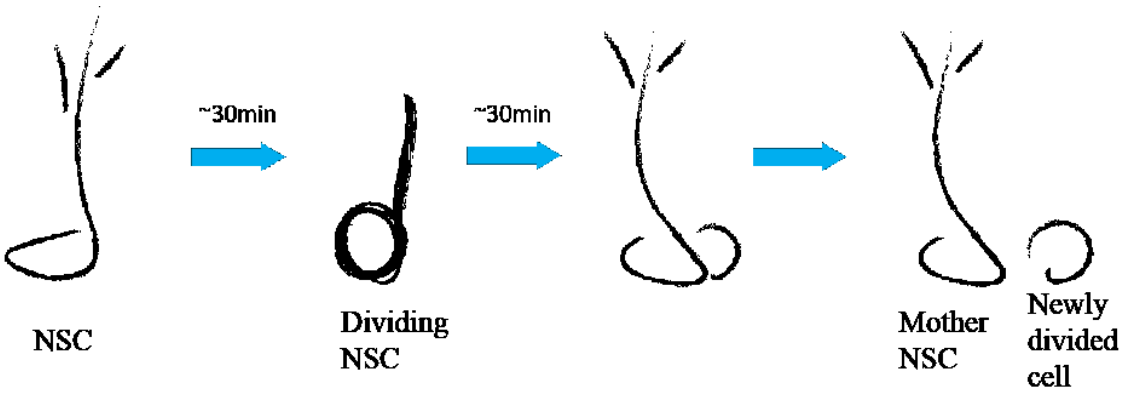
~30min
~30min
NSC
Dividing NSC
Mother NSC
Newly divided cell

Movie 2. A representative movie showing two neighboring NSCs divided one after the other

The dentate gyrus section was taken from a 2 month-old adult *Ascl1-CreERT2; mT/mG*$^{f/-}$ mice, tamoxifen-induced for 3 days. The induced GFP-labeled cells are *Ascl1* radial-glia like NSCs. Two neighboring NSCs, indicated by yellow arrows, both underwent asymmetrical divisions within 6 hours apart.

Imaging interval: 2.5 min; total imaging time: 12 hours.

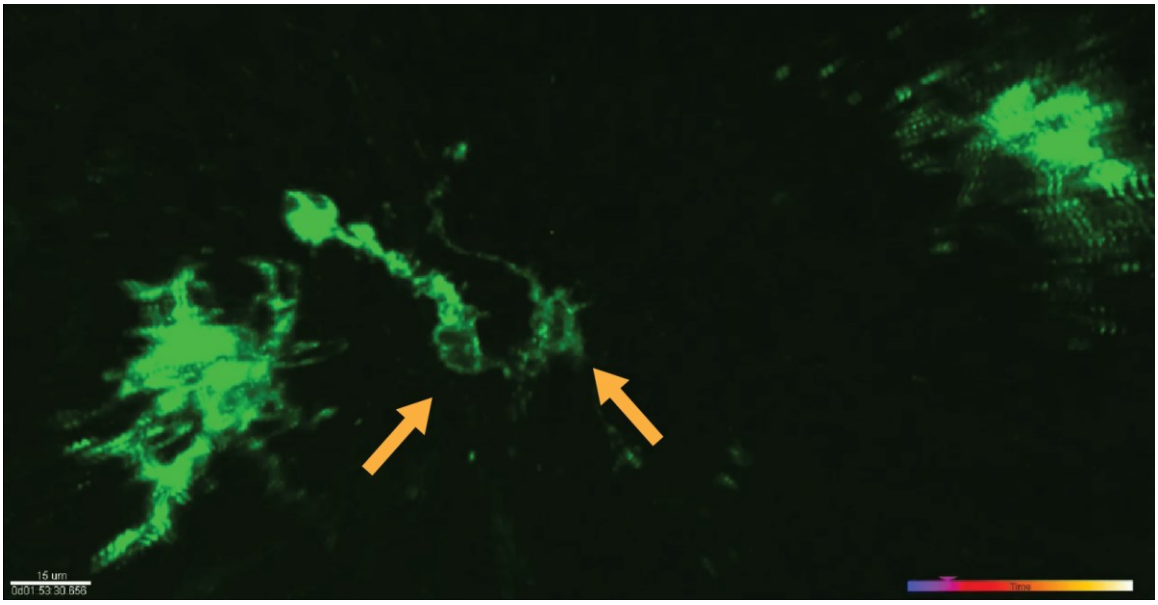
15 um
0d01:53:30.658

Movie 3. A representative movie showing two neighboring NSCs dividing simultaneously

The dentate gyrus section was taken from a 2 month-old adult *Ascl1-CreERT2; mT/mG*$^{f/-}$ mice, tamoxifen-induced for 3 days. The induced GFP-labeled cells are *Ascl1* radial-glia like NSCs. Blood vessels were labeled by Texas Red dextran (D1864, Molecular Probes) in 1x DPBS. Two neighboring NSCs divided simultaneously, indicated by yellow arrows. Imaging interval: 15 min; total imaging time: 13 hours.

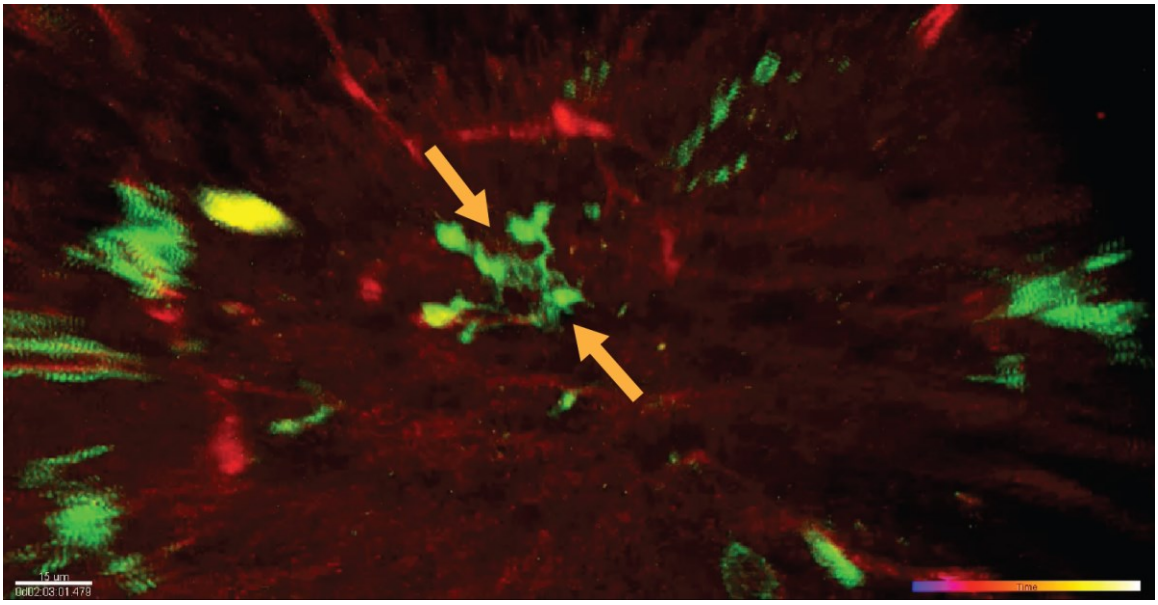
15 um
Time

Movie 4. A representative movie showing a NSC asymmetrical division

The dentate gyrus section was taken from a 2 month-old adult *Ascl1-CreERT2; mT/mG*$^{f/-}$ mice, tamoxifen-induced for 3 days. The induced GFP-labeled cell is an *Ascl1* radial-glia like NSC. Blood vessel was labeled by Texas Red dextran (D1864, Molecular Probes) in 1x DPBS. A NSC, indicated in yellow arrow, asymmetrically divided to give rise to a progenitor cell.

Imaging interval: 16 min; total imaging time: 13.5 hours.

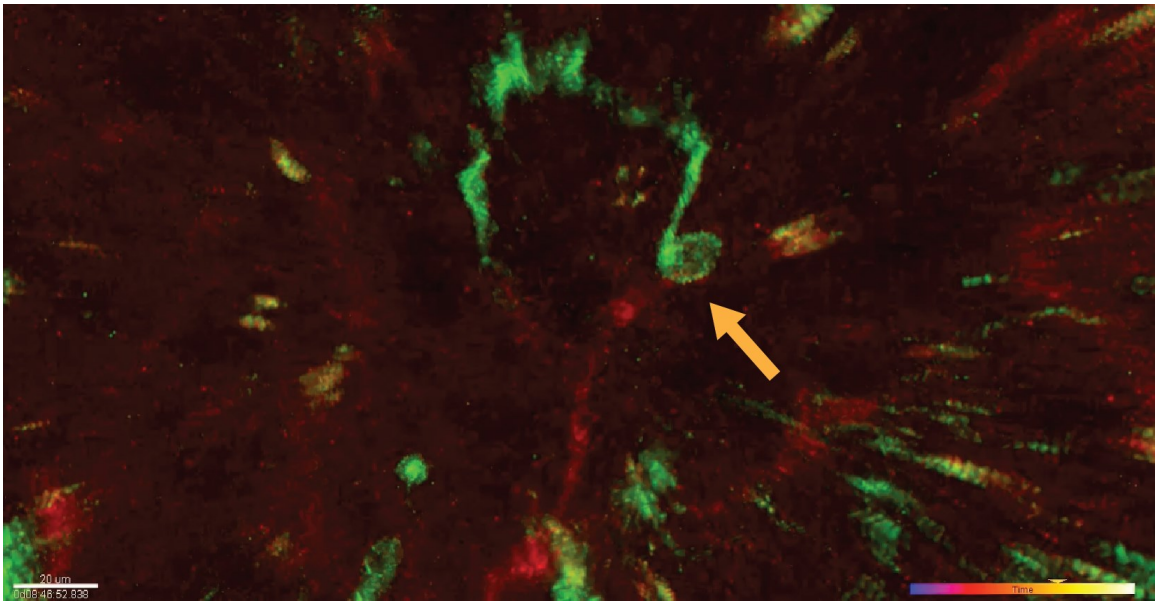
20 µm
Time

5 – Tangential migration of neuronal precursors of glutamatergic neurons in the adult mammalian brain

(This chapter was published (Sun et al., 2015b). I am the co-first author, and was involved in all aspects of the study.)

5.1 Introduction

The nervous system is formed by migration of neuronal precursors and immature neurons to specific locations during development. The classical radial unit hypothesis of mammalian brain development postulates that in the developing neocortex, glutamatergic, excitatory, principal neurons migrate radially to form discrete information processing columns of ontogenetic origin (Rakic, 2009), whereas GABAergic, inhibitory, modulatory interneurons migrate tangentially across columns (Corbin et al., 2001).

Neurogenesis persists in the adult mammalian brain in two brain regions and is thought to follow the classical migration model (Fuentealba et al., 2012; Ming and Song, 2011). In the subventricular zone (SVZ) of lateral ventricles, new neurons generated from neural precursors migrate tangentially to the olfactory bulb to become GABAergic interneurons (Braun and Jessberger, 2013; Lois and Alvarez-Buylla, 1994). In contrast, in the subgranular zone (SGZ) of the dentate gyrus, new neurons generated from radial glia-like neural stem cells (RGLs) migrate radially into the granule cell layer to become principal glutamatergic granule cells (Toni et al., 2007). However due to technical challenges, migratory patterns have only been examined at the cell population level, thus we still lack detailed information about the spatial relationship between individual precursors and their progeny *in vivo*.

Both adult neurogenic niches are highly vascularized, and this property is hypothesized to play a critical role in adult neurogenesis (Fuentealba et al., 2012). In the adult SVZ, neural precursors contact blood vessels (Mirzadeh et al., 2008; Shen et al., 2008; Tavazoie et al., 2008). In the adult SGZ, proliferating progenitor cells have been shown to be in close association with vasculature (Palmer et al., 2000). Despite these observations, the functional role of the vasculature in the niche remains to be fully explored.

Unexpectedly, and contrary to the classical model, our recent clonal lineage-tracing of individual quiescent RGLs showed tangential distribution of glutamatergic dentate granule neurons with respect to their parental RGL in the adult dentate gyrus (Bonaguidi et al., 2011). We therefore systematically investigated the migration pattern and trajectory of these newborn cells. Using a novel clonal lineage-tracing approach that preferentially targets active RGLs in the adult mouse dentate gyrus, thereby birth-dating their newborn progeny *in vivo*, we found significant tangential distribution of newborn neuroblasts from their parental RGL. Furthermore, we found direct contact of neuroblasts with the vascular network, suggesting an important function of blood vessels as a substrate for migration. Together, our results reveal a new mode of glutamatergic neuron migration under physiological conditions in the adult mammalian brain.

5.2 Materials and Methods

5.2.1 Animals and tamoxifen administration

Ascl1^{CreERT2}*;Rosa-YFP*$^{f/+}$and *Ascl1*^{CreERT2}*;Confetti*$^{f/+}$ mice were generated by crossing *Ascl1*^{CreERT2} (*Ascl1*$^{tm1.1(Cre/ERT2)Jejo}$/J, knock-in line, Jackson Labs) (Kim et al., 2011) with *Rosa-YFP*$^{f/+}$ (B6.129X1-*Gt(ROSA)26Sor*$^{tm1(EYFP)Cos}$/J, Jackson Labs) and *Confetti*$^{f/+}$ (B6.129P2-*Gt(ROSA)26Sor*$^{tm1(CAG-Brainbow2.1)Cle}$/J, Jackson Labs) mice, respectively. We used two different reporters in the present study to validate reporter independence of cell migration phenomena. *Nestin-GFP* transgenic mice were from Dr. Grigori N. Enikolopov (Encinas et al., 2006). All mice in the study were backcrossed to the C57BL/6 background for at least six generations. Animals were housed in a 14 hour light/10 hour dark cycle and had free access to food and water. Tamoxifen (66.67 mg/ml, Sigma, T5648) was prepared in a 5:1 corn oil (Sigma) to ethanol mixture. To achieve sparse labeling for clonal analysis (~ 8-16 clones per hemisphere), a single dose of tamoxifen (77.5 mg/kg for the *Rosa-YFP*$^{f/+}$ reporter, 250 mg/kg for the *Confetti*$^{f/+}$ reporter) was intraperitoneally injected into adult 8-10 week-old male and female mice. Animals were analyzed at 1, 3, or 7 days post-tamoxifen injection (dpi), or 1-2 months post-tamoxifen injection (mpi). All animal procedures were performed in accordance to institutional guidelines of Johns Hopkins University School of Medicine.

5.2.2 Tissue processing, immunostaining and confocal imaging

Animals were transcardiac perfused with cold 4% paraformaldehyde (wt/vol, in 0.1 M phosphate buffer, PB, pH 7.4), and cryoprotected with 30% sucrose (wt/vol). Serial 40 μm-thick coronal brain sections were cut on a frozen sliding microtome (Leica,

SM2010R) for immunohistology as previously described (Bonaguidi et al., 2011). For partial "whole-mount" dentate gyrus SGZ preparations, the whole hippocampus was dissected from cortex, mounted dentate-side-up on a frozen sliding microtome, and serial 50 μm horizontal sections were collected. Antibodies diluted in TBS with 0.05% Triton X-100 and 3% donkey serum, were used against GFP (Aves Labs, chicken, 1:500; Rockland, goat, 1:500), Tbr2 (Abcam, rabbit, 1:250), CD31 (BD Biosciences, rat, 1:500), DCX (Santa Cruz, goat, 1:100), GFAP (Millipore, mouse, rabbit, 1:1000), GM130 (BD Biosciences, mouse, 1:250), Nestin (Aves Labs, chicken, 1:500), γ-tubulin (BioLegend, rabbit, 1:500), Prox1 (Abcam, rabbit, 1:500), and NeuN (Millipore, guinea pig, 1:500). Nestin and NeuN antigens were retrieved by incubating brain sections in 1X DAKO target retrieval solution (DAKO) at 68°C for 20 minutes, followed by 10 minutes cooling to room temperature. Serial sections from the entire dentate gyrus were first immunostained for GFP to allow identification of prospective clone-containing sections on an epifluorescence microscope (Zeiss, Axiovert 200M). Labeled clone-containing sections were taken for further processing and confocal imaging at 40X on a Zeiss LSM 710 confocal microscope using multi-track or spectral linear unmixing 'online fingerprinting' configurations (Carl Zeiss).

5.2.3 Image processing and data analyses

Clonal analysis of adult hippocampal neural stem cells and their progeny was performed as previously described (Bonaguidi et al., 2011). Simulations to estimate the probability of two cells belonging to a clone, based upon numbers of initially labeled cells per hemisphere, were performed from 3D-reconstructed dentate gyri also as previously

described (Bonaguidi et al., 2011). For data acquisition, clones that spanned multiple serial sections were reconstructed using Reconstruct software (John C. Fiala, NIH). All aligned images were exported at full resolution for 3D visualization into Imaris (Bitplane) and analyzed. For illustrative purposes, some cells and features were volume-rendered using the Surface module in Imaris. Distance measurements were collected from 7 hemispheres (5 animals) at 3 dpi, 9 hemispheres (6 animals) at 7 dpi, and 12 hemispheres (7 animals) at 1-2 mpi. The Spots module in Imaris was used to digitize cell nucleus locations in the 3D space and to code cell type classifications, according to distinct morphological and molecular markers. The Clipping Plane module in Imaris was used to estimate the local SGZ plane for 2D clone projections. Spots and clipping planes were exported to Matlab (The MathWorks) for further distance measurements, calculations, and analyses. The distance between an RGL and a given newborn progeny in the local SGZ plane was calculated for tangential distance measurements. The shortest distance between a given labeled newborn cell and the SGZ was calculated for radial distance measurements. Cells at the dentate gyrus genu were excluded from analysis due to the potential ambiguity of tangential versus radial migration. Clones with multiple RGLs were also excluded due to ambiguity in distinguishing the cell of origin.

For vasculature association analysis at the clonal level, cells were classified into one of three groups: (1) those with no $CD31^+$ vasculature contact, (2) those with their soma directly contacting a $CD31^+$ blood vessel, and (3) those which contacted $CD31^+$ vasculature only through one or more processes. All labeled clones and the percentage of their vasculature association were quantified and averaged across 10 hemispheres (5 animals). For vasculature association analysis at the population level, all cells in a

horizontal section from 3 *Nestin-GFP* animals were quantified and results were averaged across animals. Locations of cell nuclei were digitized according to GFP, Tbr2, and DCX expression using Spots. Blood vessels were digitized using the Filament Tracer module in Imaris. 3D coordinates were exported to Matlab and distance between cells and vasculature was measured. Cells with nuclei within 7 μm of a blood vessel centerline were considered to be in contact with the blood vessel. Simulated vasculature associations were performed by randomly placing cells in the same 2D SGZ space, as estimated by a third-degree polynomial plane fit. One-hundred iterations of the simulation were performed for each cell type.

5.2.4 Electron microscopy analysis

Adult C57BL/6 female mice were stereotaxically injected with engineered murine oncoretrovirus expressing GFP as previously described (Song et al., 2012). Mice were processed 2 days after injection and transcardiac-perfused with 4% paraformaldehyde (wt/vol) with 0.1% glutaraldehyde (vol/vol; Sigma) in 0.1 M PB, pH 7.4. Coronal sections (50 μm thick) were sectioned on a vibrating microtome (VT1200S, Leica Biosystems). Sections were immunostained in phosphate-buffered saline (PBS) for CD31 and examined using an epifluorescence microscope to identify GFP^+ retrovirally-labeled newborn cells. Sections containing clearly labeled newborn progeny in close association with the $CD31^+$ vasculature were placed in cryoprotectant (25% sucrose wt/vol, 10% glycerol vol/vol, in 0.05 M PB) for 2 hours and freeze-thawed three times in liquid nitrogen. After three washes in PBS and then 0.5% bovine serum albumin in 0.1 M PB (vol/vol, BSA-C, Aurion) to block the tissue, sections were incubated overnight in the

primary antibody (biotinylated rabbit anti-GFP, Vector Laboratories, 1:1000; BA-0702) in 0.1% BSA-C in 0.1 M PB, shaking at room temperature). Sections were washed out of the primary antibody with one wash in 0.1% BSA-C in 0.1 M PB and three washes in PBS, before incubation for 90 minutes in avidin biotin peroxidase complex (ABC Elite, Vector Laboratories). After three washes in PBS and then Tris buffer, a 3,3-diaminobenzidine (DAB) peroxidase reaction was performed (Vector Laboratories Kit, 4 minutes). The sections were then washed three times in Tris buffer, three times in PBS and left overnight at 4°C. The next day, sections were washed in 0.1M PB in glass vials and post-fixed in 1% osmium tetroxide in 0.1M PB for 30 minutes. They were then dehydrated in ascending concentrations of ethanol (two 50% ethanol washes, one 70% wash with 1% uranyl acetate, one 95% wash and two 100% washes) and three washes in acetone, before being lifted into resin (Durcupan ACM, Fluka) and left overnight at room temperature. The resin was then warmed to decrease its viscosity and sections were placed onto microscope slides with coverslips, before the resin was cured at 65°C over three days. Locations of clearly labeled newborn progeny in close association with $CD31^+$ blood vessels were identified at the light microscopic level and followed through to the electron microscopic level. Serial sections (70 nm thick) were collected onto Formvar-coated, single-slot copper grids and contrasted with a lead stain (15 minutes). Sections were then examined using a Philips CM10 transmission electron microscope and serial images of the labeled structures were captured using a digital camera (Morada SIS, Olympus). These images were used to create 3D reconstructions with Fiji Image J software and individual images were processed using Adobe Creative Suite software.

5.2.5 Statistical analysis

Statistical analysis was performed with one-way ANOVA (with Tukey *post hoc* test), one-tailed unpaired Student's *t* test, two-sample Kolmogorov-Smirnov test, or Wilcoxon rank sum test (with Bonferroni correction for multiple comparisons, where applicable), as indicated in the text and figures. When applicable, validation of normality and homogeneity of variance assumptions was performed for all compared data groups using a Shapiro-Wilk test and Monte-Carlo simulation, respectively. All statistical analyses were performed in Origin Software (OriginLab) or Matlab.

5.3 Results

5.3.1 Spatial distribution of clonally-related newborn neuronal progeny with defined birthdate

We utilized a tamoxifen inducible *Ascl1*^{CreERT2} knock-in mouse line (Kim et al., 2011) to sparsely label (~8-16 cells per dentate gyrus) and lineage-trace clones of neural precursors in the adult dentate gyrus (**Figure 12A**), following our previous strategy of clonally labeling RGLs using the *Nestin*^{CreERT2} mouse line (Bonaguidi et al., 2011). At one day post-tamoxifen injection (1 dpi), labeled cells in the adult SGZ consisted of over 90% Nestin^{+}GFAP^{+} RGLs and few early intermediate progenitor cells (IPCs; n = 8 dentate gyri), as assessed by morphology and molecular marker expression (**Table 5**). Computational simulations (Bonaguidi et al., 2011) estimated that given 8 initially labeled cells, any two labeled cells within 200 μm of each other had a 99% probability of belonging to the same clone (**Figure 12B**). Thus, although few isolated IPCs were labeled at 1 dpi, the probability of their mis-assignment to an RGL clone was 1% or lower. Crucially, given our simulation results, we conservatively conducted all our analyses by excluding clones in which progeny were >150 μm from their parent RGL, thus only focusing on clones with a maximum diameter of 300 μm.

In contrast to *Nestin*^{CreERT2}-based clonal lineage-tracing of quiescent RGLs that exhibited stochastic activation over time (Bonaguidi et al., 2011), at 1 dpi the majority of *Ascl1*^{CreERT2}-labeled RGLs (96 ± 2%, n = 10 dentate gyri) had just divided (with one adjacent progeny) or were in the process of cell division (**Figure 12A**). Therefore, our current approach selectively targets activating RGLs, allowing, for the first time, birth-dating of RGL progeny to track their development with high temporal precision. At 1-

month post-tamoxifen injection (mpi), we observed clones in which Prox-1^{+}NeuN^{+} mature dentate granule cells were distributed a long distance (15 cell bodies or more than 100 μm) away from their mother RGL along the SGZ plane (**Figure 12C**; **Movie 5**). These results suggest, in contrast to the classic model, tangential migration of a glutamatergic neuronal subtype in the adult mammalian brain under physiological conditions.

Cell type	Molecular markers	Morphology
Radial glia-like cell (RGL) with neurogenic division	Nestin, GFAP	RGL has its soma in the SGZ, radial process in the GCL and ML, nuclear cleavage with only one GFAP+ nucleus
Intermediate progenitor cell (IPC)	Tbr2 ($GFAP^{-}$)	IPC is spherical with short, multipolar processes in the SGZ
Neuroblast (NB)	DCX, Prox1	NB has elongated soma, bipolar processes
Immature neuron (IN)	DCX, Prox1, NeuN	IN has soma in the apical GCL, thin dendrite through the GCL
Mature neuron (N)	Prox1, NeuN (DCX^{-})	N has multi-branched spiny dendrites in the ML and axon to CA3

Table 6. Summary of the morphological markers used in the current study for identification of each cell type during adult hippocampal neurogenesis.

Figure 12. Tangential distribution of newborn granule neurons away from their parental RGLs of origin in the adult dentate gyrus as revealed by *in vivo* clonal analysis.

(**A**) Sample projected confocal image of an *Ascl1*^{CreERT2}; *Rosa-YFP*$^{f/+}$-labeled RGL in the dentate gyrus at 1 dpi. As shown in a high magnification image (bottom panels), this GFAP^{+} RGL (filled arrowhead) underwent an asymmetric division to produce a GFAP^{-} neuronal progeny (open arrowhead, on a different focal plane). Scale bars: 100 μm (top panel) and 10 μm (bottom panels). (**B**) Computational simulations of nearest distances between two cells in the 3D dentate gyrus space. Each colored line represents the reverse cumulative distribution of nearest cell distances from a simulation with a given number of total cells. (**C**) Sample projection confocal image of a labeled clone in *Ascl1*^{CreERT2}; *Rosa-YFP*$^{f/+}$ mouse at 1 mpi (see **Movie 5**), showing tangential distribution of Prox1^{+}NeuN^{+} mature glutamatergic granule neurons and their parental GFAP^{+} RGL. Inset: 2-dimensional SGZ plane projection in 200 μm square windows of all clonally related cell locations. RGL is represented as center open circle; neural progeny are represented as closed circles. Shown on the right top panel is a schematic diagram for measurements of tangential and radial distance of neuronal progeny from the parental RGL. Shown on the right bottom panel are enlarged confocal images for a GFAP^{+} RGL (1) and Prox1^{+}NeuN^{+} mature neuronal progeny (2). Scale bar: 10 μm. GCL: granule cell layer; SGZ: subgranular zone. (**D**) Distribution plot of tangential distance between labeled RGL and its progeny within each clone at 3 dpi, 7 dpi, and 1-2 mpi (*$P < 0.05$; two-sample Kolmogorov-Smirnov test statistic = 0.85 for 3 vs 7 dpi and = 0.66 for 3 dpi vs 1-2 mpi). Raw distributions are shown as bar graphs; curved lines correspond to

smoothed distributions. (**E**) Dot plot of tangential versus radial distance from the parental RGL for each neural progeny in all labeled RGL-containing clones at 3 dpi, 7 dpi, and 1-2 mpi. Inset: tangential distance of each neural progeny to its parental RGL.

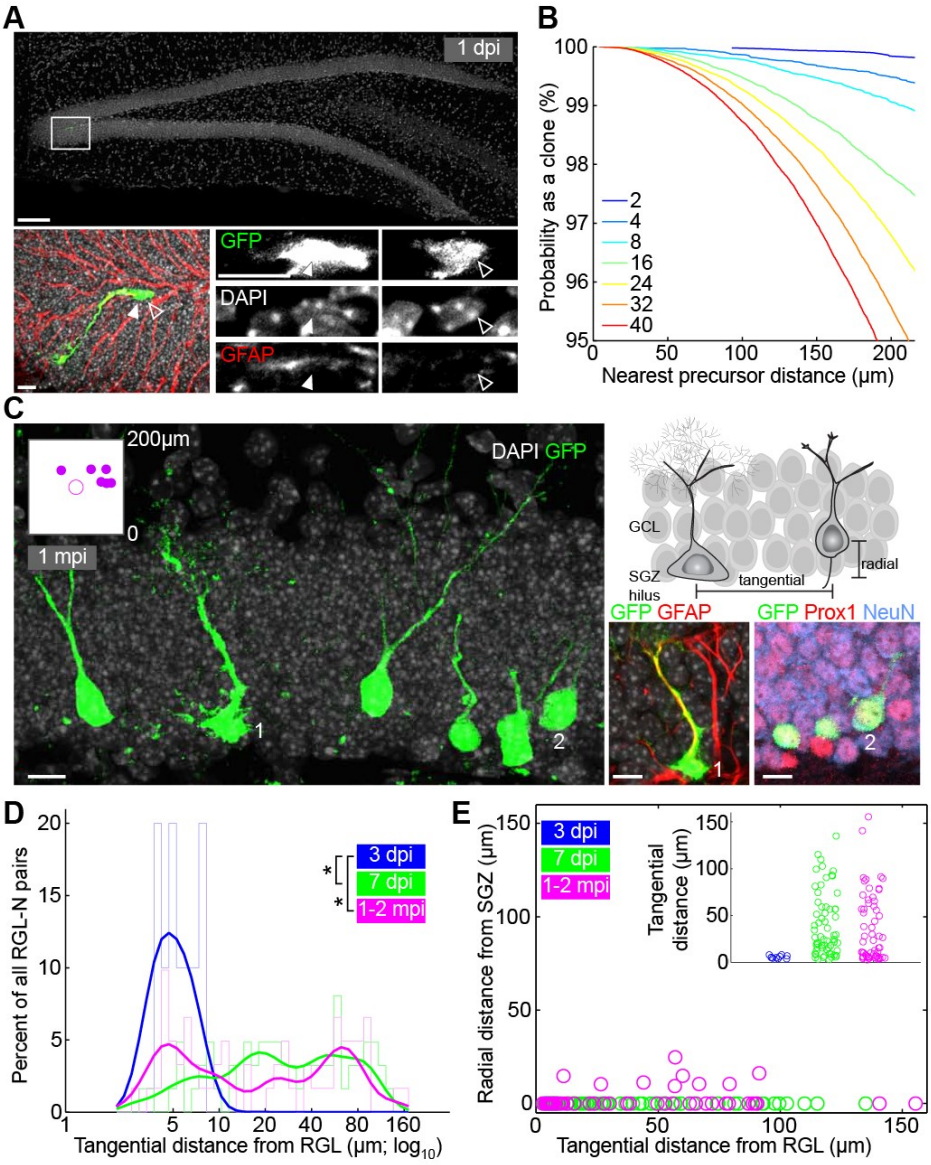
A
1 dpi
GFP
DAPI
GFAP
B
Probability as a clone (%)
100
99
98
97
96
95
2
4
8
16
24
32
40
0
50
100
150
200
Nearest precursor distance (μm)
C
200μm
DAPI GFP
0
1 mpi
1
2
GCL
SGZ
hilus
tangential
radial
GFP GFAP
GFP Prox1 NeuN
D
Percent of all RGL-N pairs
20
15
10
5
0
3 dpi
7 dpi
1-2 mpi
*
*
1
5
10
20
40
80
160
Tangential distance from RGL (μm; log10)
E
Radial distance from SGZ (μm)
150
100
50
0
3 dpi
7 dpi
1-2 mpi
Tangential distance (μm)
150
100
50
0
0
50
100
150
Tangential distance from RGL (μm)

Movie 5. Widespread distribution of clonally related cells in the adult dentate gyrus. Shown is a sample 3D reconstruction of a GFP-labeled clone showing distribution of adult-born dentate granule neurons away from their parental RGL at 1 month post-tamoxifen induction in *Ascl1*^{CreERT2}; *Rosa-YFP*$^{f/+}$ mouse. The projection view of the same clone is shown in **Figure 12C**.

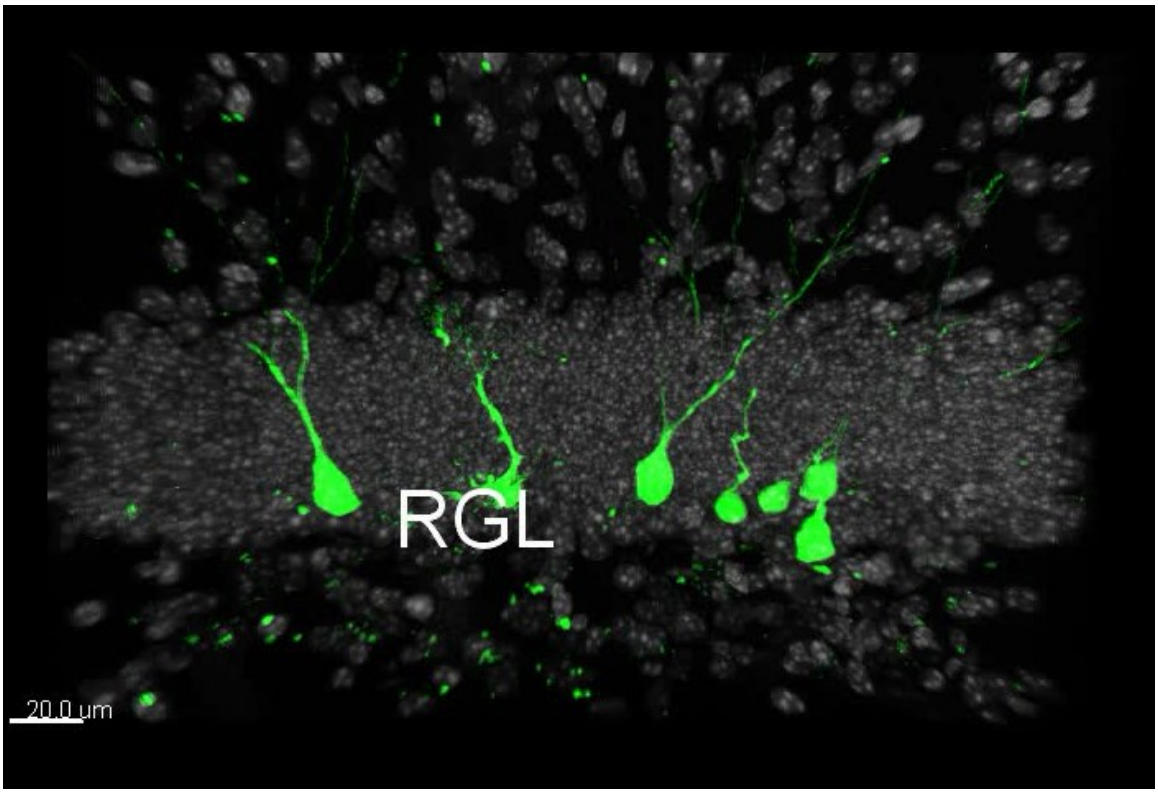
RGL
20.0 µm

5.3.2 Developmental stage-specific tangential distribution

Newborn cells may have exhibited tangential distribution due to passive mechanisms such as displacement upon cell division. To provide further evidence for active tangential migration, we explored the dynamics of cell distribution by time-course analysis. At 3 dpi, labeled cells exhibited little displacement from each other, despite all being identified as highly proliferative IPCs (Berg et al., 2015) (**Figure 12D**). In contrast, at 7 dpi there was significant distance along the tangential plane of the SGZ between labeled newborn neural progenitors and their parental RGLs, the distribution of which was very similar to that at 1-2 mpi (**Figure 12D**). Only ~15% of labeled newborn neurons exhibited measurable radial displacement away from the SGZ into the granule cell layer even at 1 or 2 mpi (all < 25 μm), yet among these cells, ~47% spread more than 25 μm tangentially away from their parental RGL (**Figure 12E**). The average tangential distance exceeded that of radial distance by almost 18-fold. Notably, radial migration was absent at 7 dpi, suggesting that tangential movement preceded any radial migration (**Figure 12E**); no correlation between tangential and radial migration was observed among individual cells that exhibited both (**Figure 12E**; $R = 0.08$, $p = 0.85$). Taken together, these results establish that tangential distribution of newborn progeny from their parental RGL could not have arisen by chance and instead represents a dominant mode of migration in the adult dentate gyrus.

We next asked whether tangential migration occurred during a specific developmental stage (or stages) during adult neurogenesis. Adult hippocampal neurogenesis proceeds in a stereotypic sequence – dividing RGLs give rise to IPCs, which in turn develop through neuroblast (NB) and immature neuron (IN) stages before

becoming mature glutamatergic granule neurons (**Figure 13A**) (Ming and Song, 2011). Utilizing distinct morphological and molecular markers to distinguish labeled cells at different developmental stages (**Figure 13A** and **Table 5**), we found that neuroblasts, corresponding to 3-7 day-old DCX^+ cells with a bipolar, elongated morphology, were the earliest cells in the developmental lineage that showed significant tangential distribution away from their parental RGL (**Figure 13B**; $p = 5.4\times10^{-7}$; Kolmogorov-Smirnov test). On average, neuroblasts, immature neurons, and mature neurons exhibited similar tangential distances away from their parental RGLs (**Figure 13B**). These results suggest that the majority of tangential migration occurs within the neuroblast stage during adult hippocampal neurogenesis.

Figure 13. Developmental stage-specific tangential distribution of newborn neural progeny.

(**A**) Summary of molecular markers used for identification of each cell type during adult hippocampal neurogenesis. Newborn cells are generated from $GFAP^{+}Nestin^{+}$ RGLs that undergo asymmetric neuronal divisions, which develop into $Tbr2^{+}$ intermediate progenitor cells (IPC) with short, multipolar processes within three days of birth. Within 3-7 days, newborn cells possess long, bipolar processes and elongated somas in a $Tbr2^{+/-}$ DCX^{+} neuroblast stage (NB) before penetrating the granule cell layer and becoming a polarized $Prox1^{+}DCX^{+}$ immature neuron (IN) with axon and dendrite. Over the next month, newborn cells mature into $Prox1^{+}NeuN^{+}$ neurons (N) with spiny dendrites and long axons that project to CA3. See also **Table 5**. (**B**) Summary of tangential distance of each neural progeny from its parental RGL for progeny at each developmental stage. IPC: intermediate progenitor cell; NB: neuroblast; IN: immature neuron; N: mature granule neuron. Values represent mean ± s.e.m. ($^{*}P < 0.01$; $^{\#}P \approx 1$; Wilcoxon rank-sum test with Bonferroni correction for multiple comparisons; test statistic, $z = -5.58$ and -0.72, respectively). (**C**) Histogram and cumulative distribution plot of the maximum distance between clonally related neural progeny for all clones, including non-RGL containing clones. See **Figure 14** for 2D SGZ plane projection of representative clones ($^{*}P < 0.1$; two-sample Kolmogorov-Smirnov test statistic = 0.38).

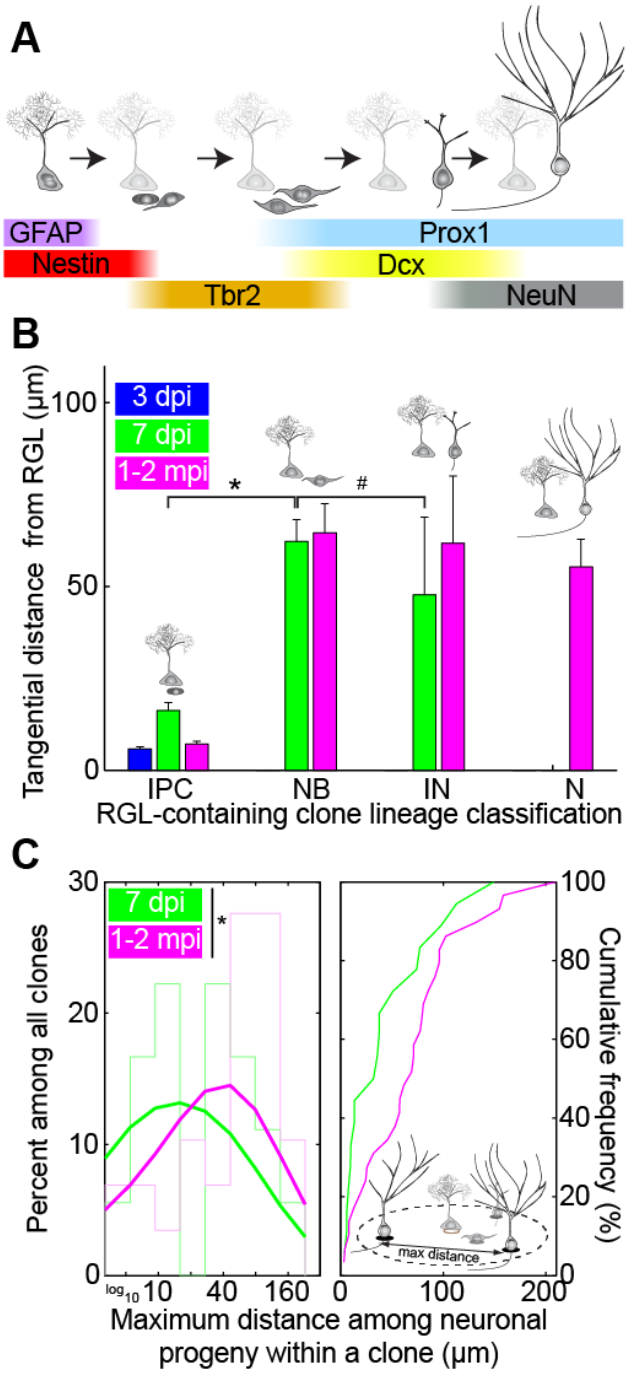
A
GFAP
Prox1
Nestin
Dcx
Tbr2
NeuN
B
Tangential distance from RGL (μm)
100
50
0
3 dpi
7 dpi
1-2 mpi
*
#
IPC
NB
IN
N
RGL-containing clone lineage classification
C
Percent among all clones
30
20
10
0
7 dpi
1-2 mpi
*
log10 10
40
160
0
100
200
Cumulative frequency (%)
100
80
60
40
20
0
max distance
Maximum distance among neuronal progeny within a clone (μm)

Figure 14. Tangential distribution among newborn neural progeny at 3 dpi, 7 dpi, and 1-2 mpi in the adult dentate gyrus.

(**A-C**) 2-dimensional SGZ plane projection of all RGL-containing clones containing at least IPCs at (**A**) 3 dpi, (**B**) 7 dpi, and (**C**) 1-2 mpi, plotted in a 300 μm square window. RGLs are represented as open circles; neural progeny are represented as closed circles. Different time points or developmental stages are encoded with color. Clones that lack RGLs at 1-2 mpi were also plotted in gray boxes and included in histogram in **Figure 13C**.


A
3 dpi
RGL 3 dpi 7 dpi 1-2 mpi
Progeny IPC NB IN N
Distance (µm)
100
0
-100
B
7 dpi
C
1-2 mpi

5.3.3 Pattern and magnitude of tangential distribution

A consequence of tangential migration of neuronal progeny is that individual clones disperse over areas beyond that of a radial unit, potentially allowing individual RGLs to modify a large domain of the hippocampal circuitry via neurogenesis. We visualized 2D SGZ projections of clones over time in 300 μm square windows (**Figure 14A-C**; excluding clones with single RGLs that had not completed division). RGLs exhibit depletion over time (Bonaguidi et al., 2011) and we included non RGL-containing clones only for 1-2 mpi. Qualitatively, clones dispersed over large areas, strongly suggestive of widespread tangential migration (**Figure 14A-C**).

We next quantitatively determined the extent of tangential distribution of neuronal progeny in each clone under 2D SGZ projection. As opposed to measuring the distance of each newborn neural progeny to its mother RGL as we did in the previous analysis (**Figure 12**), we instead measured the maximum distance amongst all newborn neural progeny within each clone. The mean values were ~ 43 ± 16 μm and ~ 69 ± 19 μm, whereas the maximum values were 149 μm and 210 μm at 7 dpi and 1-2 mpi, respectively. The distribution of maximum distances was modestly shifted from 7 dpi to 1-2 mpi (**Figure 13C**; $p = 0.06$; Kolmogorov-Smirnov test). The considerable spacing between neural progeny supports our model of neuronal migration as opposed to motility of only the RGLs.

5.3.4 Vascular substrate for putative tangential migration

We then investigated a potential cellular mechanism underlying tangential migration of neuronal precursors in the adult hippocampus *in vivo*. Tangential migration of

GABAergic interneurons has been shown to be facilitated by a combination of homotypic and heterotypic cellular interactions, such as migration in chains and along existing axonal processes, respectively (Ghashghaei et al., 2007). We therefore searched for potential substrates that could support tangential migration during adult hippocampal neurogenesis. In the adult dentate gyrus, BrdU-incorporating cells are known to be in close association with the vasculature (Palmer et al., 2000). Indeed, we found that labeled neuroblasts mostly stayed in very close contact with $CD31^+$ vasculature (**Figure 15A, B** and **Movie 6**). Notably, these neuroblasts exhibited polarized organelles, such as $GM130^+$ Golgi apparatus (**Figure 15C**) and γ-tubulin$^+$ centrosomes (**Figure 15D**), characteristic of migrating, mobile cells (Ghashghaei et al., 2007).

Quantitative analysis further showed that, among all labeled cells, $Tbr2^+DCX^+$ and $Tbr2^-DCX^+$ neuroblasts were two major cell types in contact with the vasculature, either via cell soma or processes (**Figure 16A**; left graph). 88% of $Tbr2^+DCX^+$ and 80% of $Tbr2^-DCX^+$ cells with tangential processes were closely associated with the vasculature (**Figure 16A**; right column). In contrast, $Tbr2^+DCX^-$ IPCs or $Tbr2^-DCX^+$ immature neurons with radial processes mostly lacked vascular contact (**Figure 16A**). We further examined the interaction between neural progeny and endothelial cells at the ultrastructural level using electron microscopy. Remarkably, the process and soma of some labeled neuroblasts were in direct contact with blood vessels (**Figure 16B**). These data support the model that neuroblasts represent the dominant cell stage of active migration via a vascular substrate.

Figure 15. Close association between tangentially migrating neuroblasts and blood vessels in the adult dentate gyrus.

(**A**) Sample confocal image (left panels) and 3D rendering (right panel) of a CFP^+ clone at 7 dpi with a neuroblast whose soma and tangential processes closely associated with a $CD31^+$ blood vessel. (**B**) Sample confocal image and 3D rendering of a GFP^+ clone at 7 dpi containing a parental RGL and dispersed $Tbr2^+DCX^+$ neuroblasts (NB) in close association with $CD31^+$ blood vessels (see also **Movie 6**). Note that CD31 and Tbr2 shared the same channel due to limited availability of channels, but could be distinguished by different morphology (Tbr2, nuclear staining; CD31, tubular staining). (**C**) Sample confocal image and 3D rendering of a GFP^+ clone at 7 dpi with a neuroblast whose tangential process extended along a blood vessel and contained polarized $GM130^+$ Golgi apparatus at its base, proximal to the cell soma. (**D**) Sample confocal image and 3D rendering of GFP^+ neuroblasts at 7 dpi with polarized γ-$tubulin^+$ centrosomes and $GM130^+$ Golgi apparatus, and in close association with $CD31^+$ blood vessels. All scale bars: 10 μm.

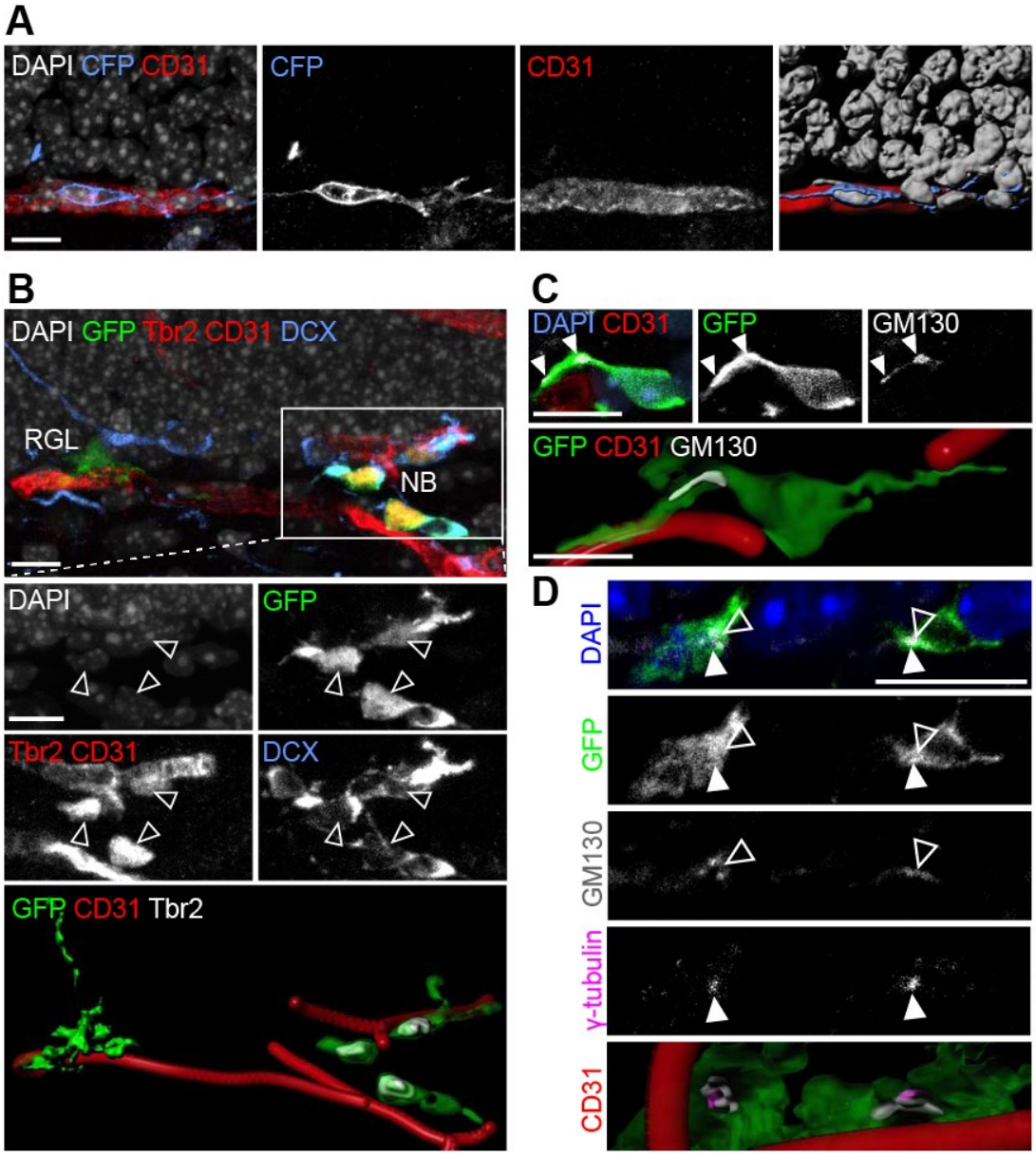
A
DAPI CFP CD31
CFP
CD31
B
DAPI GFP Tbr2 CD31 DCX
RGL
NB
DAPI
GFP
Tbr2 CD31
DCX
GFP CD31 Tbr2
C
DAPI CD31
GFP
GM130
GFP CD31 GM130
D
DAPI
GFP
GM130
γ-tubulin
CD31

Movie 6. Close association of neuroblasts with blood vessels in the adult dentate gyrus.

Shown is a confocal image of immunostaining for GFP, Tbr2, CD31 and DCX in *Ascl1*^{CreERT2}; *Rosa-YFP*$^{f/+}$ mouse at 7 dpi. Note the close association of neuroblasts on blood vessels in the SGZ, away from their parental RGL. The projection confocal image is shown in **Figure 15B**. Also shown is a surface rendering of all cells and their association to the vasculature. GFP, green; Tbr2 & CD31, red; DCX, blue.

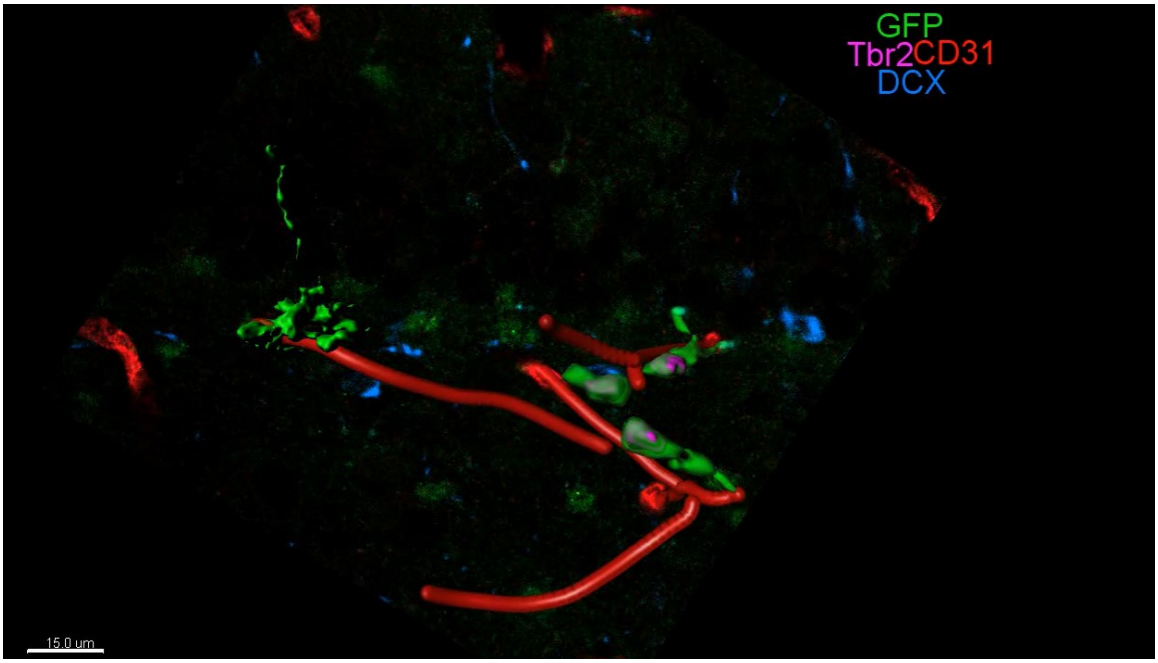
GFP
Tbr2CD31
DCX
15.0 um

Figure 16. Direct contact between tangentially migrating neuroblasts and blood vessels in the adult dentate gyrus.

(**A**) Quantification of distribution of various labeled precursors in close association with the vasculature at 7 dpi. Values represent mean ± s.e.m. Also shown are summaries of precursor cell molecular marker expression and the percentage of a given cell subtype in close association with vasculature (right panels). (**B**) 3D reconstruction, from serial electron microscopic sections, of a GFP^+ SGZ neuronal precursor (NP1) extending a tangential process along a blood vessel (BV). The immunofluorescence-identified, immunoperoxidase-labeled cell (top panels) sits alongside another neuronal precursor (NP2) and apposes the blood vessel with both its tangential process (mid-left panel) and its cell body (top right panel, arrowhead). SGZ: subgranular zone; GCL: granule cell layer; BV: blood vessel. Scale bars: 5 μm.

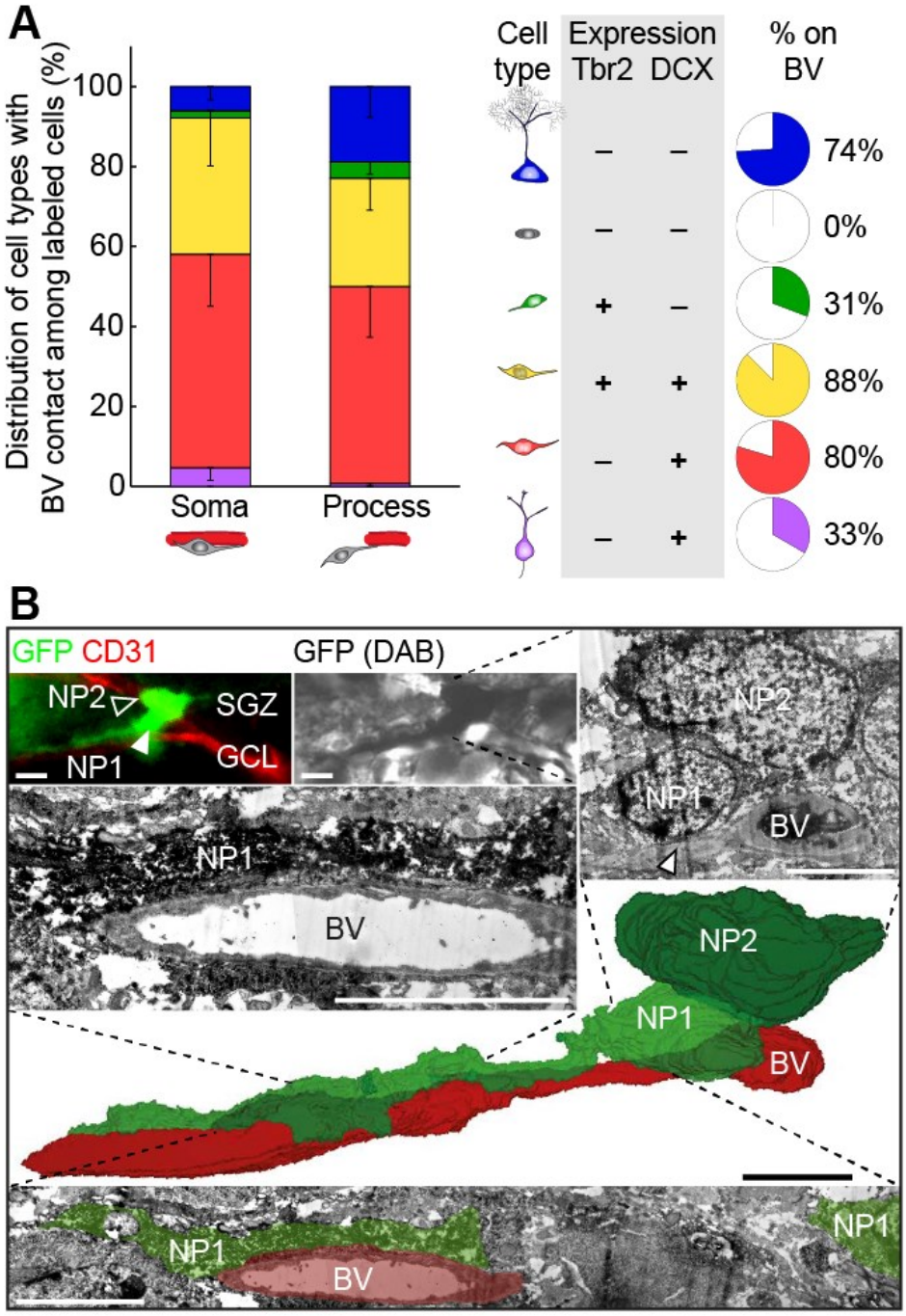
A
Distribution of cell types with BV contact among labeled cells (%)
100
80
60
40
20
0
Soma
Process
Cell type
Expression
Tbr2
DCX
% on BV
–
–
74%
–
–
0%
+
–
31%
+
+
88%
–
+
80%
–
+
33%
B
GFP CD31
GFP (DAB)
NP2
SGZ
NP1
GCL
NP1
BV
NP2
NP1
BV
NP2
NP1
BV
NP1
BV
NP1

5.3.5 Global view of neural precursors and niche-wide vascular-mediated migration

To determine whether the general population of neural precursors exhibited properties similar to those clonally labeled in *Ascl1*^{CreERT2} mice, we developed a partial "whole-mount" preparation by sectioning the hippocampus parallel to the SGZ (**Figure 17A** and **Movie 7**). This preparation enabled large sheets of SGZ to be visualized in a single section. We first visualized CD31^{+} vasculature and found a dense bed of blood vessels within the SGZ, in contrast to a sparse, columnar architecture of vessels within the granule cell layer (**Figure 17B**). The SGZ vascular architecture may therefore be uniquely suited to support tangential migration of newborn progeny within the adult SGZ.

Using *Nestin-GFP* reporter mice (Encinas et al., 2006) in combination with the same immunohistological and morphological markers as for clonal analysis (**Figure 13A** and **Table 5**), we examined the association of SGZ progenitors with vasculature (**Figure 17C**). Given that by chance a fraction of different cell types would be in close proximity to blood vessels, we simulated vascular association of the same number of each cell type randomly placed in the same SGZ space. We found that Tbr2^{+}DCX^{+} or Tbr2^{-}DCX^{+} neuroblasts were most associated with CD31^{+} blood vessels significantly above chance levels (**Figure 17D** and **Movie 8**). These neuroblasts on blood vessels also contained polarized GM130^{+} Golgi apparatus that is characteristic of migrating cells (**Figure 17E**). Together with findings from clonal analysis (**Figures 15 and 16**), these results support a model whereby vasculature serves as a substrate for tangential migration of newborn neural progeny during adult hippocampal neurogenesis.

Figure 17. Neuroblast–vasculature interaction using a partial "whole-mount" dentate gyrus SGZ preparation.

(**A**) Schematic illustration of the partial "whole-mount" dentate gyrus SGZ preparation. See **Movie 7**. (**B**) $CD31^+$ blood vessels using "whole-mount" preparation visualized in SGZ (left panel) and GCL (right panel). Scale bar: 100 μm. (**C**) Sample projected confocal image of *Nestin-GFP* tissue from "whole-mount" preparation immunostained for Tbr2, CD31 and DCX. Scale bar: 100 μm. See **Movie 8**. (**D**) Quantification of vascular association of different cell types expressing various combinations of Nestin-GFP, Tbr2, and DCX, utilizing the "whole-mount" preparation to view population of progenitors in the SGZ. Association was defined as having cell soma on a blood vessel and compared with simulated random distributions of same numbers of cells in the same space. Values represent means ± s.e.m. (n = 3 animals; *P < 0.05; **P < 0.01; one-tailed unpaired Student's t-test, observed > simulated; $Tbr2^+$: $t(4) = 2.20$; $Tbr2^+DCX^+$: $t(4) = 2.44$; DCX^+(neuroblast): $t(4) = 3.76$). (**E**) Sample confocal image and 3D rendering of $Tbr2^+DCX^+$ neuroblast migrating on $CD31^+$ blood vessel with polarized $GM130^+$ Golgi apparatus from "whole-mount" preparation in *Nestin-GFP* mouse. Scale bar: 10 μm.

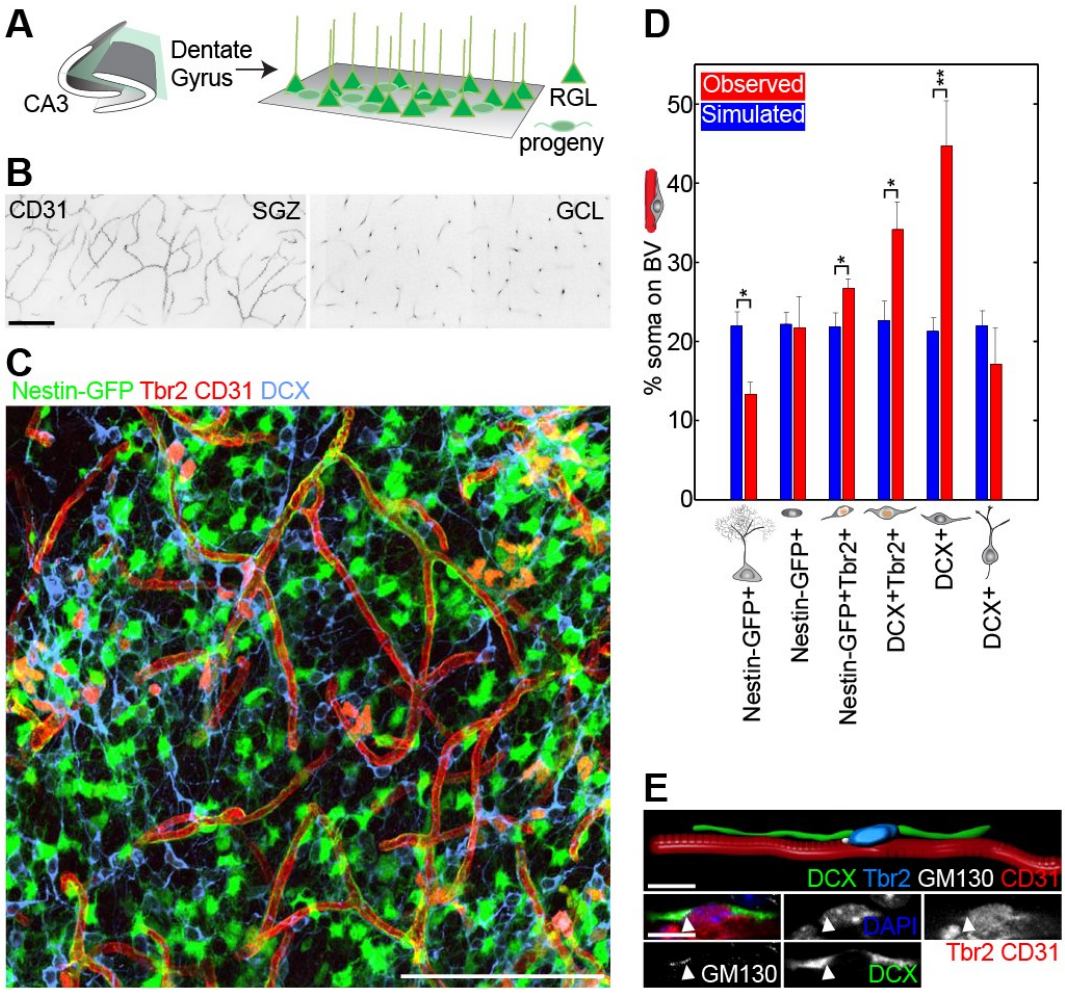
A
Dentate Gyrus
CA3
RGL
progeny
B
CD31
SGZ
GCL
C
Nestin-GFP Tbr2 CD31 DCX
D
Observed
Simulated
% soma on BV
50
40
30
20
10
0
*
*
*
**
Nestin-GFP+
Nestin-GFP+
Nestin-GFP+Tbr2+
DCX+Tbr2+
DCX+
DCX+
E
DCX Tbr2 GM130 CD31
DAPI
Tbr2 CD31
GM130
DCX

Movie 7. A partial "whole-mount" dentate gyrus SGZ preparation.

Shown is a confocal image of a "whole-mount" preparation section from adult *Nestin-GFP* mouse hippocampus and immunostained with GFP (green) and Nestin (red). A schematic illustration of this preparation is shown in **Figure 17A**.

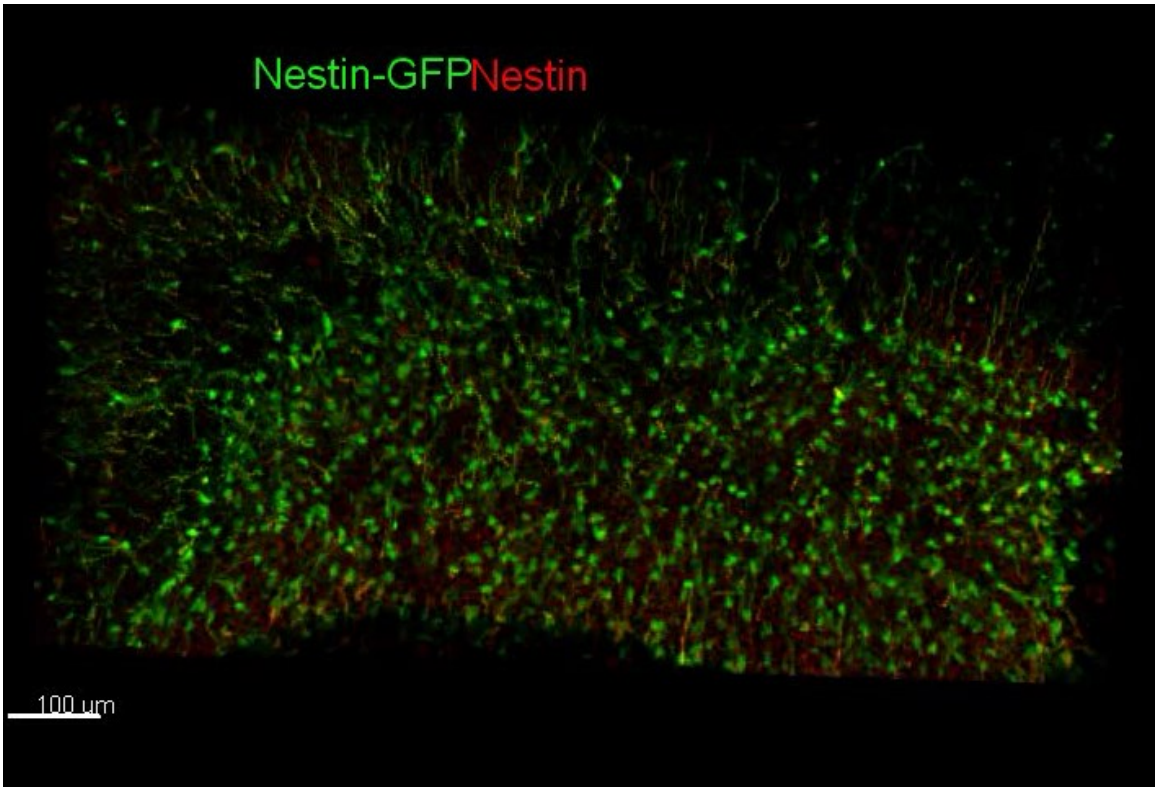
Nestin-GFPNestin
100 µm

Movie 8. Association of neuroblasts with the vasculature in the "whole-mount" dentate gyrus SGZ preparation.

Shown is a confocal image of a "whole-mount" preparation section from adult *Nestin-GFP* mouse hippocampus and immunostained with GFP (green), Tbr2 & CD31 (red), and DCX (blue). Also shown are surface renderings of representative neuroblasts on blood vessels in the adult SGZ.

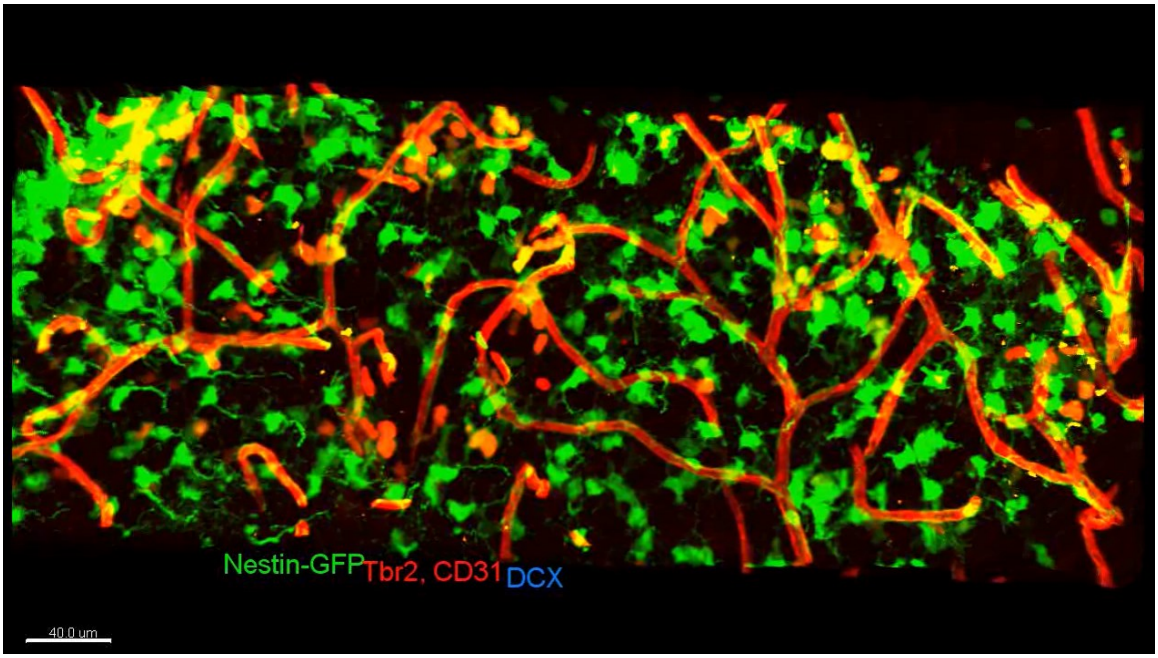
Nestin-GFP
Tbr2, CD31
DCX
40.0 um

5.4 Discussion

In contrast to the prevailing model that glutamatergic neurons migrate radially whereas interneurons migrate tangentially during development, we demonstrated for the first time in the adult mammalian brain that neuroblast precursors of principal, glutamatergic neurons exhibit significant tangential distribution away from their parental stem cell under physiological conditions. We revealed a two-step migration process during adult hippocampal neurogenesis, in which significant tangential migration of neuroblasts is followed by limited radial migration of immature neurons (**Figure 18**). Tangentially migrating neuroblasts may utilize the vasculature as a migration substrate, revealing an important role of this neurogenic niche component (**Figure 18**).

Figure 18. A two-step model for neuronal migration during adult hippocampal neurogenesis.

During adult hippocampal neurogenesis, radial glia-like cells (RGLs) give rise to Tbr2+ intermediate progenitor cells (IPCs) within 3 days. In the next 4 days, the cells become DCX+ proliferating neuroblasts (NBs) that extend long processes tangential to the SGZ, and contact blood vessels directly. During this phase, neuroblasts utilize blood vessels as a substrate to migrate tangentially away from their parental RGL. After 7 days, newborn neural progeny extend radial dendritic processes and develop into mature, $NeuN^{+}Prox1^{+}$ dentate granule neurons and exhibit limited radial migration through the granule cell layer. Shown on the lower panel is a global-view illustration of RGLs, neural progeny, and vasculature in the adult SGZ. The SGZ contains a dense bed of capillaries on which neuroblasts with tangential morphology migrate.

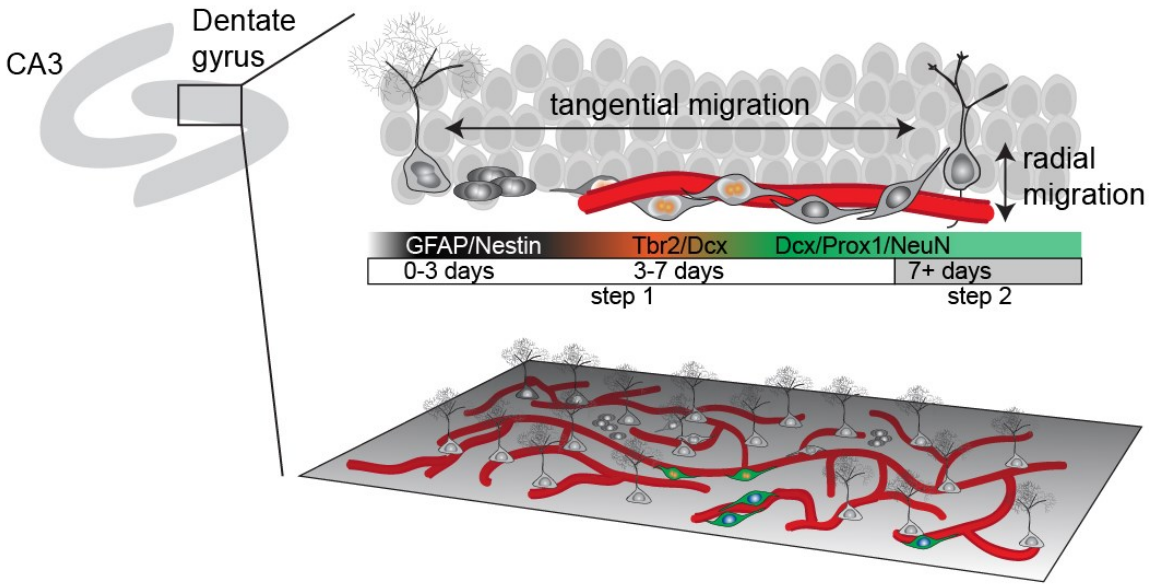
CA3
Dentate
gyrus
tangential migration
radial
migration
GFAP/Nestin
Tbr2/Dcx
Dcx/Prox1/NeuN
0-3 days
3-7 days
7+ days
step 1
step 2

Our finding of dominant tangential migration of neural precursors of glutamatergic dentate granule cells in the adult brain is a departure from the classical radial unit hypothesis of early cortical development (Rakic, 2009). Although early studies described tangential neuronal migration of presumed excitatory cells in the embryonic cortex, they may have actually been describing tangentially migrating inhibitory neurons, which were discovered later (Marin and Rubenstein, 2001). Interestingly, several recent studies do support the notion that at least some rare (Britanova et al., 2006), although usually transient (Bielle et al., 2005; Teissier et al., 2010), populations of excitatory cortical neurons migrate tangentially in the developing brain. Tangential migration of neural precursors in the developing hippocampus has previously only been observed in early post-natal developmental stages, during which the hippocampus is still immature and marked by ongoing growth and development (Li and Pleasure, 2014; Seki et al., 2007). Radial and tangential migration modes may not be specific to a given cell type but depend instead on both intrinsic and extrinsic mechanisms. Indeed, in the cerebellum, inhibitory principal Purkinje neurons exhibit radial migration, whereas excitatory modulatory granule neurons migrate tangentially as well as radially (Komuro et al., 2001). A very small number of glutamatergic interneurons are also generated in the adult SVZ and migrate to the olfactory bulb (Brill et al., 2009). Motor neurons in the spinal cord possess both radial and tangential migration (Leber and Sanes, 1995). Additionally, neurons originating from the diencephalon can migrate tangentially to populate the amygdala, a telencephalic nucleus (Garcia-Moreno et al., 2010).

Here, we have for the first time described an example of tangential migration of neuronal precursors of excitatory principal neurons in the adult mammalian brain. The

magnitude of migration observed, although significant and not due to chance via cell displacement upon division, is much less than that of migrating SVZ neuroblasts or even radially migrating neocortical neurons. This may be due to differences in tissue architecture. Neuroblasts in the SVZ are born far from their target brain region and the neocortex is a multi-layered structure, both requiring cells to travel longer distances to populate all target regions. By comparison, the dentate gyrus is a thin single-layer sheet whereby newborn neurons were presumed, before the present study, to be born, develop, and integrate all in the same location. Due to the limitation of single-color reporters in resolving different clones and probabilities of clonality calculated from our simulations, we took an inherently conservative approach by imposing a 300 μm maximum for clone diameter. Our reported magnitude of tangential migration distance may therefore be an underestimation.

Vasculature has been previously proposed as a crucial niche component for adult neurogenesis in both SGZ and SVZ (Mirzadeh et al., 2008; Palmer et al., 2000; Shen et al., 2008; Tavazoie et al., 2008), however its functional role is not well-understood. We showed that neuroblasts exhibit several features of migrating cells, such as polarized organelle distribution, and there exists a tight, direct association between neuroblasts and vasculature at cellular and ultrastructural levels. Although our data leave open the possibility of vasculature-independent tangential migration, our findings suggest that one function of the vascularized niche is to support migration of neuronal progeny away from their parental origin. Interestingly, GABAergic neurons generated in the adult SVZ have also been shown to migrate along blood vessels in the rostral migratory stream (Snapyan et al., 2009; Whitman et al., 2009) and towards injury sites following stroke (Grade et al.,

2013). Thus, in the adult brain, vasculature may serve as a common substrate for migration of different neuronal subtypes. This mechanism to support cell migration may be important during early development, as vascular outgrowth often precedes neural outgrowth, and migrating cells can be found in regions lacking classic substrates such as glial fibers (Saghatelyan, 2009; Tam and Watts, 2010).

We and others have previously only been able to document radial migration during adult hippocampal neurogenesis (Altman, 1966; Duan et al., 2007), having been limited to population level analyses that lacked lineage relationship information of individual stem cells and their progeny. Our new approach permits clonal analysis of activating RGLs in the adult dentate gyrus using the *Ascl1*^{CreERT2} knock-in mouse line (Kim et al., 2011) and direct examination of cell dispersion of individual newborn progeny with respect to their parental RGL. With the high temporal and spatial resolution our approach allows, we were able to directly compare tangential and radial migration of single cells for the first time. Interestingly, the two forms of migration appeared to be temporally segregated, with tangential migration preceding and exceeding radial migration. Together, these data suggest that independent mechanisms may regulate the two modes of migration. Future studies combining our new clonal analysis with conditional gene inactivation could elucidate shared or independent molecular mechanisms governing different forms of migration.

We also developed a novel partial "whole-mount" preparation to optimize visualization of the SGZ niche and showed that the general population of neuroblasts is in close contact with the blood vessel network and exhibits polarized Golgi apparatus, characteristic of migrating cells. This technical advance will allow for systematic

characterization of the complete global architecture of the hippocampal niche in the future. Such a characterization could potentially reveal important motifs to understand the underlying structure of the vascular network and migrating cells we have observed. Ultimately, our technique can help broaden our knowledge of the general principles of neurogenic niches, especially in combination with knowledge gained from similar approaches in the adult SVZ (Mirzadeh et al., 2008; Shen et al., 2008; Tavazoie et al., 2008).

Our clonal analyses of activating radial glia-like neural stem cells suggest a new mode of neuronal migration during adult hippocampal neurogenesis. Given that adult neural stem cells are dynamically regulated by their local environment, including neuronal activity (Jang et al., 2013; Song et al., 2012), our findings have significant implications for understanding how individual neural stem cells could impact the function of the existing microcircuitry via delivery of newborn neurons that are primed to undergo a critical period of enhanced plasticity (Ge et al., 2007). Our findings also provide a new framework in which to investigate the aberrant migration of newborn granule cells under pathological conditions, such as epilepsy (Jessberger et al., 2007; Parent et al., 1997). In addition, the identification of a novel mode of glutamatergic cell migration tangentially along the vasculature suggests a new strategy to overcome current challenges in targeting glutamatergic neurons to injured or degenerating regions for successful cell transplantation therapy in the adult mammalian brain (Ladewig et al., 2014). Together, our results suggest that diverse modes of migration may be ubiquitous among different neuron classes in the adult mammalian brain, providing important

conceptual groundwork for future studies of neural development, plasticity, regeneration, repair and brain disorders.

Figure 19. A summary: neural development in the adult mouse hippocampus from stem cell to nerve cell.

The work I accomplished during graduate school, including the thesis work presented here, has contributed significant novel discoveries in neural development in the adult brain. I have found novel molecular and cellular mechanisms regulating adult neural stem cell quiescence and persistence (Chapter 3) (Zhou et al., 2018), division (Chapter 4), fate decision (Sun et al., 2015a), and newborn neuron migration (Chapter 5) (Sun et al., 2015b). I developed live imaging technology allowing real-time observation on single-cell behaviors (Chapter 4), as well as the ongoing work (not included in this thesis) where I utilize single-cell RNA sequencing technology with bioinformatics pipeline to identify novel key molecular signature during human hippocampal neurogenesis. Overall, my findings have great relevance to better understanding brain development and regenerative medicine.

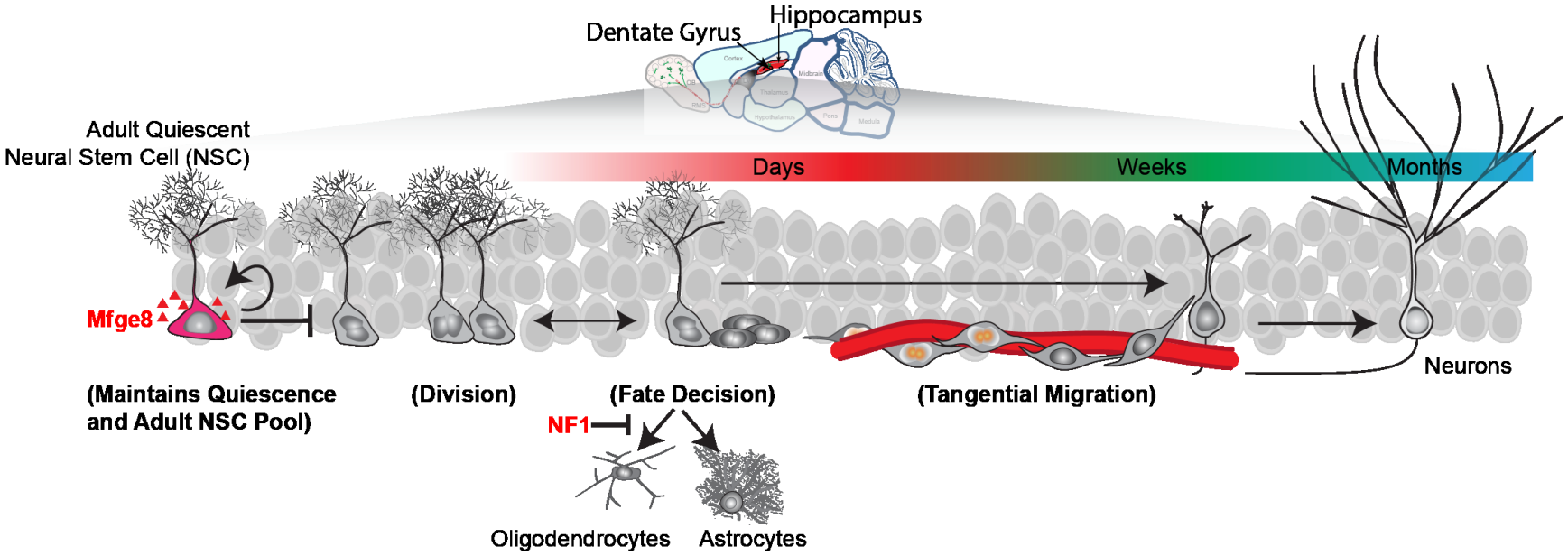
Dentate Gyrus
Hippocampus
Adult Quiescent
Neural Stem Cell (NSC)
Days
Weeks
Months
Mfge8
Neurons
(Maintains Quiescence
and Adult NSC Pool)
(Division)
(Fate Decision)
(Tangential Migration)
NF1
Oligodendrocytes
Astrocytes

References

Ahn, S., and Joyner, A.L. (2005). In vivo analysis of quiescent adult neural stem cells responding to Sonic hedgehog. Nature *437*, 894-897.

Altman, J. (1966). Autoradiographic and histological studies of postnatal neurogenesis. II. A longitudinal investigation of the kinetics, migration and transformation of cells incorporating tritiated thymidine in infant rats, with special reference to postnatal neurogenesis in some brain regions. The Journal of comparative neurology *1966*, 431-474.

Altman, J., and Das, G.D. (1965). Autoradiographic and histological evidence of postnatal hippocampal neurogenesis in rats. The Journal of comparative neurology *124*, 319-335.

Anacker, C., and Hen, R. (2017). Adult hippocampal neurogenesis and cognitive flexibility - linking memory and mood. Nat Rev Neurosci *18*, 335-346.

Asai, A., Aihara, E., Watson, C., Mourya, R., Mizuochi, T., Shivakumar, P., Phelan, K., Mayhew, C., Helmrath, M., Takebe, T.*, et al.* (2017). Paracrine signals regulate human liver organoid maturation from induced pluripotent stem cells. Development *144*, 1056-1064.

Barbosa, J.S., Sanchez-Gonzalez, R., Di Giaimo, R., Baumgart, E.V., Theis, F.J., Gotz, M., and Ninkovic, J. (2015). Neurodevelopment. Live imaging of adult neural stem cell behavior in the intact and injured zebrafish brain. Science *348*, 789-793.

Berg, D.A., Belnoue, L., Song, H., and Simon, A. (2013). Neurotransmitter-mediated control of neurogenesis in the adult vertebrate brain. Development *140*, 2548-2561.

Berg, D.A., Bond, A.M., Ming, G.L., and Song, H. (2018). Radial glial cells in the adult dentate gyrus: what are they and where do they come from? F1000Res *7*, 277.

Berg, D.A., Yoon, K.-J., Will, B., Xiao, A.Y., Kim, N.-S., Christian, K.M., Song, H., and Ming, G.-l. (2015). Tbr2-expressing intermediate progenitor cells in the adult mouse hippocampus are unipotent neuronal precursors with limited amplification capacity under homeostasis. Frontiers in Biology *in press*.

Bielle, F., Griveau, A., Narboux-Neme, N., Vigneau, S., Sigrist, M., Arber, S., Wassef, M., and Pierani, A. (2005). Multiple origins of Cajal-Retzius cells at the borders of the developing pallium. Nature neuroscience *8*, 1002-1012.

Bonaguidi, M.A., Wheeler, M.A., Shapiro, J.S., Stadel, R.P., Sun, G.J., Ming, G.L., and Song, H. (2011). In vivo clonal analysis reveals self-renewing and multipotent adult neural stem cell characteristics. Cell *145*, 1142-1155.

Bond, A.M., Ming, G.-l., and Song, H. (2015). Adult mammalian neural stem cells and neurogenesis: Five decades later. Cell Stem Cell *17*, 385-395.

Braun, S.M.G., and Jessberger, S. (2013). Adult neurogenesis in the mammalian brain. Frontiers in Biology *8*, 295-304.

Brill, M.S., Ninkovic, J., Winpenny, E., Hodge, R.D., Ozen, I., Yang, R., Lepier, A., Gascon, S., Erdelyi, F., Szabo, G.*, et al.* (2009). Adult generation of glutamatergic olfactory bulb interneurons. Nat Neurosci *12*, 1524-1533.

Britanova, O., Alifragis, P., Junek, S., Jones, K., Gruss, P., and Tarabykin, V. (2006). A novel mode of tangential migration of cortical projection neurons. Developmental biology *298*, 299-311.

Brooker, S.M., Bond, A.M., Peng, C.Y., and Kessler, J.A. (2016). beta1-integrin restricts astrocytic differentiation of adult hippocampal neural stem cells. Glia *64*, 1235-1251.

Calzolari, F., Michel, J., Baumgart, E.V., Theis, F., Gotz, M., and Ninkovic, J. (2015). Fast clonal expansion and limited neural stem cell self-renewal in the adult subependymal zone. Nat Neurosci *18*, 490-492.

Cheung, T.H., and Rando, T.A. (2013). Molecular regulation of stem cell quiescence. Nature reviews Molecular cell biology *14*, 329-340.

Christian, K.M., Song, H., and Ming, G.L. (2014). Functions and dysfunctions of adult hippocampal neurogenesis. Annual review of neuroscience *37*, 243-262.

Corbin, J.G., Nery, S., and Fishell, G. (2001). Telencephalic cells take a tangent: non-radial migration in the mammalian forebrain. Nature neuroscience *4 Suppl*, 1177-1182.

Delgado, A.C., Ferron, S.R., Vicente, D., Porlan, E., Perez-Villalba, A., Trujillo, C.M., D'Ocon, P., and Farinas, I. (2014). Endothelial NT-3 delivered by vasculature and CSF promotes quiescence of subependymal neural stem cells through nitric oxide induction. Neuron *83*, 572-585.

Duan, X., Chang, J.H., Ge, S., Faulkner, R.L., Kim, J.Y., Kitabatake, Y., Liu, X.B., Yang, C.H., Jordan, J.D., Ma, D.K.*, et al.* (2007). Disrupted-In-Schizophrenia 1 regulates integration of newly generated neurons in the adult brain. Cell *130*, 1146-1158.

Dulken, B.W., Leeman, D.S., Boutet, S.C., Hebestreit, K., and Brunet, A. (2017). Single-Cell Transcriptomic Analysis Defines Heterogeneity and Transcriptional Dynamics in the Adult Neural Stem Cell Lineage. Cell Rep *18*, 777-790.

Encinas, J.M., Michurina, T.V., Peunova, N., Park, J.H., Tordo, J., Peterson, D.A., Fishell, G., Koulakov, A., and Enikolopov, G. (2011). Division-coupled astrocytic

differentiation and age-related depletion of neural stem cells in the adult hippocampus. Cell stem cell *8*, 566-579.

Encinas, J.M., Vaahtokari, A., and Enikolopov, G. (2006). Fluoxetine targets early progenitor cells in the adult brain. Proc Natl Acad Sci U S A *103*, 8233-8238.

Eriksson, P.S., Perfilieva, E., Bjork-Eriksson, T., Alborn, A.M., Nordborg, C., Peterson, D.A., and Gage, F.H. (1998). Neurogenesis in the adult human hippocampus. Nature medicine *4*, 1313-1317.

Fricker, M., Neher, J.J., Zhao, J.W., Thery, C., Tolkovsky, A.M., and Brown, G.C. (2012). MFG-E8 mediates primary phagocytosis of viable neurons during neuroinflammation. J Neurosci *32*, 2657-2666.

Fuentealba, L.C., Obernier, K., and Alvarez-Buylla, A. (2012). Adult neural stem cells bridge their niche. Cell stem cell *10*, 698-708.

Fuentealba, L.C., Rompani, S.B., Parraguez, J.I., Obernier, K., Romero, R., Cepko, C.L., and Alvarez-Buylla, A. (2015). Embryonic Origin of Postnatal Neural Stem Cells. Cell *161*, 1644-1655.

Furutachi, S., Miya, H., Watanabe, T., Kawai, H., Yamasaki, N., Harada, Y., Imayoshi, I., Nelson, M., Nakayama, K.I., Hirabayashi, Y*., et al.* (2015). Slowly dividing neural progenitors are an embryonic origin of adult neural stem cells. Nat Neurosci *18*, 657-665.

Gage, F.H. (2000). Mammalian neural stem cells. Science *287*, 1433-1438.

Garcia-Moreno, F., Pedraza, M., Di Giovannantonio, L.G., Di Salvio, M., Lopez-Mascaraque, L., Simeone, A., and De Carlos, J.A. (2010). A neuronal migratory pathway crossing from diencephalon to telencephalon populates amygdala nuclei. Nature neuroscience *13*, 680-689.

Ge, S., Yang, C.H., Hsu, K.S., Ming, G.L., and Song, H. (2007). A critical period for enhanced synaptic plasticity in newly generated neurons of the adult brain. Neuron *54*, 559-566.

Ghashghaei, H.T., Lai, C., and Anton, E.S. (2007). Neuronal migration in the adult brain: are we there yet? Nature reviews Neuroscience *8*, 141-151.

Goh, E.L., Young, J.K., Kuwako, K., Tessier-Lavigne, M., He, Z., Griffin, J.W., and Ming, G.L. (2008). beta1-integrin mediates myelin-associated glycoprotein signaling in neuronal growth cones. Molecular brain *1*, 10.

Goncalves, J.T., Schafer, S.T., and Gage, F.H. (2016). Adult Neurogenesis in the Hippocampus: From Stem Cells to Behavior. Cell *167*, 897-914.

Gotz, M., and Huttner, W.B. (2005). The cell biology of neurogenesis. Nature reviews Molecular cell biology *6*, 777-788.

Grade, S., Weng, Y.C., Snapyan, M., Kriz, J., Malva, J.O., and Saghatelyan, A. (2013). Brain-derived neurotrophic factor promotes vasculature-associated migration of neuronal precursors toward the ischemic striatum. PloS one *8*, e55039.

Groszer, M., Erickson, R., Scripture-Adams, D.D., Dougherty, J.D., Le Belle, J., Zack, J.A., Geschwind, D.H., Liu, X., Kornblum, H.I., and Wu, H. (2006). PTEN negatively regulates neural stem cell self-renewal by modulating G0-G1 cell cycle entry. Proceedings of the National Academy of Sciences of the United States of America *103*, 111-116.

Hanayama, R., Tanaka, M., Miwa, K., Shinohara, A., Iwamatsu, A., and Nagata, S. (2002). Identification of a factor that links apoptotic cells to phagocytes. Nature *417*, 182-187.

Hanayama, R., Tanaka, M., Miyasaka, K., Aozasa, K., Koike, M., Uchiyama, Y., and Nagata, S. (2004). Autoimmune disease and impaired uptake of apoptotic cells in MFG-E8-deficient mice. Science *304*, 1147-1150.

Hochgerner, H., Zeisel, A., Lonnerberg, P., and Linnarsson, S. (2018). Conserved properties of dentate gyrus neurogenesis across postnatal development revealed by single-cell RNA sequencing. Nature neuroscience *21*, 290-299.

Homem, C.C., Repic, M., and Knoblich, J.A. (2015). Proliferation control in neural stem and progenitor cells. Nature reviews Neuroscience *16*, 647-659.

Horsley, V., Aliprantis, A.O., Polak, L., Glimcher, L.H., and Fuchs, E. (2008). NFATc1 balances quiescence and proliferation of skin stem cells. Cell *132*, 299-310.

Hu, X.L., Chen, G., Zhang, S., Zheng, J., Wu, J., Bai, Q.R., Wang, Y., Li, J., Wang, H., Feng, H.*, et al.* (2017). Persistent Expression of VCAM1 in Radial Glial Cells Is Required for the Embryonic Origin of Postnatal Neural Stem Cells. Neuron *95*, 309-325 e306.

Jang, M.H., Bonaguidi, M.A., Kitabatake, Y., Sun, J., Song, J., Kang, E., Jun, H., Zhong, C., Su, Y., Guo, J.U.*, et al.* (2013). Secreted frizzled-related protein 3 regulates activity-dependent adult hippocampal neurogenesis. Cell stem cell *12*, 215-223.

Jensen, K.B., Collins, C.A., Nascimento, E., Tan, D.W., Frye, M., Itami, S., and Watt, F.M. (2009). Lrig1 expression defines a distinct multipotent stem cell population in mammalian epidermis. Cell stem cell *4*, 427-439.

Jessberger, S., Zhao, C., Toni, N., Clemenson, G.D., Jr., Li, Y., and Gage, F.H. (2007). Seizure-associated, aberrant neurogenesis in adult rats characterized with retrovirus-

mediated cell labeling. The Journal of neuroscience : the official journal of the Society for Neuroscience *27*, 9400-9407.

Ka, M., Condorelli, G., Woodgett, J.R., and Kim, W.Y. (2014). mTOR regulates brain morphogenesis by mediating GSK3 signaling. Development *141*, 4076-4086.

Karadottir, R.T., and Kuo, C.T. (2018). Neuronal Activity-Dependent Control of Postnatal Neurogenesis and Gliogenesis. Annual review of neuroscience.

Kawaguchi, D., Furutachi, S., Kawai, H., Hozumi, K., and Gotoh, Y. (2013). Dll1 maintains quiescence of adult neural stem cells and segregates asymmetrically during mitosis. Nature communications *4*, 1880.

Kempermann, G., and Gage, F.H. (1999). New nerve cells for the adult brain. Sci Am *280*, 48-53.

Khalifeh-Soltani, A., Ha, A., Podolsky, M.J., McCarthy, D.A., McKleroy, W., Azary, S., Sakuma, S., Tharp, K.M., Wu, N., Yokosaki, Y.*, et al.* (2016). alpha8beta1 integrin regulates nutrient absorption through an Mfge8-PTEN dependent mechanism. Elife *5*.

Khalifeh-Soltani, A., McKleroy, W., Sakuma, S., Cheung, Y.Y., Tharp, K., Qiu, Y., Turner, S.M., Chawla, A., Stahl, A., and Atabai, K. (2014). Mfge8 promotes obesity by mediating the uptake of dietary fats and serum fatty acids. Nature medicine *20*, 175-183.

Khlghatyan, J., and Saghatelyan, A. (2012). Time-lapse imaging of neuroblast migration in acute slices of the adult mouse forebrain. J Vis Exp, e4061.

Kim, E.J., Ables, J.L., Dickel, L.K., Eisch, A.J., and Johnson, J.E. (2011). Ascl1 (Mash1) defines cells with long-term neurogenic potential in subgranular and subventricular zones in adult mouse brain. PloS one *6*, e18472.

Kim, J.H., Han, G.C., Seo, J.Y., Park, I., Park, W., Jeong, H.W., Lee, S.H., Bae, S.H., Seong, J., Yum, M.K., *et al.* (2016). Sex hormones establish a reserve pool of adult muscle stem cells. Nat Cell Biol *18*, 930-940.

Kim, J.Y., Duan, X., Liu, C.Y., Jang, M.H., Guo, J.U., Pow-anpongkul, N., Kang, E., Song, H., and Ming, G.L. (2009). DISC1 regulates new neuron development in the adult brain via modulation of AKT-mTOR signaling through KIAA1212. Neuron *63*, 761-773.

Knoblich, J.A. (2008). Mechanisms of asymmetric stem cell division. Cell *132*, 583-597.

Komuro, H., Yacubova, E., Yacubova, E., and Rakic, P. (2001). Mode and tempo of tangential cell migration in the cerebellar external granular layer. The Journal of neuroscience : the official journal of the Society for Neuroscience *21*, 527-540.

Ladewig, J., Koch, P., and Brustle, O. (2014). Auto-attraction of neural precursors and their neuronal progeny impairs neuronal migration. Nature neuroscience *17*, 24-26.

Lay, K., Kume, T., and Fuchs, E. (2016). FOXC1 maintains the hair follicle stem cell niche and governs stem cell quiescence to preserve long-term tissue-regenerating potential. Proceedings of the National Academy of Sciences of the United States of America *113*, E1506-1515.

Leber, S.M., and Sanes, J.R. (1995). Migratory paths of neurons and glia in the embryonic chick spinal cord. The Journal of neuroscience : the official journal of the Society for Neuroscience *15*, 1236-1248.

Li, G., and Pleasure, S.J. (2014). The development of hippocampal cellular assemblies. Wiley interdisciplinary reviews Developmental biology *3*, 165-177.

Lie, D.C., Colamarino, S.A., Song, H.J., Desire, L., Mira, H., Consiglio, A., Lein, E.S., Jessberger, S., Lansford, H., Dearie, A.R., *et al.* (2005). Wnt signalling regulates adult hippocampal neurogenesis. Nature *437*, 1370-1375.

Llorens-Bobadilla, E., Zhao, S., Baser, A., Saiz-Castro, G., Zwadlo, K., and Martin-Villalba, A. (2015). Single-Cell Transcriptomics Reveals a Population of Dormant Neural Stem Cells that Become Activated upon Brain Injury. Cell stem cell *17*, 329-340.

Lois, C., and Alvarez-Buylla, A. (1994). Long-distance neuronal migration in the adult mammalian brain. Science *264*, 1145-1148.

Ma, D.K., Chiang, C.H., Ponnusamy, K., Ming, G.L., and Song, H. (2008). G9a and Jhdm2a regulate embryonic stem cell fusion-induced reprogramming of adult neural stem cells. Stem Cells *26*, 2131-2141.

Marin, O., and Rubenstein, J.L. (2001). A long, remarkable journey: tangential migration in the telencephalon. Nature reviews Neuroscience *2*, 780-790.

Mills, E.A., Davis, C.H., Bushong, E.A., Boassa, D., Kim, K.Y., Ellisman, M.H., and Marsh-Armstrong, N. (2015). Astrocytes phagocytose focal dystrophies from shortening myelin segments in the optic nerve of Xenopus laevis at metamorphosis. Proceedings of the National Academy of Sciences of the United States of America *112*, 10509-10514.

Ming, G.L., and Song, H. (2011). Adult neurogenesis in the mammalian brain: significant answers and significant questions. Neuron *70*, 687-702.

Mira, H., Andreu, Z., Suh, H., Lie, D.C., Jessberger, S., Consiglio, A., San Emeterio, J., Hortiguela, R., Marques-Torrejon, M.A., Nakashima, K., *et al.* (2010). Signaling through BMPR-IA regulates quiescence and long-term activity of neural stem cells in the adult hippocampus. Cell Stem Cell *7*, 78-89.

Mirzadeh, Z., Merkle, F.T., Soriano-Navarro, M., Garcia-Verdugo, J.M., and Alvarez-Buylla, A. (2008). Neural stem cells confer unique pinwheel architecture to the ventricular surface in neurogenic regions of the adult brain. Cell stem cell *3*, 265-278.

Morrison, S.J., and Kimble, J. (2006). Asymmetric and symmetric stem-cell divisions in development and cancer. Nature *441*, 1068-1074.

Mosher, K.I., Andres, R.H., Fukuhara, T., Bieri, G., Hasegawa-Moriyama, M., He, Y., Guzman, R., and Wyss-Coray, T. (2012). Neural progenitor cells regulate microglia functions and activity. Nature neuroscience *15*, 1485-1487.

Muzumdar, M.D., Tasic, B., Miyamichi, K., Li, L., and Luo, L. (2007). A global double-fluorescent Cre reporter mouse. Genesis *45*, 593-605.

Nagata, S., Hanayama, R., and Kawane, K. (2010). Autoimmunity and the clearance of dead cells. Cell *140*, 619-630.

Neher, J.J., Emmrich, J.V., Fricker, M., Mander, P.K., Thery, C., and Brown, G.C. (2013). Phagocytosis executes delayed neuronal death after focal brain ischemia. Proceedings of the National Academy of Sciences of the United States of America *110*, E4098-4107.

Ninkovic, J., and Gotz, M. (2007). Signaling in adult neurogenesis: from stem cell niche to neuronal networks. Curr Opin Neurobiol *17*, 338-344.

Paez-Gonzalez, P., Asrican, B., Rodriguez, E., and Kuo, C.T. (2014). Identification of distinct ChAT(+) neurons and activity-dependent control of postnatal SVZ neurogenesis. Nat Neurosci *17*, 934-942.

Paik, J.H., Ding, Z., Narurkar, R., Ramkissoon, S., Muller, F., Kamoun, W.S., Chae, S.S., Zheng, H., Ying, H., Mahoney, J.*, et al.* (2009). FoxOs cooperatively regulate diverse pathways governing neural stem cell homeostasis. Cell stem cell *5*, 540-553.

Palmer, T.D., Willhoite, A.R., and Gage, F.H. (2000). Vascular niche for adult hippocampal neurogenesis. The Journal of comparative neurology *425*, 479-494.

Parent, J.M., Yu, T.W., Leibowitz, R.T., Geschwind, D.H., Sloviter, R.S., and Lowenstein, D.H. (1997). Dentate granule cell neurogenesis is increased by seizures and contributes to aberrant network reorganization in the adult rat hippocampus. The Journal of neuroscience : the official journal of the Society for Neuroscience *17*, 3727-3738.

Paul, A., Chaker, Z., and Doetsch, F. (2017). Hypothalamic regulation of regionally distinct adult neural stem cells and neurogenesis. Science *356*, 1383-1386.

Pilz, G.A., Bottes, S., Betizeau, M., Jorg, D.J., Carta, S., Simons, B.D., Helmchen, F., and Jessberger, S. (2018). Live imaging of neurogenesis in the adult mouse hippocampus. Science *359*, 658-662.

Pollen, A.A., Nowakowski, T.J., Chen, J., Retallack, H., Sandoval-Espinosa, C., Nicholas, C.R., Shuga, J., Liu, S.J., Oldham, M.C., Diaz, A.*, et al.* (2015). Molecular identity of human outer radial glia during cortical development. Cell *163*, 55-67.

Porcheri, C., Suter, U., and Jessberger, S. (2014). Dissecting integrin-dependent regulation of neural stem cell proliferation in the adult brain. J Neurosci *34*, 5222-5232.

Rakic, P. (2009). Evolution of the neocortex: a perspective from developmental biology. Nature reviews Neuroscience *10*, 724-735.

Ramon y Cajal, S. (1930). Degeneration and regeneration of the nervous system. Nature *125*, 230-231.

Raymond, A., Ensslin, M.A., and Shur, B.D. (2009). SED1/MFG-E8: a bi-motif protein that orchestrates diverse cellular interactions. J Cell Biochem *106*, 957-966.

Renault, V.M., Rafalski, V.A., Morgan, A.A., Salih, D.A., Brett, J.O., Webb, A.E., Villeda, S.A., Thekkat, P.U., Guillerey, C., Denko, N.C.*, et al.* (2009). FoxO3 regulates neural stem cell homeostasis. Cell stem cell *5*, 527-539.

Saghatelyan, A. (2009). Role of blood vessels in the neuronal migration. Seminars in cell & developmental biology *20*, 744-750.

Sato, A., Sunayama, J., Matsuda, K., Tachibana, K., Sakurada, K., Tomiyama, A., Kayama, T., and Kitanaka, C. (2010). Regulation of neural stem/progenitor cell maintenance by PI3K and mTOR. Neurosci Lett *470*, 115-120.

Seib, D.R., Corsini, N.S., Ellwanger, K., Plaas, C., Mateos, A., Pitzer, C., Niehrs, C., Celikel, T., and Martin-Villalba, A. (2013). Loss of Dickkopf-1 restores neurogenesis in old age and counteracts cognitive decline. Cell stem cell *12*, 204-214.

Seki, T., Namba, T., Mochizuki, H., and Onodera, M. (2007). Clustering, migration, and neurite formation of neural precursor cells in the adult rat hippocampus. The Journal of comparative neurology *502*, 275-290.

Seri, B., Garcia-Verdugo, J.M., Collado-Morente, L., McEwen, B.S., and Alvarez-Buylla, A. (2004). Cell types, lineage, and architecture of the germinal zone in the adult dentate gyrus. The Journal of comparative neurology *478*, 359-378.

Shaw, R.J., Bardeesy, N., Manning, B.D., Lopez, L., Kosmatka, M., DePinho, R.A., and Cantley, L.C. (2004). The LKB1 tumor suppressor negatively regulates mTOR signaling. Cancer Cell *6*, 91-99.

Shen, Q., Wang, Y., Kokovay, E., Lin, G., Chuang, S.M., Goderie, S.K., Roysam, B., and Temple, S. (2008). Adult SVZ stem cells lie in a vascular niche: a quantitative analysis of niche cell-cell interactions. Cell Stem Cell *3*, 289-300.

Shin, J., Berg, D.A., Zhu, Y., Shin, J.Y., Song, J., Bonaguidi, M.A., Enikolopov, G., Nauen, D.W., Christian, K.M., Ming, G.L.*, et al.* (2015). Single-Cell RNA-Seq with Waterfall Reveals Molecular Cascades underlying Adult Neurogenesis. Cell stem cell *17*, 360-372.

Snapyan, M., Lemasson, M., Brill, M.S., Blais, M., Massouh, M., Ninkovic, J., Gravel, C., Berthod, F., Gotz, M., Barker, P.A.*, et al.* (2009). Vasculature guides migrating neuronal precursors in the adult mammalian forebrain via brain-derived neurotrophic factor signaling. The Journal of neuroscience : the official journal of the Society for Neuroscience *29*, 4172-4188.

Song, H., Stevens, C.F., and Gage, F.H. (2002). Astroglia induce neurogenesis from adult neural stem cells. Nature *417*, 39-44.

Song, J., Zhong, C., Bonaguidi, M.A., Sun, G.J., Hsu, D., Gu, Y., Meletis, K., Huang, Z.J., Ge, S., Enikolopov, G.*, et al.* (2012). Neuronal circuitry mechanism regulating adult quiescent neural stem-cell fate decision. Nature *489*, 150-154.

Spalding, K.L., Bergmann, O., Alkass, K., Bernard, S., Salehpour, M., Huttner, H.B., Bostrom, E., Westerlund, I., Vial, C., Buchholz, B.A.*, et al.* (2013). Dynamics of hippocampal neurogenesis in adult humans. Cell *153*, 1219-1227.

Sun, G.J., Zhou, Y., Ito, S., Bonaguidi, M.A., Stein-O'Brien, G., Kawasaki, N.K., Modak, N., Zhu, Y., Ming, G.L., and Song, H. (2015a). Latent tri-lineage potential of adult

hippocampal neural stem cells revealed by Nf1 inactivation. Nature neuroscience *18*, 1722-1724.

Sun, G.J., Zhou, Y., Stadel, R.P., Moss, J., Yong, J.H., Ito, S., Kawasaki, N.K., Phan, A.T., Oh, J.H., Modak, N.*, et al.* (2015b). Tangential migration of neuronal precursors of glutamatergic neurons in the adult mammalian brain. Proceedings of the National Academy of Sciences of the United States of America *112*, 9484-9489.

Tam, S.J., and Watts, R.J. (2010). Connecting vascular and nervous system development: angiogenesis and the blood-brain barrier. Annual review of neuroscience *33*, 379-408.

Tavazoie, M., Van der Veken, L., Silva-Vargas, V., Louissaint, M., Colonna, L., Zaidi, B., Garcia-Verdugo, J.M., and Doetsch, F. (2008). A specialized vascular niche for adult neural stem cells. Cell stem cell *3*, 279-288.

Teissier, A., Griveau, A., Vigier, L., Piolot, T., Borello, U., and Pierani, A. (2010). A novel transient glutamatergic population migrating from the pallial-subpallial boundary contributes to neocortical development. The Journal of neuroscience : the official journal of the Society for Neuroscience *30*, 10563-10574.

Tong, C.K., Chen, J., Cebrian-Silla, A., Mirzadeh, Z., Obernier, K., Guinto, C.D., Tecott, L.H., Garcia-Verdugo, J.M., Kriegstein, A., and Alvarez-Buylla, A. (2014). Axonal control of the adult neural stem cell niche. Cell Stem Cell *14*, 500-511.

Toni, N., Teng, E.M., Bushong, E.A., Aimone, J.B., Zhao, C., Consiglio, A., van Praag, H., Martone, M.E., Ellisman, M.H., and Gage, F.H. (2007). Synapse formation on neurons born in the adult hippocampus. Nat Neurosci *10*, 727-734.

Whitman, M.C., Fan, W., Rela, L., Rodriguez-Gil, D.J., and Greer, C.A. (2009). Blood vessels form a migratory scaffold in the rostral migratory stream. The Journal of comparative neurology *516*, 94-104.

Xu, Q., Fitzsimmons, B., Steinauer, J., O'Neill, A., Newton, A.C., Hua, X.Y., and Yaksh, T.L. (2011). Spinal phosphinositide 3-kinase-Akt-mammalian target of rapamycin signaling cascades in inflammation-induced hyperalgesia. The Journal of neuroscience : the official journal of the Society for Neuroscience *31*, 2113-2124.

Yan, L., Yang, M., Guo, H., Yang, L., Wu, J., Li, R., Liu, P., Lian, Y., Zheng, X., Yan, J.*, et al.* (2013). Single-cell RNA-Seq profiling of human preimplantation embryos and embryonic stem cells. Nat Struct Mol Biol *20*, 1131-1139.

Yuzwa, S.A., Borrett, M.J., Innes, B.T., Voronova, A., Ketela, T., Kaplan, D.R., Bader, G.D., and Miller, F.D. (2017). Developmental Emergence of Adult Neural Stem Cells as Revealed by Single-Cell Transcriptional Profiling. Cell Rep *21*, 3970-3986.

Zeisel, A., Munoz-Manchado, A.B., Codeluppi, S., Lonnerberg, P., La Manno, G., Jureus, A., Marques, S., Munguba, H., He, L., Betsholtz, C.*, et al.* (2015). Brain structure. Cell types in the mouse cortex and hippocampus revealed by single-cell RNA-seq. Science *347*, 1138-1142.

Zhou, Y., Bond, A.M., Shade, J.E., Zhu, Y., Davis, C.O., Wang, X., Su, Y., Yoon, K.J., Phan, A.T., Chen, W.J.*, et al.* (2018). Autocrine Mfge8 Signaling Prevents Developmental Exhaustion of the Adult Neural Stem Cell Pool. Cell stem cell.

Curriculum Vitae

YI ZHOU

BCMB Graduate Program | Departments of Neuroscience and Neurology |

Institute for Cellular Engineering

The Johns Hopkins University, School of Medicine

Department of Neuroscience | Hongjun Song Lab

University of Pennsylvania, Perelman School of Medicine

Address: 415 Curie Boulevard, Suite 118 | Philadelphia PA 19104 | U.S.A.

Phone: +1 (410) 929-1033 | Email: zhou.joey.yi@gmail.com | LinkedIn

Research Summary

Yi Zhou is a productive neuroscientist from the Johns Hopkins University, School of Medicine. He performs innovative research and has obtained breakthroughs in understanding the brain and brain repair. In particular, he has made significant contributions investigating mechanisms underlying adult neural stem cells and neurogenesis, neural development, stroke, and neural protection (*P.N.A.S.*, 2014; *P.N.A.S.*, 2015; *Nature Neuroscience*, 2015; *Cell Stem Cell*, 2018). Yi, a recipient of fellowships/awards from American Heart Association and New York Academy of Sciences, was invited to present at international conferences, including the Society for Neuroscience. His long term career interests lie in bridging science and technology breakthroughs with business resources to generate impact.

Education

2012-2018	Ph.D. expected	BCMB Program Mentor: Hongjun Song, Ph.D.	Johns Hopkins School of Medicine
2008-2012	B.S.	Biological Sciences	East China Normal University
2008-2012	B.S.	Microbiology	Colorado State University

Research Experience

2017-present Ph.D. student in Hongjun Song lab, University of Pennsylvania

- Lab moved
- Investigate key molecular signature defining human neural stem cells and progenitors

2013-2017 Ph.D. student in Hongjun Song lab, Johns Hopkins

- Overall goal is to identify key cellular and molecular mechanisms regulating neural stem cells and neurogenesis
- Published 3 (first or second author) papers in leading peer-reviewed journals
- Thesis committee: Jeremy Nathans (Chair), Seth Blackshaw, and Erika Matunis
- Funding: American Heart Association Fellowship

2013 Rotation student in Alex L. Kolodkin lab, Johns Hopkins/HHMI

- Research topic: semaphorin 6A and plexin A2 regulate dendritic development of mouse retinal starburst amacrine cells

2012 Rotation student in Nicholas Marsh-Armstrong lab, Johns Hopkins

- Contributed to discovery of local astroyctes' transmitophagy in retina, which suggested novel neuroprotection mechanism (co-authorship in *P.N.A.S.*)

2011-2012 Undergraduate researcher in James R. Bamburg lab, Colorado State

- Research topic: human Huntington's disease progression by accumulation of cofilin-actin rods, a stress-induced protein
- Funding: International Merit Work-Study Award

2011 Summer intern in John O'Brien lab, University of Texas at Houston

- Collaboration project with John Rash Lab. Identified colocalization of retinal connexin 34.7 and 35 using immunocytochemistry
- Funding: Summer Internship Award

2010-2012 Undergraduate researcher in John E. Rash lab, Colorado State

- Research topic: mechanisms underlying retinal light response, focusing on gap junctions' role in electrical signal transduction between photoreceptors in retina

- Identified ultrastructure evidence of presence of retinal connexin 34.7 and 35
- Funding: Experiential Learning Stipend

Fellowship

2016-2018 American Heart Association Fellowship (**Top 10% nationally**)

2012-2016 Johns Hopkins BCMB Full Fellowship

Selected Peer-Reviewed Publications

1. **Zhou, Y.**, Bond, A.m., Shade, J.e., Zhu, Y., Davis, C.-h.O., Wang, X., Yoon, K.-j., Su, Y., Phan, A.t., Chen, W.j., Oh, J.h., Marsh-Armstrong, N., Atabai, K., Ming, G.-l., Song, H. Autocrine Mfge8 Signaling Prevents Developmental Exhaustion of the Adult Neural Stem Cell Pool. (2018) *Cell Stem Cell*. 23(3), 444-452 (PMCID: PMC6128767)
   - Highlighted in *Cell Stem Cell*

2. Sun, G. j*, **Zhou, Y.***, Stadel, R. p*, Moss, J., Yong, J.H. a, Ito, S., Kawasaki, N. k, Phan, A. t, Oh, J. h, Modak, N., Reed, R. r, Toni, N., Song, H., Ming, G.-l. Tangential migration of neuronal precursors of glutamatergic neurons in the adult mammalian brain. (2015) *P.N.A.S.*, 112(30), 9484-9 (PMCID: PMC4522763) (***co-first authorship**)

3. Sun, G. j, **Zhou, Y.**, Ito, S., Bonaguidi, M. a, O'Brien, G. s, Kawasaki, N., Modak, N., Zhu, Y., Ming, G.-l., Song, H. Latent tri-lineage potential of adult neural stem cells in the hippocampus revealed by Nf1 inactivation. (2015) *Nature Neuroscience*, 18, 1722-4 (PMCID: PMC4661096)
    - Highlighted in *Nature Reviews Neuroscience*, and *F1000 Research*
    - Earned a *Faculty of 1000* Factor of 2.0

4. Davis, C.-H.O., Kim, K.-Y., Bushong, E. a, Mills, E. a, Boassa, D., Shih, T., Kinebuchi, M., Phan, S., **Zhou, Y.**, Bihlmeyer, N. a, Nguyen, J.V., Jin, Y., Ellisman, M.H., Marsh-Armstrong, N. (2014). Transcellular degradation of axonal mitochondria. *P.N.A.S.*, 111(26), 9633-8 (PMCID: PMC4084443)
    - Featured as cover article
    - Highlighted in *Science*, *The Scientist*, and *Science Daily*
    - Earned a *Faculty of 1000* Factor of 3.0
    - Cited over 150 times by peer-reviewed journals

5. Minamide, L. s, Bernstein, B. w, Shaw, A. e, Mi, J., Walsh, K. p, **Zhou, Y.**, Bamburg, J. r. *Manuscript in review*.

Conference Oral Presentations

Zhou, Y., Sun, G.j., Ming, G.-l., Song, H. Latent tri-lineage potential of adult hippocampal neural stem cells revealed by Nf1 inactivation. The 12th Annual

Christopher Reeve "Hot Topics" in Stem Cell Biology Symposium, Society for Neuroscience 2015, Chicago, IL. (2015). *Received Travel Award.*

Zhou, Y., Sun, G.j., Ming, G.-l., Song, H. Latent tri-lineage potential of adult hippocampal neural stem cells revealed by Nf1 inactivation. 2015 BCMB Annual Retreat, St. Michaels, MD. (2015)

Zhou, Y., Ming, G.-l., Song, H. Dynamics of adult neural stem and progenitor cells. 'Journey through Science', New York Academy of Sciences, New York City, NY. (2013). *Received 'Excellence in Research' Award (**Top 3/78**)*

Zhou, Y., Sun, G.j., Ming, G.-l., Song, H. Tangential migration of neuronal precursors of glutamatergic neurons in the adult mammalian brain. 2013 Johns Hopkins BCMB Annual Retreat, St. Michaels, MD. (2013). *Received Presentation Award (**Top 5%**)*

Honors and Awards

2008	F500 Scholarship (**Top 0.5%**, highest-honor graduate), High School Affiliated to Fudan University, Shanghai, China
2010	Second Class Scholarship for Outstanding Students (**Top 10%**), China
2010-2012	International Partnership Scholarship (**Top 2%**), Colorado State
2010-2012	Multiple Dean's Honor Lists (**Top 10%**), Colorado State
2011/7/22	GRE General: Verbal 730/800 (**94% below**) + Quantitative 800/800 (**98% below**)

2013 'Excellence in Research' Award (**Top 3/78**), New York Academy of Sciences

Invited Peer-Reviews for Scientific Journals

2015-present *Scientific Reports (SREP)*

2015-present *Cellular and Molecular Neurobiology (CEMN)*

2015-present *Advances in Bioscience and Biotechnology (ABB)*

2017-present *Computers and Mathematics with Applications (CAMWA)*

2017-present *Journal of Neurological Research and Therapy (JNRT)*

2017-present *The Scientific Pages of Minimally Invasive Surgeries (SPMIS)*

2017-present *Data in Brief (DIB)*

2018-present *Annals of Case Reports (ACRT)*

Journal Editorial Board

2017-present *Peer Reviewed Academia Sciences (PRAS)*

2018-present *Cient Periodique Medicine (CPQ Medicine)*

2018-present *Journal of Spine & Neurological Disorders (JSND)*

Teaching and Mentoring

2011 Served as teaching assistant in General Microbiology, Colorado State

2013-present Mentor students for research. Students' list,

- Johns Hopkins rotation student: Jing Hui (Adeline) Yong (now in Richard Huganir lab)

- Johns Hopkins undergraduate students: Shiori Ito (now medical student at Shiga University, Japan), Zhengyun Ji (now master's student at McGill University), Nick Kawasaki, Nik Modak, Justin Oh, Alex Phan (now medical student at St. George's University), Jamie Shade

Work Experience

2016 Sage Growth Partners, Baltimore, MD Consulting Associate (Intern)

A consulting firm specialized in healthcare strategy, technology and marketing.

- Streamlined an innovative approach to increase efficiency by 60% in identifying market size and 2,800+ potential buyer's profiles for a healthcare data service provider.
- Built market sizing model and competitive overview for 3 healthcare products. Interviewed physicians and hospitals managers on their market perception.
- Wrote industrial report on telehealth, analyzing market SWOT and growth potential.
- Contributed to report forecasting future of healthcare in the new administration.

2016 T. Rowe Price, Baltimore, MD Equity Research Analyst Intern

Didactic and experiential training in buy and sell sides of equity research.

- Analyzed biotechnology small-/mid- capital companies emphasizing fundamentals, competitive advantage, valuation and other quantitative and qualitative factors to identify stock to competitively pitch.
- Placed **Top 3**/10 groups. The stock exceeded target price by 28% between Pick and Pitch.

2016 NextCure Inc., Beltsville, MD Consultant Intern

An immuno-oncology drug development firm with a record $67M series-A financing from Pfizer.

- Identified competitive landscape for current immuno-oncology market. Generated databases for 300+ pipelined therapeutics.
- Performed M&A due diligence for strategic partnerships with a pharma start-up.
- Prepared presentations and memos to support investment decisions for CEO and COO.
- Recruited and liaised collaboration with Johns Hopkins consulting *pro bono* team.

Student Leadership

2015-2017 President, Johns Hopkins Graduate Consulting Club

Dedicated to help 700+ graduate student members prepare for a career in consulting.

- Lead publicity of case competitions: 30+ team applications from 9 major U.S. universities.
- Maintain active collaboration and raised $14,000+ funding from 12 consulting firms.
- Established collaboration with career office, 4 student groups at JHU, NIH. Organize 20+ career workshops and networking events. Raised and oversee a budget of ~$25,000.
- Revitalized consulting boot camp series, 200+ attendees. Founded round-robin case interview practice series, 20+ participants/week.

2010-2012 Vice President, Biomedical Student Association, Colorado State

- Invited local biotech and healthcare firms for career workshops.
- Organized bioscience resume competition, 60+ participants.

Case Competition Experience

2015/11 **Top 1**/8 teams in 2015 Pfizer Case Competition at Johns Hopkins

- Combined psychological studies with market analysis to provide strategic plan to overcome anti-vaccine stigma via social media

2015/7 **Finalist** (**Top 4**/20 teams) in 2015 Princeton University Graduate Case Competition

- Performed SWOT and cost-benefit analysis for the Unlimited Data Plan from T-Mobile Inc.

2015/4 **Top 4**/28 teams in 2015 University of Pennsylvania Graduate Case Competition

- Benchmarked competitors and pinpointed value propositions for unmanned aircrafts market for Identified Tech Inc., a start-up

Hobbies

Singing **Best Ten Singers** in 'The Voice of Baltimore' Singing Championship. Served as pub singer in Shanghai

Writing Editor and contributing writer at City Weekend, a popular high-end bilingual leisure magazine in Shanghai in 2012. Published two articles on Shanghai historic sites